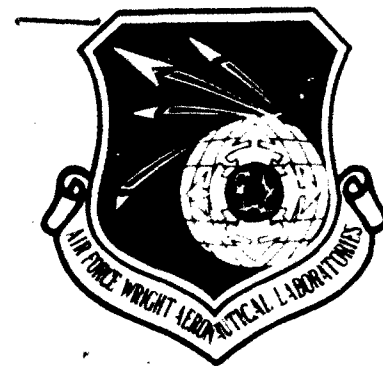


AFWAL-TR-80-2094

LEVEL

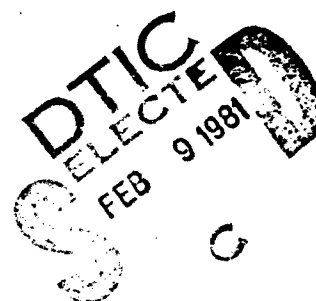
2



NON-AQUEOUS ELECTRODE RESEARCH

R. G. Keil  
W. E. Moddeman  
T. N. Wittberg  
J. R. Hoenigman  
P. S. Zaidain  
J. A. Peters

UNIVERSITY OF DAYTON  
RESEARCH INSTITUTE  
300 College Park  
Dayton, Ohio 45469



AD A094699

October 1980

Technical Report AFWAL-TR-80-2094  
Final Technical Report for the period 1 October 1977 to 25 July 1980

Approved for public release; distribution unlimited

DEC FILE COPY

AERO PROPULSION LABORATORY  
AIR FORCE WRIGHT AERONAUTICAL LABORATORIES  
AIR FORCE SYSTEMS COMMAND  
WRIGHT-PATTERSON AIR FORCE BASE, OHIO 45433


Best Available Copy


NOTICE

*When Government drawings, specifications, or other data are used for any purpose other than in connection with a definitely related Government procurement operation, the United States Government thereby incurs no responsibility nor any obligation whatsoever; and the fact that the government may have formulated, furnished, or in any way supplied the said drawings, specifications, or other data, is not to be regarded by implication or otherwise as in any manner licensing the holder or any other person or corporation, or conveying any rights or permission to manufacture use, or sell any patented invention that may in any way be related thereto.*

*This report has been reviewed by the Office of Public Affairs (ASD/PA) and is releasable to the National Technical Information Service (NTIS). At NTIS, it will be available to the general public, including foreign nations.*

*This technical report has been reviewed and is approved for publication.*

  
DAVID H. FRITTS  
Project Engineer

  
DONALD P. MORTEL  
TAM, Batteries & Fuel Cells  
Energy Conversion Branch

FOR THE COMMANDER  
  
JAMES D. REAMS  
Chief, Aerospace Power Division  
Aero Propulsion Laboratory

*"If your address has changed, if you wish to be removed from our mailing list, or if the addressee is no longer employed by your organization please notify AFAPL/POE-1 (D. H. Fritts), Wright-Patterson Air Force Base, Ohio 45433 to help us maintain a current mailing list".*

*Copies of this report should not be returned unless return is required by security considerations, contractual obligations, or notice on a specific document.*

SECURITY CLASSIFICATION OF THIS PAGE (When Data Entered)

19 REPORT DOCUMENTATION PAGE		READ INSTRUCTIONS BEFORE COMPLETING FORM	
1. REPORT NUMBER AFWAL-TR-80-2794	2. GOVT ACCESSION NO. AD-A094699	3. RECIPIENT'S CATALOG NUMBER	
4. TITLE (and Subtitle) NON-AQUEOUS ELECTRODE RESEARCH.	5. TYPE OF REPORT & PERIOD COVERED Final Technical Report. 1 Oct 1977-25 July 1980	6. PERFORMING ORG. REPORT NUMBER UDR-NM-TR-80-27	
7. AUTHOR R. G. Keil J. R. Hoenigman E. Moddeman P. S. Zaidain T. N. Wittberg J. A. Peters	8. CONTRACT OR GRANT NUMBER(s) F33615-77-C-3156	9. PROGRAM ELEMENT PROJECT, TASK AREA & WORK UNIT NUMBERS 23035408	
10. PERFORMING ORGANIZATION NAME AND ADDRESS University of Dayton Research Institute 300 College Park Dayton, OH 45469	11. REPORT DATE October 1980	12. NUMBER OF PAGES 102	
13. CONTROLLING OFFICE NAME AND ADDRESS Aero Propulsion Laboratory AF Wright Aeronautical Laboratories (AFSC) Wright-Patterson Air Force Base, OH 45433	14. MONITORING AGENCY NAME & ADDRESS (if different from Controlling Office)	15. SECURITY CLASS. (of this report) Unclassified	
16. DISTRIBUTION STATEMENT (of this Report) Approved for public release; distribution unlimited.			
17. DISTRIBUTION STATEMENT of the abstract entered in Block 20, if different from Report)			
18. SUPPLEMENTARY NOTES			
19. KEY WORDS (Continue on reverse side if necessary and identify by block number) Lithium Thionyl chloride Passivation reactivity Auger electron spectroscopy X-ray photoelectron spectroscopy Scanning electron microscope Gases electrochemistry			
20. ABSTRACT (Continue on reverse side if necessary and identify by block number) The faradaic and non-faradaic reactivity of lithium in the thionyl chloride battery system has been studied using AES, XPS, and SEM/EDAX. The passivating film has been characterized as lithium chloride and found to contain substantial quantities of aluminum and sulfur. XPS results show definitely that in battery discharged lithium sulfur occluded within the passive film is present in multiple oxidation states, including sulfide. The reactivity of the			

DD FORM 1 JAN 73 1473 EDITION OF 1 NOV 65 IS OBSOLETE

SECURITY CLASSIFICATION OF THIS PAGE (When Data Entered)

105400

## 20. ABSTRACT (Concluded)

lithium metal surface with  $O_2$ ,  $CO_2$ , CO, and  $N_2$  was studied. The "black spots" were synthesized and analyzed as a lithium oxynitride. A model for ion transport across the passivating lithium chloride film was postulated and its implications discussed. The current interrupt method was tested on a model system. An A/D interface and associated software was developed to enable rapid, accurate data acquisition.

## FOREWORD

This report was prepared by the University of Dayton Research Institute under Air Force Contract No. F33615-77-C-3156 (Project, Task, and Work Unit Numbers 23035408). The work was administered under the direction of the Aerospace Power Division, Energy Conversion Branch, Aero Propulsion Laboratory, with Dr. D. H. Fritts, acting as Contract Monitor. The work reported herein is a summary of a three year research effort. Previously published interim annual reports for the first two years, AFAPL-TR-79-2003 and AFWAL-TR-80-2018, are used as a basis in part together with results obtained during the last year. This report presents the final results of research work conducted from 1 October 1977 through 25 July 1980.

The financial support of this work by the Aero Propulsion Laboratory (AFWAL/POOC) at Wright-Patterson Air Force Base is gratefully acknowledged.

A special note of thanks and appreciation are hereby made to Dr. David Fritts, the Project Monitor. In addition, the authors acknowledge the encouragement and technical support of the following: Dr. Robert McDonald and Dr. Nicolai Marincic of GTE Laboratories, Waltham, Massachusetts; Dr. David Chau and Mr. Donald Bartlett of the Honeywell Power Sources Center, Horsham, Pennsylvania; Dr. Hal Grady of Foote Mineral Company, Exton, Pennsylvania; and to Dr. William Moddeman, who is presently on a leave of absence to the Department of Energy Facility at Mound Laboratories, Miamisburg, Ohio.

Accession For	
NRIS GRA&I	<input checked="checked" type="checkbox"/>
DTIC TAB	<input type="checkbox"/>
Unannounced	<input type="checkbox"/>
Justification	
By	
Distribution/	
Availability Codes	
Dist	Avail and/or Special
A	

## TABLE OF CONTENTS

SECTION		PAGE
1	INTRODUCTION	1
2	EQUIPMENT	5
	A. Dry Box	5
	B. XPS Spectrometer	5
	C. Sample Holder and Vacuum Interlock System	7
	D. Gas Manifold System	12
	E. Spectrometer	12
	F. Electroanalytical Components	14
	G. Chemicals	14
3	PREPARATION OF CLEAN LITHIUM SURFACES	18
4	THE NON-FARADAIC REACTIVITY OF LITHIUM WITH GASES	22
5	NON-FARADAIC REACTIVITY OF LITHIUM	29
6	THE NON-FARADAIC REACTIVITY OF LITHIUM WITH ELECTROLYTE	34
7	THE FARADAIC REACTIVITY OF LITHIUM IN ELECTROLYTE	48
8	XPS OF THE LITHIUM SURFACE	62
9	ELECTROCHEMICAL STUDIES: A MODEL FOR THE LITHIUM/ELECTROLYTE INTERFACE	68
10	SUMMARY AND CONCLUSIONS	89
	REFERENCES	90

## LIST OF ILLUSTRATIONS

Figure		Page
1	Block Diagram of Helium Dry Box and Purification System.	6
2	XPS System Showing the Redesigned Vacuum System. A. Turbomolecular pump; B. Ion pump; C. Titanium sublimation pump.	8
3	Sample Insertion Probe for the XPS System. A. Bellows assembly; B. Ultrahigh vacuum rotary feedthrough.	9
4	Lithium Sample Transfer Chamber. A. Ultrahigh vacuum gate valve; B. Sample chamber; C. Viewing port.	10
5	Lithium Sample Holder for the XPS System. A. Banana plug support; B. Sample rod; C. Set screw fastener; D. Threaded sample probe fastener.	11
6	Gas Manifold for Vapor Exposure Studies on "Fresh" Lithium Surfaces.	13
7	Circuit Schematic for Step-Function Galvanostat and Voltage Follower.	15
8	Auger Spectrum of a Lithium Metal Surface As-Cut Under n-Hexane Using the Improved Sample Preparation Technique.	19
9	Auger Spectrum of a Clean Lithium Metal Surface Obtained by Repeated Sputtering and Pumping.	20
10	High Resolution Auger Spectra of Lithium. a) clean surface; b) exposed to $1.6 \times 10^8$ Langmuirs of nitrogen; c) exposed to $5.0 \times 10^8$ Langmuirs of nitrogen; d) exposed to $4.8 \times 10^3$ Langmuirs of oxygen; e) exposed to $8.9 \times 10^3$ Langmuirs of carbon dioxide.	23
11	Relative Response Ratios of $H_2O$ , $N_2$ , $CO_2$ , and $O_2$ versus Dose. a) $O$ (509 eV)/Li(51 eV) Auger peak ratios for $H_2O$ exposures; b) Li (38 eV)/Li(51 eV) Auger peak ratios for $H_2O$ exposures; c) $N$ (380 eV)/Li(51 eV) Auger peak ratios for $N_2$ exposures; d) $O$ (509 eV)/Li (51 eV) Auger peak ratios for $CO_2$ exposures; e) $O$ (509 eV)/Li(51 eV) Auger peak ratios for $O_2$ exposures; f) Li(38 eV)/Li(51 eV) Auger peak ratios for $CO_2$ exposures; g) Li(38 eV)/Li(51 eV) Auger peak ratios for $O_2$ exposures.	24
12	Typical Overall XPS Scan of Foote Mineral Lithium Freshly Cut in Inert Atmosphere.	25

# LIST OF ILLUSTRATIONS (Continued)

Figure		Page
13	High Resolution O 1s XPS Spectra of: a) Lithium hydroxide, b) approximately equal amount of Lithium hydroxide and Lithium oxide, and c) Lithium oxide.	26
14	Auger Spectrum of Black Spot on a Lithium Surface After an Overnight Exposure to Nitrogen.	28
15	Overall AES Spectra of a Typical GTE Lithium Anode Surface "as received" Which was Exposed to: a) $\text{SOCl}_2$ liquid, 11 days, and b) $\text{SOCl}_2$ vapor, 11 days.	30
16	SEM Photomicrographs for Lithium Aged in Thionyl Chloride, $55^\circ\text{C}$ , Four Days.	32
17	Sputtering Time Required to Read 10 Percent Signal versus Lithium Exposure Temperature for a Four-Day Exposure to "neat" Thionyl Chloride and 1.8 M Lithium Tetrachloroaluminate in Thionyl Chloride.	35
18	SEM Photomicrographs for Lithium Aged in Electrolyte, $25^\circ\text{C}$ , Four Days.	36
19	SEM Photomicrographs for Lithium Aged in Electrolyte, $55^\circ\text{C}$ , Four Days.	38
20	SEM Photomicrographs for Lithium Aged in Electrolyte, $70^\circ\text{C}$ , Four Days.	40
21	SEM Photomicrographs for Lithium Samples Soaked in Electrolyte for 90 Minutes and Receiving Two Thionyl Chloride Washings.	42
22	SEM (3000X) Photomicrographs of Aggregate Crystal Formed During a 90 Minute Electrolyte Soak.	43
23	SEM (1000X) Photomicrograph and EDAX Trace of "mudcracked" Region for a Lithium Sample Soaked in Electrolyte 90 Minutes and Receiving No Thionyl Chloride Wash.	44
24	AES Spectrum of Lithium Exposed for 90 Minutes to $\text{LiAlCl}_4/\text{SOCl}_2$ , No Wash.	46
25	AES Spectrum of Lithium Exposed for 90 Minutes to $\text{LiAlCl}_4/\text{SOCl}_2$ , One Wash.	47
26	SEM Photomicrographs for Lithium Discharged Ten Percent at One $\text{mA}/\text{cm}^2$ , Room Temperature, Unwashed.	49
27	SEM Photomicrographs for Lithium Discharged Ten Percent at One $\text{mA}/\text{cm}^2$ , Room Temperature, One Washing.	51



# LIST OF ILLUSTRATIONS (Continued)

Figure		Page
28	AES Spectrum of Lithium Discharged One-Half Percent in Electrolyte at One mA/cm <sup>2</sup> , Room Temperature, No Thionyl Chloride Wash.	53
29	AES Spectrum of Lithium Discharged One-Half Percent in Electrolyte at One mA/cm <sup>2</sup> , Room Temperature, One Thionyl Chloride Washing.	54
30	AES Spectrum of Lithium Discharged One-Half Percent in Electrolyte at One mA/cm <sup>2</sup> , Room Temperature, Two Thionyl Chloride Washings.	55
31	AES Spectrum of Lithium Discharged One-Half Percent in Electrolyte at One mA/cm <sup>2</sup> , Room Temperature, Three Thionyl Chloride Washings.	56
32	AES Spectrum of Lithium Discharged One-Half Percent in Electrolyte at One mA/cm <sup>2</sup> , Room Temperature, Four Thionyl Chloride Washings.	57
33	AES Oxygen and Aluminum Peak from a Lithium Anode Discharged Ten Percent at One mA/cm <sup>2</sup> , and Room Temperature Receiving Thionyl Chloride Washings. a) no wash; b) one wash; c) two washings; d) three washings; e) four washings.	58
34	High Resolution XPS of Sulfur 2p in a) Na <sub>2</sub> SO <sub>4</sub> initial scan; b) Na <sub>2</sub> SO <sub>4</sub> after 11 hour beam exposure; and c) ten percent discharged lithium at one mA/cm <sup>2</sup> , 50,000 counts, 11-hour beam exposure.	60
35	XPS Spectra of Lithium Surface a) "as received" and from the dry box; b) after argon ion sputtering; c) after short exposure to SOCl <sub>2</sub> vapor; and d) after short exposure to SOCl <sub>2</sub> liquid.	63
36	XPS Spectra of a) after 90 minutes exposure of "as received" lithium to 1.8 M LiAlCl <sub>4</sub> /SOCl <sub>2</sub> , no wash; b) after one SOCl <sub>2</sub> wash; c) after three SOCl <sub>2</sub> washes; d) after four SOCl <sub>2</sub> washes.	64
37	High Resolution XPS Spectra of Chlorine 2p on Lithium Metal Surfaces, a) "as received" and transferred from the dry box, b) after 90 minutes exposure to SOCl <sub>2</sub> liquid, c) after 90 minutes exposure to electrolyte, no wash, d) after 90 minutes exposure to electrolyte, one SOCl <sub>2</sub> wash; and e) after 90 minutes exposure to electrolyte, four washings.	65

# LIST OF ILLUSTRATIONS (Concluded)

Figure		Page
38	High Resolution XPS Spectra of Oxygen 1s on Lithium Metal Surfaces a) "as received" and transferred from the dry box; b) after receiving 90 minutes argon ion sputter; c) after exposure to $\text{SOCl}_2$ vapor; d) after 90 minutes exposure to electrolyte, no $\text{SOCl}_2$ wash; and e) after 90 minutes exposure to electrolyte, four $\text{SOCl}_2$ washings.	66
39	Plot of Minus $V_o$ versus Formation Potential (Volts) for Tantalum Anodized in an Aqueous Boric Acid-Sodium Tetraborate Solution at Room Temperature.	87

# LIST OF TABLES

TABLE		PAGE
I	THIONYL CHLORIDE COMPOSITION	17
II	EXPERIMENTAL CONDITIONS AND TABLE SOURCE FOR VOLTAGE DATA OBTAINED WITH TANTALUM METAL IN AQUEOUS BORIC ACID - SODIUM TETRABORATE SOLUTIONS AT ROOM TEMPERATURE AFTER CURRENT INTERRUPT	73
III	OVERVOLTAGE TRANSIENT DATA FOR A 3.7 VOLT TANTALUM FILM ANODIZED IN AN AQUEOUS BORIC ACID SODIUM TETRABORATE SOLUTION AT 2,174 $\mu\text{a}/\text{cm}^2$ AND AT ROOM TEMPERATURE: TIME RESOLUTION 158.5 $\mu$ SEC, VOLTAGE RESOLUTION 2.4414 MILLIVOLTS, DATA PRESENTED IN MILLIVOLTS	74
IV	OVERVOLTAGE TRANSIENT DATA FOR A 5.3 VOLT TANTALUM FILM ANODIZED IN AN AQUEOUS BORIC ACID SODIUM TETRABORATE SOLUTION AT 2,174 $\mu\text{a}/\text{cm}^2$ AND AT ROOM TEMPERATURE: TIME RESOLUTION 158.5 $\mu$ SEC, VOLTAGE RESOLUTION 2.4414 MILLIVOLTS, DATA PRESENTED IN MILLIVOLTS	75
V	OVERVOLTAGE TRANSIENT DATA FOR A 7.0 VOLT TANTALUM FILM ANODIZED IN AN AQUEOUS BORIC ACID SODIUM TETRABORATE SOLUTION AT 2,174 $\mu\text{a}/\text{cm}^2$ AND AT ROOM TEMPERATURE: TIME RESOLUTION 158.5 $\mu$ SEC, VOLTAGE RESOLUTION 2.4414 MILLIVOLTS, DATA PRESENTED IN MILLIVOLTS	76
VI	OVERVOLTAGE TRANSIENT DATA FOR A 9.0 VOLT TANTALUM FILM ANODIZED IN AN AQUEOUS BORIC ACID SODIUM TETRABORATE SOLUTION AT 2,174 $\mu\text{a}/\text{cm}^2$ AND AT ROOM TEMPERATURE: TIME RESOLUTION 158.5 $\mu$ SEC, VOLTAGE RESOLUTION 2.4414 MILLIVOLTS, DATA PRESENTED IN MILLIVOLTS	77
VII	OVERVOLTAGE TRANSIENT DATA FOR A 3.0 VOLT TANTALUM FILM ANODIZED IN AN AQUEOUS BORIC ACID SODIUM TETRABORATE SOLUTION AT 1,087 $\mu\text{a}/\text{cm}^2$ AND AT ROOM TEMPERATURE: TIME RESOLUTION 158.8 $\mu$ SEC, VOLTAGE RESOLUTION 2.4414 MILLIVOLTS, DATA PRESENTED IN MILLIVOLTS	78
VIII	OVERVOLTAGE TRANSIENT DATA FOR A 5.0 VOLT TANTALUM FILM ANODIZED IN AN AQUEOUS BORIC ACID SODIUM TETRABORATE SOLUTION AT 1,087 $\mu\text{a}/\text{cm}^2$ AND AT ROOM TEMPERATURE: TIME RESOLUTION 158.8 $\mu$ SEC, VOLTAGE RESOLUTION 2.4414 MILLIVOLTS, DATA PRESENTED IN MILLIVOLTS	79
IX	OVERVOLTAGE TRANSIENT DATA FOR A 7.0 VOLT TANTALUM FILM ANODIZED IN AN AQUEOUS BORIC ACID SODIUM TETRABORATE SOLUTION AT 1,087 $\mu\text{a}/\text{cm}^2$ AND AT ROOM TEMPERATURE: TIME RESOLUTION 158.8 $\mu$ SEC, VOLTAGE RESOLUTION 2.4414 MILLIVOLTS, DATA PRESENTED IN MILLIVOLTS	80

# LIST OF TABLES (Concluded)

TABLE		PAGE
X	OVERVOLTAGE TRANSIENT DATA FOR A 9.0 VOLT TANTALUM FILM ANODIZED IN AN AQUEOUS BORIC ACID SODIUM TETRABORATE SOLUTION AT 1,087 $\mu\text{a}/\text{cm}^2$ AND AT ROOM TEMPERATURE: TIME RESOLUTION 158.8 $\mu$ SEC, VOLTAGE RESOLUTION 2.4414 MILLIVOLTS, DATA PRESENTED IN MILLIVOLTS	81
XI	OVERVOLTAGE TRANSIENT DATA FOR A 3.1 VOLT TANTALUM FILM ANODIZED IN AN AQUEOUS BORIC ACID SODIUM TETRABORATE SOLUTION AT 217 $\mu\text{a}/\text{cm}^2$ AND AT ROOM TEMPERATURE: TIME RESOLUTION 158.8 $\mu$ SEC, VOLTAGE RESOLUTION 2.4414 MILLIVOLTS, DATA PRESENTED IN MILLIVOLTS	82
XII	OVERVOLTAGE TRANSIENT DATA FOR A 7.0 VOLT TANTALUM FILM ANODIZED IN AN AQUEOUS BORIC ACID SODIUM TETRABORATE SOLUTION AT 217 $\mu\text{a}/\text{cm}^2$ AND AT ROOM TEMPERATURE: TIME RESOLUTION 158.8 $\mu$ SEC, VOLTAGE RESOLUTION 2.4414 MILLIVOLTS, DATA PRESENTED IN MILLIVOLTS	83
XIII	OVERVOLTAGE TRANSIENT DATA FOR A 9.0 VOLT TANTALUM FILM ANODIZED IN AN AQUEOUS BORIC ACID SODIUM TETRABORATE SOLUTION AT 217 $\mu\text{a}/\text{cm}^2$ AND AT ROOM TEMPERATURE: TIME RESOLUTION 158.8 $\mu$ SEC, VOLTAGE RESOLUTION 2.4414 MILLIVOLTS, DATA PRESENTED IN MILLIVOLTS	84
XIV	OVERVOLTAGE TRANSIENT DATA FOR A 5.0 VOLT TANTALUM FILM ANODIZED IN AN AQUEOUS BORIC ACID SODIUM TETRABORATE SOLUTION AT 217 $\mu\text{a}/\text{cm}^2$ AND AT ROOM TEMPERATURE: TIME RESOLUTION 158.8 $\mu$ SEC, VOLTAGE RESOLUTION 2.4414 MILLIVOLTS, DATA PRESENTED IN MILLIVOLTS	85
XV	ELECTROCHEMICAL RESULTS; CALCULATED VALUES OF "k", " $V_o$ ", AND "s" FOR FILM GROWN AT SPECIFIED CURRENT DENSITY AND VOLTAGE. THE VALUE OF $\theta$ WHICH YIELDS THE MINIMAL VALUE IS "s" IS PRESENTED	86

## SECTION 1

### INTRODUCTION

In recent years, attention has focused upon lithium as an anode material for high energy density (H.E.D.) battery systems. Because of the ease of oxidation of metallic lithium, such systems necessarily use a non-aqueous solvent/electrolyte. From practical considerations, the anode and cathode materials which will provide the largest emf are selected from a list of standard electrode potentials (1). Lithium immediately becomes a prime anode candidate. The large emf that can be obtained, coupled with the possibility of high energy densities (500 W-hr/kg), prompted research interest in lithium batteries since about 1960. Cathode materials are chosen on the basis of the cell voltage, reaction products formed, availability and stability. A much larger list of potential cathode systems exists which include heavy metal halides (2-4) sulfides (5) and oxides (6)

Auburn et al (7) and Behl et al (8) reported on cells utilizing oxyhalides with the addition of 1-2M  $\text{LiAlCl}_4$  as an electrolyte and either graphite, carbon black, or polycarbon monofluoride  $(\text{CF})_n$  as the cathode. Lithium was found to be stable in the three major oxyhalides studied; phosphorus oxytrichloride ( $\text{POCl}_3$ ), sulfuryl chloride ( $\text{SO}_2\text{Cl}_2$ ), and thionyl chloride ( $\text{SOCl}_2$ ). It was concluded from observations of the appearance of lithium anode surfaces, from cell performance, and from opinions based on the established reactivity of lithium that this stability was due to the formation of a passivation layer. Solvent reduction occurred during operation of the cell as a battery and energy densities in excess of 500W-hr/kg were reported (7). The thionyl chloride system showed the best performance compared to the other two oxyhalides due to its higher energy density even though the cell voltage of the  $\text{SO}_2\text{Cl}_2$  system is higher than that of the  $\text{SOCl}_2$  system (3.9V vs. 3.6V), respectively (9). These factors then prompted further investigation and development of the lithium thionyl chloride system.

Many reactions (and reaction products) can be proposed, consistent with a complex system, and a favorable thermodynamic situation. The reactivity at the electrode surface is further complicated because the kinetics for each reaction are apt to be markedly different and a mixed potential situation probably exists. Since surface lithium reactions in a simple system are not yet understood, an analytical determination of these reaction products might yield insights into basic phenomena affecting cell performance.

Thionyl chloride is used as an electrolyte carrier and cathode depolarizer because of its ability to undergo electrochemical reduction. The continued development and investigation of primary lithium batteries based on  $\text{SOCl}_2$  has highlighted three problems: first, a voltage delay after storage at high temperature (10-14), second, a tendency of the cells to explode at high rates of discharge, short circuit, or overdischarge (13), and third, limited cell capacity based on the ability of the carbon cathode to accommodate products of reaction before passivation (9).

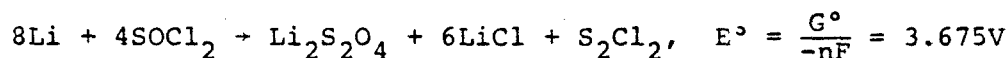
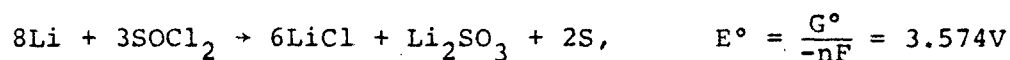
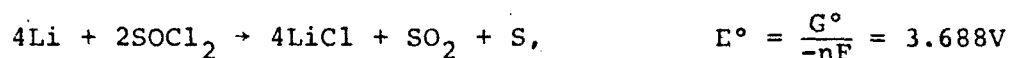
Approaches to alleviate the safety hazards associated with the use of these batteries have been investigated (15,16). It appears that the explosion problem can be solved by providing for automatic venting, limiting the rate of discharge, and protecting against short circuit by the use of thermal fusing within the cell. The problem is further complicated, however, by the observation that  $\text{SO}_2$  gas, a primary reaction product, is not produced at a linear rate when a battery is discharged at constant current; rather it is expelled in a non-linear fashion toward the end of the discharge (17). The cathode limitation can be overcome by using a porous cathode with greater surface area while limiting the cell anode by controlling the quantity of lithium utilized (18).

The voltage delay phenomenon caused by passivation of the lithium surface has been studied by a number of workers (10-14, 19). Driscoll et al. (19) reported that the voltage delay could be eliminated by pretreatment in  $1.5\text{M LiAlCl}_4/\text{SOCl}_2$  and that solution purity dramatically affected the voltage delay. Principal

products of the discharge reaction were reported to be S, SO<sub>2</sub>, and LiCl. Dey and Schlaikjer (12) examined the surface of lithium by SEM and energy dispersive x-ray analysis to characterize the passive film growth and its composition. These investigators concluded that the crystalline material on the lithium surface was LiCl.

In a separate study, Auburn et al. (7) concluded that the reaction products were mainly lithium chloride, sulfur, and lithium sulfite, while Holleck et al. (20) reported the reaction products to be lithium chloride, sulfur, and sulfur dioxide.

Several reactions were then examined thermodynamically in an effort to determine if one of the calculated voltages compared more favorably to the measured open circuit voltage of approximately 3.6V. The free energy values of formation were obtained from Lattimer (1).



Unfortunately, all of these values are within the experimental error of measurement so that no conclusion regarding the reaction can be reached based upon these calculations even if kinetic complications were to be ignored. Chua et al. (14) have reported that film growth was observed only in the presence of LiAlCl<sub>4</sub> and the addition of 5% SO<sub>2</sub> reduces the voltage delay time.

Lithium is so reactive that it is unlikely that it can exist in contact with another material without forming a protective film. The properties of this passive film upon lithium can be understood in part through electrochemical studies. The behavior of the lithium is dependent upon several film properties including its thickness, its morphology (porosity and crystal size), the type and concentration of lattice defects (interstitial ions, grain boundaries), and the transport mechanism (ions and/or electrons).

Some (21,22) have made initial use of electrochemical techniques to examine this passive film.

It appears that a first step in attempting to understand the complex phenomena and reactions occurring within a primary lithium cell, is to understand the surface reactions of lithium with its environment before it is placed in the battery. It is obvious that the surface reaction products of lithium, passive or active, can influence the operation of the battery. A second step is to study the surface reactivity with electrolyte. It is the purpose of this study to investigate the surface reactions and passive film formation on lithium using surface spectroscopy techniques and to correlate these results with electroanalytical results.



## SECTION 2

### EQUIPMENT

#### A. Dry Box

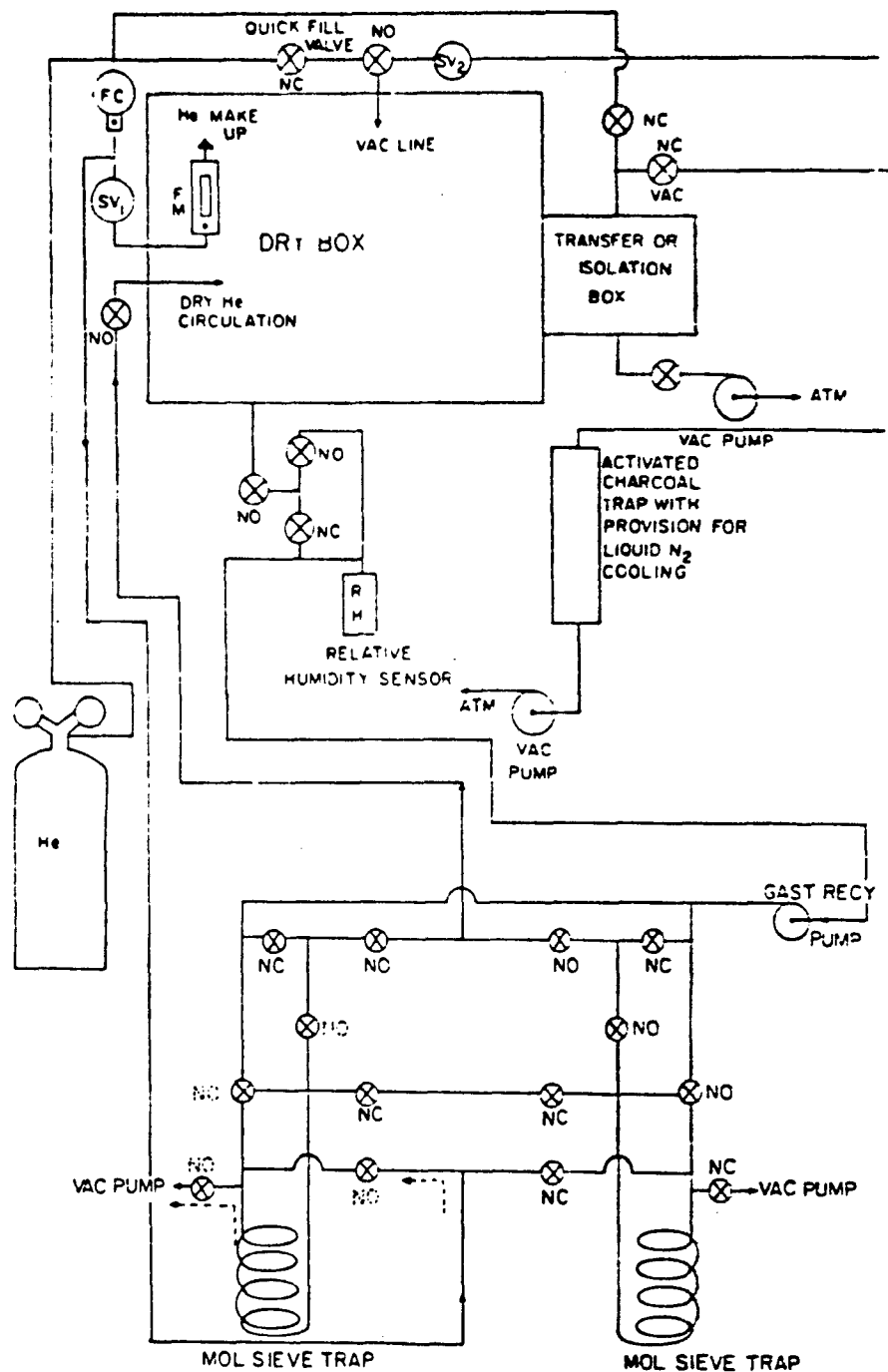
A dry box, obtained from Wright-Patterson Air Force Base was refurbished to provide an environment in which lithium and thionyl chloride could be stored, their chemical reactivity studied, and electrochemical experiments conducted. Subsequently lithium samples were transferred for surface analysis using demonstrated procedures (described later) which minimized the chance of contamination. The dry box was fitted with electrical feedthroughs to enable electrochemical experiments to be conducted.

The major components of the dry box system shown in Figure 1 are:

- (1) a provision for an inert atmosphere (helium was used;
  - (2) a recirculating pump for continual removal of any gaseous impurities such as water vapor from the helium (by pumping through molecular sieve columns);
  - (3) a provision for maintaining a continuous positive pressure;
  - (4) an isolation or transfer compartment (which allows chemicals and equipment to be introduced into the box without contaminating the atmosphere with either air or water vapor);
  - (5) a provision for regeneration of the molecular sieve;
- and
- (6) a relative humidity sensor to enable constant monitoring of the water vapor level in the dry box. A dewpoint of about  $-78^{\circ}\text{C}$  ( $<2\text{ppm H}_2\text{O}$ ) was maintained for the duration of this work.

#### B. XPS Spectrometer

XPS spectra were obtained using an AEI (KRATOS) ES-100 spectrometer modified to include ion sputtering, enhanced vacuum capabilities and microprocessor controlled data acquisition. Spectra were



----- FOR MOL SIEVE REGENERATION

Figure 1. Block Diagram of Helium Dry Box and Purification System.

obtained using a magnesium K $\alpha$  source at a beam power of 200 watts. The enhanced pumping capability was achieved through the use of a turbo-molecular pump, ion pump and a titanium sublimation pump. The XPS system was thus able to sustain a base pressure of  $1 \times 10^{-9}$  Torr ( $1.3 \times 10^{-7}$  Pa). This design (Figure 2) provides improved reliability and presents a clean environment for the analysis of samples including lithium metal samples exposed to environmental gases.

### C. Sample Holder and Vacuum Interlock System

A vacuum interlock system was used for transferring lithium, SOCl<sub>2</sub> and battery anode samples from the helium dry box in which they were prepared into the XPS sample chamber for analysis. The two sections of the vacuum interlock system are shown in Figures 3 and 4. Figure 3 is the insertion stage, and Figure 4 is the transfer chamber. The corresponding sample holder for lithium metal is shown in Figure 5.

The vacuum interlock is composed of two sections which bolt onto opposite sides of the XPS sample chamber (Figures 3 and 4). On one side is a long .375 in. diameter stainless steel rod inside a stainless steel bellows (A in Figure 3). The rod can be rotated within the bellows via a vacuum rotary feedthrough (B in Figure 3). This rod is inserted through the XPS system into the sample transfer chamber. Utilizing the bellows and rotary feedthrough, the rod is attached to the threaded end of the sample holder (D in Figure 5) and the sample is drawn into the XPS system. The other half of the interlock system is the actual transfer chamber (Figure 4). The transfer chamber consists of an ultrahigh vacuum gate valve (A in Figure 4), a sample chamber (B in Figure 4), and a viewing port (C in Figure 4). The transfer chamber is initially loaded with a sample inside the helium dry box. The gate valve is then closed and the transfer chamber is bolted onto the XPS unit. The use of a second gate valve on the XPS system permits simultaneous isolation of both the XPS system

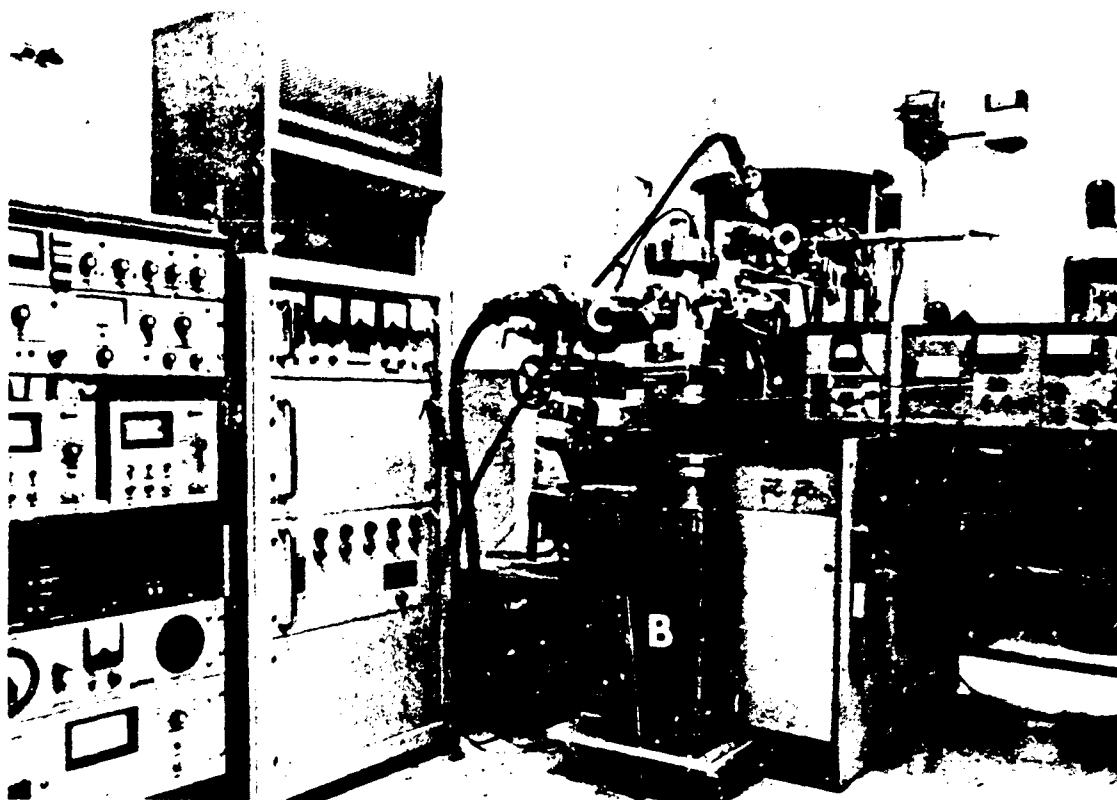


Figure 2. XPS System Showing the Redesigned Vacuum System. A. Turbomolecular pump; B. Ion pump; C. Titanium sublimation pump.

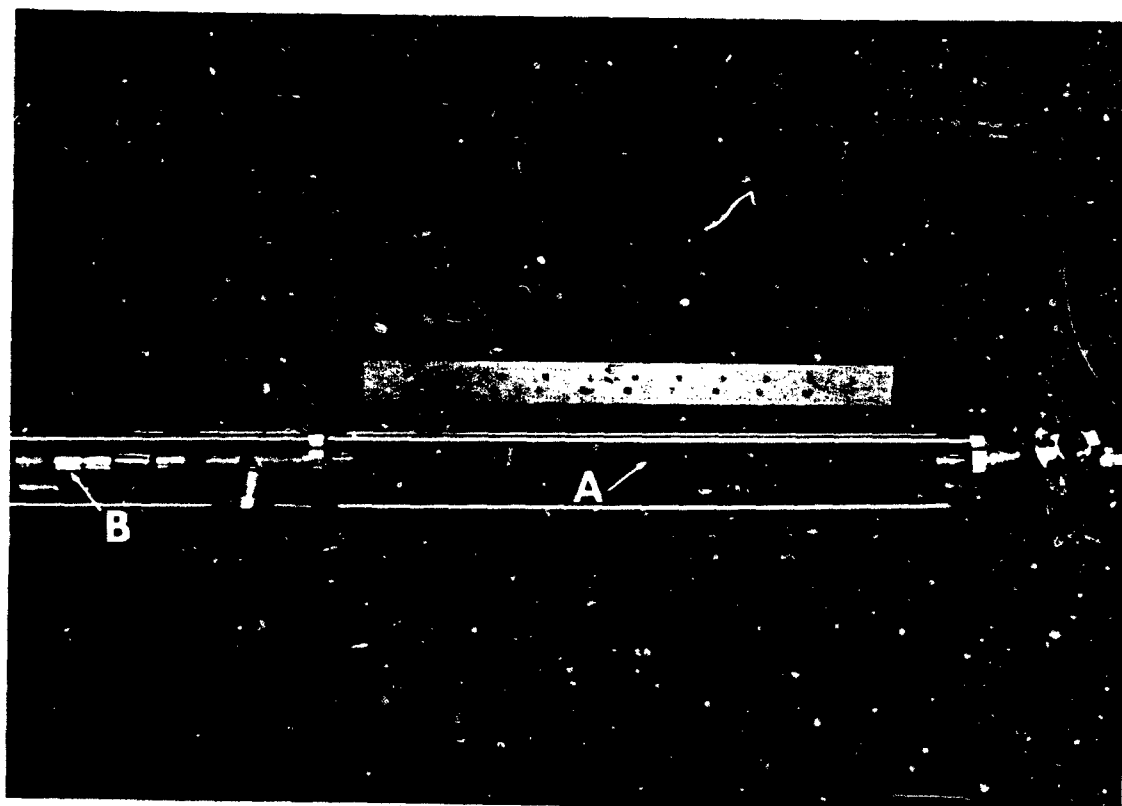


Figure 3. Sample Insertion Probe for the XPS System. A. Bellows assembly;  
B. Ultrahigh vacuum rotary feedthrough.

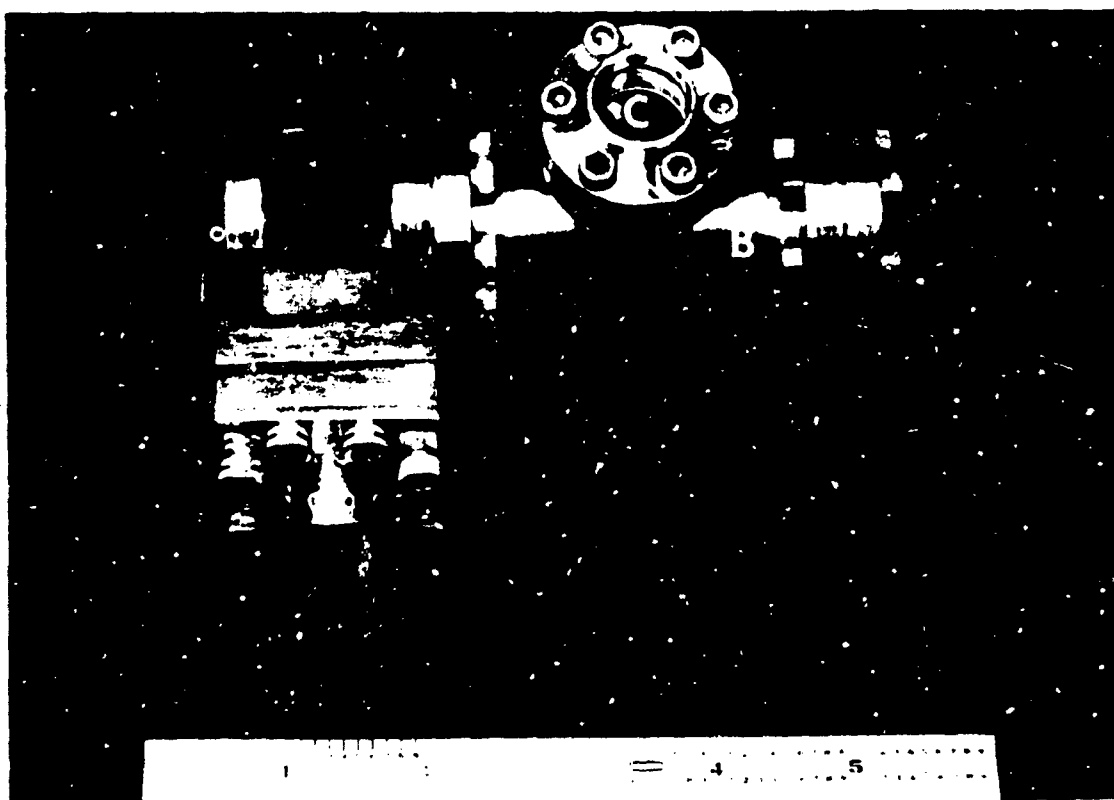


Figure 4. Lithium Sample Transfer Chamber.  
A. Ultrahigh vacuum gate valve;  
B. Sample chamber; C. Viewing port.

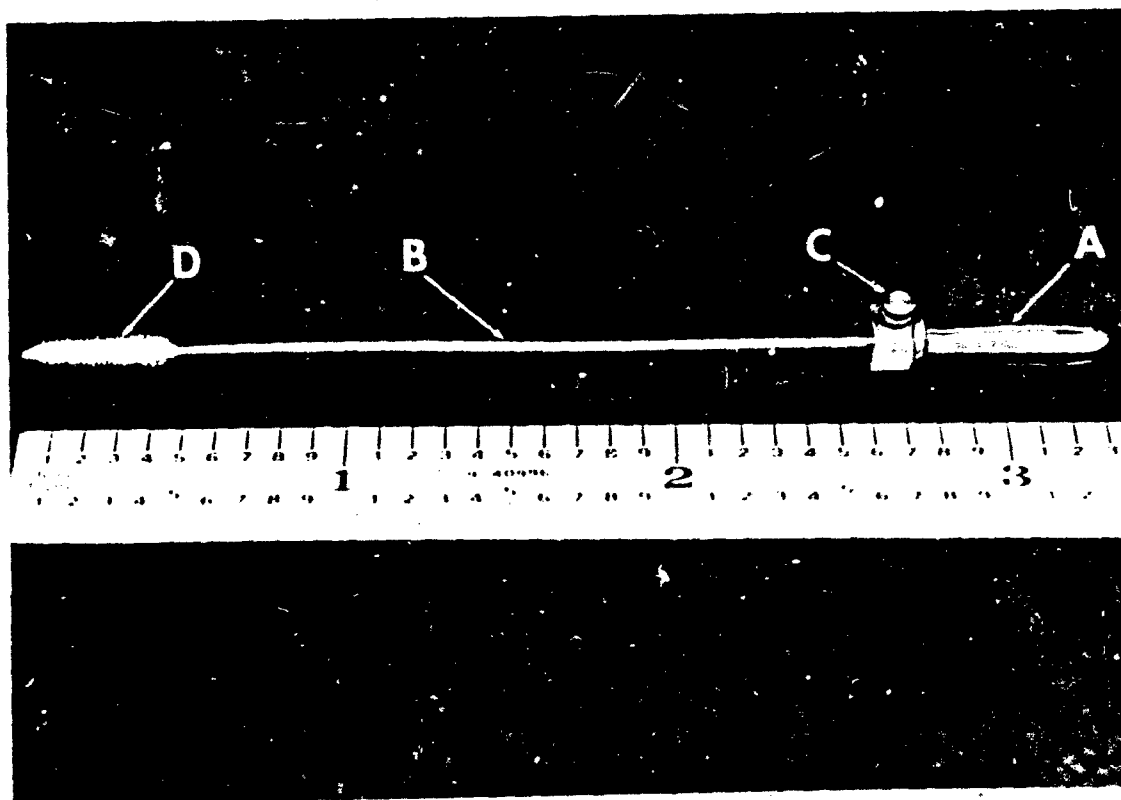


Figure 5. Lithium Sample Holder for the XPS System.  
A. Banana plug support; B. Sample rod;  
C. Set screw fastener; D. Threaded sample  
probe fastener.

and the transfer chamber from the atmosphere. Through the use of an additional valve the transfer system can be evacuated using the turbomolecular pump. The sample is then pulled into the XPS chamber. This transfer system was utilized in all the XPS studies of lithium anodes.

The sample holder functions as follows: one end of the holder is composed of a standard banana plug (A in Figure 5). The banana plug is connected to a rod (B in Figure 5) by means of a small set screw (C in Figure 5). The opposite end of the sample holder is threaded (D in Figure 5). A sample of the lithium metal is "speared" onto the holder rod such that the end faces of the lithium are parallel to the rod. The banana plug is then fastened on the rod and then inserted into a hole in the end plate of the vacuum interlock. Once the interlock system is attached to the XPS instrument and evacuated, the sample is pulled into the analysis chamber by screwing the insertion rod onto the threaded end of the sample holder and withdrawing the holder from the vacuum interlock.

#### D. Gas Manifold System

A separate system for the exposure of lithium to different gases was constructed. The gas manifold system shown in Figure 6 is composed of a central manifold with four gas cylinders connected in parallel. An ultrahigh vacuum flange on each end of the manifold allowed the manifold to be connected to the Auger spectrometer and to a portable high vacuum system simultaneously. When this system was connected to the spectrometer, gases of interest were introduced for direct reaction with the sample in the analysis chamber. In addition, the system allowed mixed gas reactions and sequential gas exposure experiments to be conducted.

#### E. Spectrometer

AES spectra were obtained with a Varian 10 keV 5 $\mu$ m spectrometer. The electron beam energy and spot size chosen for these analyses were typically 3 keV and  $5 \times 10^{-2}$  mm<sup>2</sup>, respectively. The



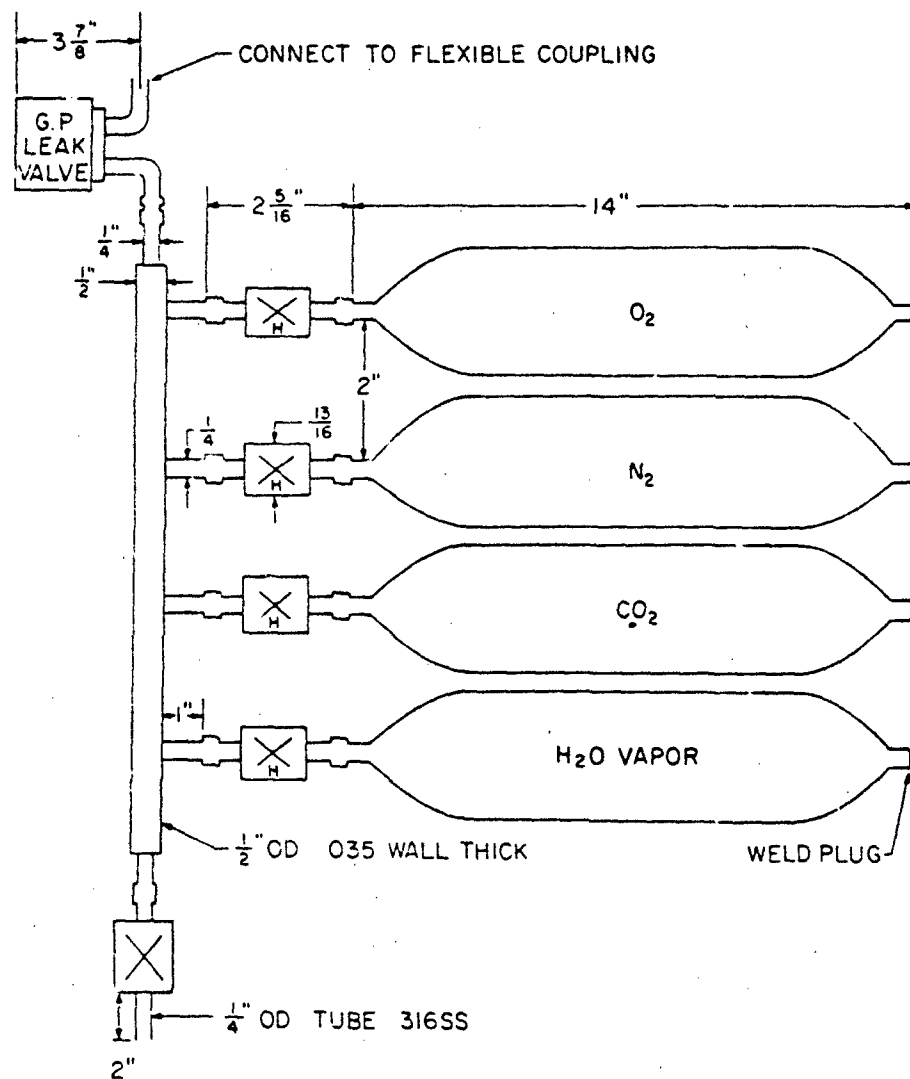


Figure 6. Gas Manifold for Vapor Exposure Studies on "Fresh" Lithium Surfaces.

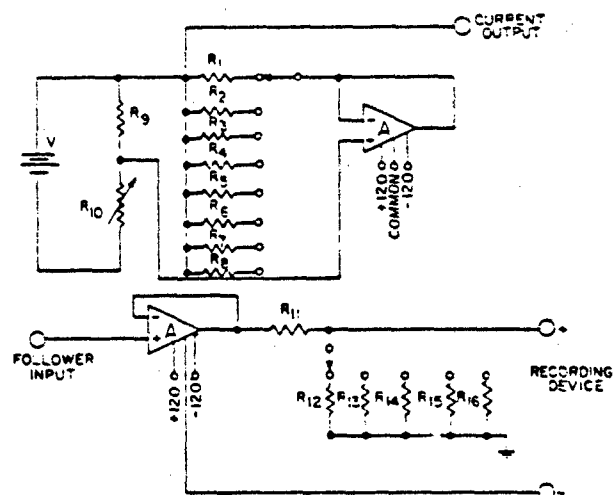
electron beam current was 1  $\mu$ A. The base pressure determined from the uncorrected nude gauge reading was typically  $1 \times 10^{-10}$  Torr ( $1.3 \times 10^{-8}$  Pa). Samples were profiled using 3 keV argon ions with the system backfilled to  $5 \times 10^{-5}$  Torr. The intensities of the element of interest e.g. chlorine (181 eV), carbon (271 eV), oxygen (503 eV) and/or aluminum (1386 eV) were monitored. Samples were transferred from the dry box to the spectrometer by placing the carousel containing several samples in a "Zip-Loc" polyethylene bag. This transporter bag was opened inside a larger bag attached to an entry port of the AES system through which dry argon gas was flowing at a rapid rate. Little or no contamination resulted when samples were transferred in this manner.

#### F. Electroanalytical Components

A galvanostat and voltage follower were constructed with a pair of Philbrick SP-102 operational amplifiers (Figure 7). These amplifiers have a compliance voltage of some  $\pm 100$  volts and as such were used to construct a system with seven current values from 0.500 to 2500  $\mu$ A. The open circuit potential of the lithium electrode versus a calomel reference electrode was monitored versus time following a galvanostatic pulse by inputting the cell to a Data! MDAS-80 A/D converter which was interfaced with a computer (TRS-80). The acquisition rate was computer limited (6500  $\sim$ /sec) which allowed transients as short as about one milliseconds to be adequately followed. The galvanostatic current was computer controlled through a National Semiconductor analogue switch (No. AH0015) whose transients (400 nsec-off, 100 nsec-on) and internal resistance (75 $\Omega$ -on, 10 $\Omega$ -off) were quite acceptable. The software for computer acquisition and processing of voltage transient data was available within the laboratory.

#### G. Chemicals

Lithium samples from discharged cells were prepared by GTE-Sylvania of Waltham, Massachusetts. They were sealed with sealing wax in screw-cap seals which had been blanketed with argon



Circuit schematic: A—operational amplifiers; V—Mallory TR-289, 12.6V battery;  $R_1$ —20 Mohms;  $R_2$ —2 Mohms;  $R_3$ —400 kohms;  $R_4$ —200 kohms;  $R_5$ —40 kohms;  $R_6$ —20 kohms;  $R_7$ —6 kohms;  $R_8$ —4 kohms;  $R_9$ —12.1 kohms;  $R_{10}$ —5 kohms;  $R_{11}$ —500 kohms;  $R_{12}$ —5 ohms;  $R_{13}$ —6.6 ohms;  $R_{14}$ —10 ohms;  $R_{15}$ —20 ohms;  $R_{16}$ —50 ohms.

Figure 7. Circuit Schematic for Step-Function Galvanostat and Voltage Follower.

within their dry box. High purity lithium was also obtained from Foote Mineral Company, Exton, Pennsylvania

This program called for GTE-Sylvania to supply lithium anode samples which had been discharged to specified depths of their theoretical capacity, at specified rates and at specified temperatures. High purity thionyl chloride (Table I) and electrolyte were also supplied by GTE-Sylvania.

TABLE I. THIONYL CHLORIDE COMPOSITION

Component	Weight %
Sulfuryl Chloride	<0.009%
Sulfur Chlorides	<0.1%
Sulfur Dioxide	<0.3%
Residue on Evaporation	<0.1%
Nickel	5 ppm
Iron	5 ppm
Lead	5 ppm
Copper	1 ppm
Zinc	1 ppm
Other Metals	10 ppm
Water	<50 ppm
Organics	Not Detected

### SECTION 3

#### PREFERRATION OF CLEAN LITHIUM SURFACES

The affinity which lithium has for most substances, e.g., water and oxygen, requires that special precautions be taken to inhibit surface reaction. Removal of contamination through sputtering and pumping is difficult. An improvement in transferring lithium metal samples which resulted in only slight oxygen contamination was achieved by immersing the lithium in n-hexane prior to transfer from the dry box. The details of this procedure have been fully described in detail (23). An AES trace of a lithium metal surface put under n-Hexane is shown in Figure 8 and a trace for the lithium metal surface after receiving repeated sputtering and pumping is shown in Figure 9. This surface (Figure 9) was deemed to be the result of an optimum lithium surface preparation procedure, and was used as a substrate to conduct gas exposure studies. The resulting "clean" lithium surfaces displayed a combined surface impurity (O, N and C) of less than one atomic percent. This determination was made by considering the relative sensitivity of these elements to the Auger process as measured from data gathered in our laboratory and elsewhere (24). In Figure 9, the major Auger peak in the K-VV spectrum of clean lithium appears at 51eV. This is in agreement with previously reported results (25,26) on lithium.

The base pressure in the XPS is greater than that in the AES,  $3 \times 10^{-7}$  Pa versus  $1.3 \times 10^{-8}$  Pa, respectively. We were not able to obtain a satisfactorily clean lithium surface within the XPS. Toward this effort glow discharge, ion sputtering and pumping techniques failed to produce a surface sufficiently devoid of oxygen to consider it a trace surface constituent. Johansson et al (27) have demonstrated that atomically clean lithium can be prepared for XPS analysis using evaporation techniques at pressures below  $2 \times 10^{-10}$  Torr ( $3 \times 10^{-8}$  Pa).

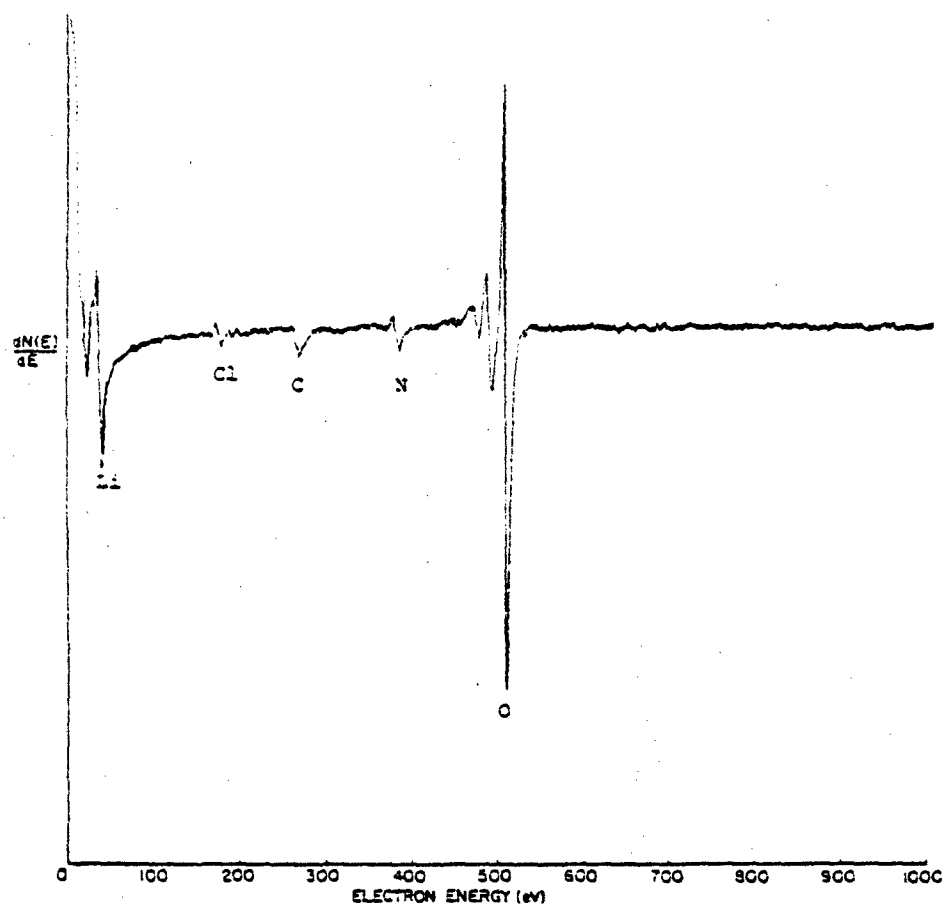


Figure 8. Auger Spectrum of a Lithium Metal Surface As-Cut Under n-Hexane Using the Improved Sample Preparation Technique.

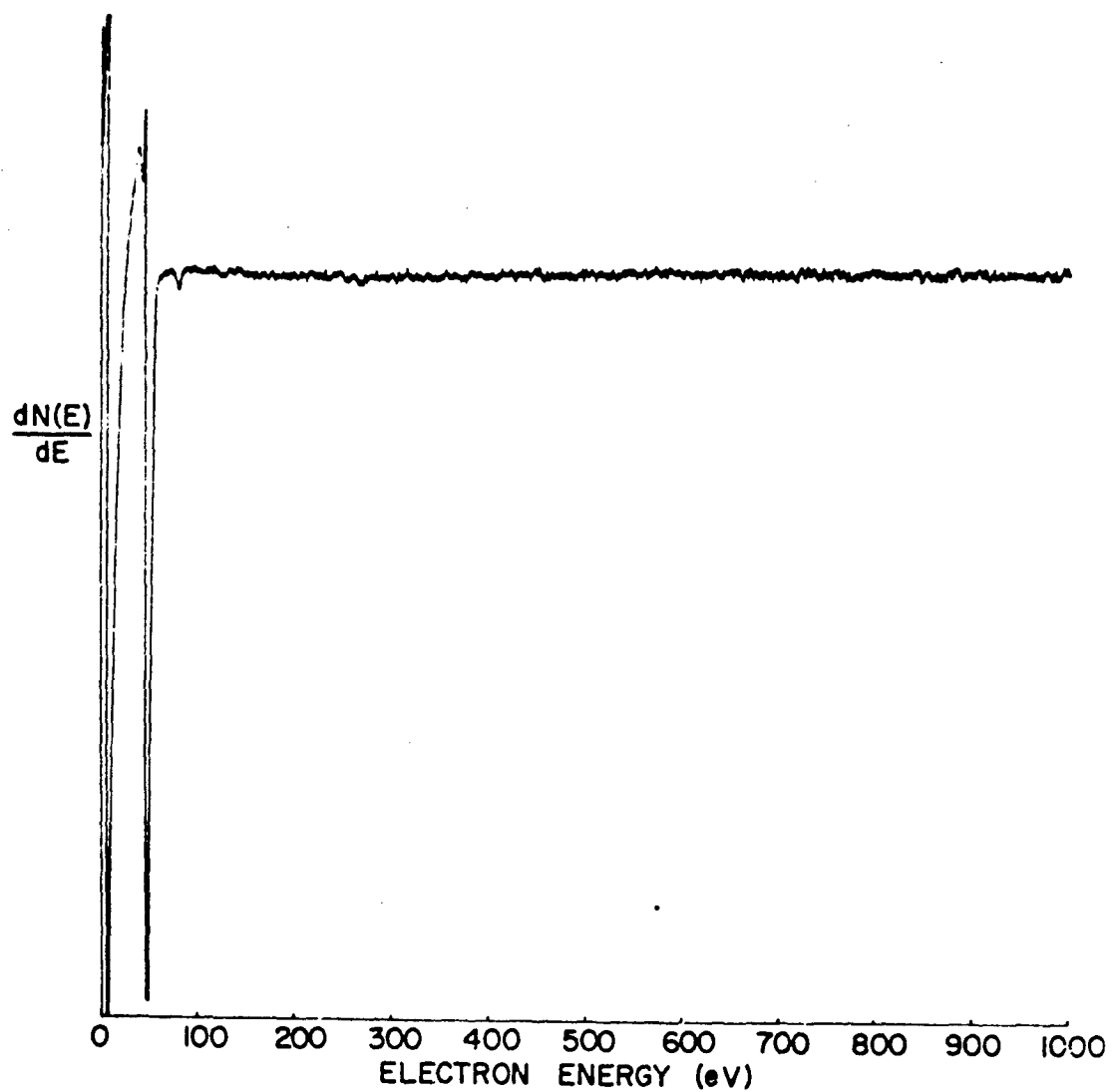


Figure 9. Auger Spectrum of a Clean Lithium Metal Surface Obtained by Repeated Sputtering and Pumping.



For the studies which involved the storage of lithium in solvent or electrolyte, lithium metal was used either as received or scraped with a clean surgical blade within the dry box.

#### SECTION 4

##### THE NON-FARADAIC REACTIVITY OF LITHIUM WITH GASES

In an effort to understand the role, lithium reactivity has in the "voltage delay" phenomenon, experiments were designed in which the specific reactivity of lithium metal with the environment, i.e., gases, solvent and electrolyte, was determined. These results are discussed below.

For the studies with gases, controlled amounts of  $O_2$ ,  $CO$ ,  $CO_2$ , and  $N_2$  were introduced through a leak valve which was an integral part of the AES vacuum system. After selected periods of time at measured pressures, the chamber was evacuated and the sample was rescanned immediately. These results are shown in Figure 10 as a composite of Li KVV spectra referenced to the peak from metallic lithium at 51 eV. The reaction rate of lithium with nitrogen is the lowest for any of the gases utilized. Evidence of reaction at the lithium surface can be inferred from the shift in the 51 eV peak (clean lithium) towards 38 eV ( $CO_2$  reacted lithium surface). The relative response ratios from N, C, and O versus dose are shown in Figure 11. It can be concluded that the passivation of lithium by  $O_2$  and  $CO_2$  is rapid and complete. The passivation of lithium by  $CO$  is not as rapid as for  $O_2$  and  $CO_2$ . The chemical affinity of lithium to the various gases in order of increasing reactivity is:

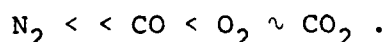


Figure 12 shows a typical overall XPS scan of high purity lithium sample transferred from our dry box. Figure 13 shows the high resolution O 1s XPS scans obtained in our laboratory from freshly cut lithium following insertion into the XPS system (Figure 13a), after some argon ion bombardment (Figure 13b) and after further ion bombardment (Figure 13c). The conversion of the hydroxide to oxide under ion bombardment is apparent. These peak assignments to hydroxide and oxide are in agreement with a previous

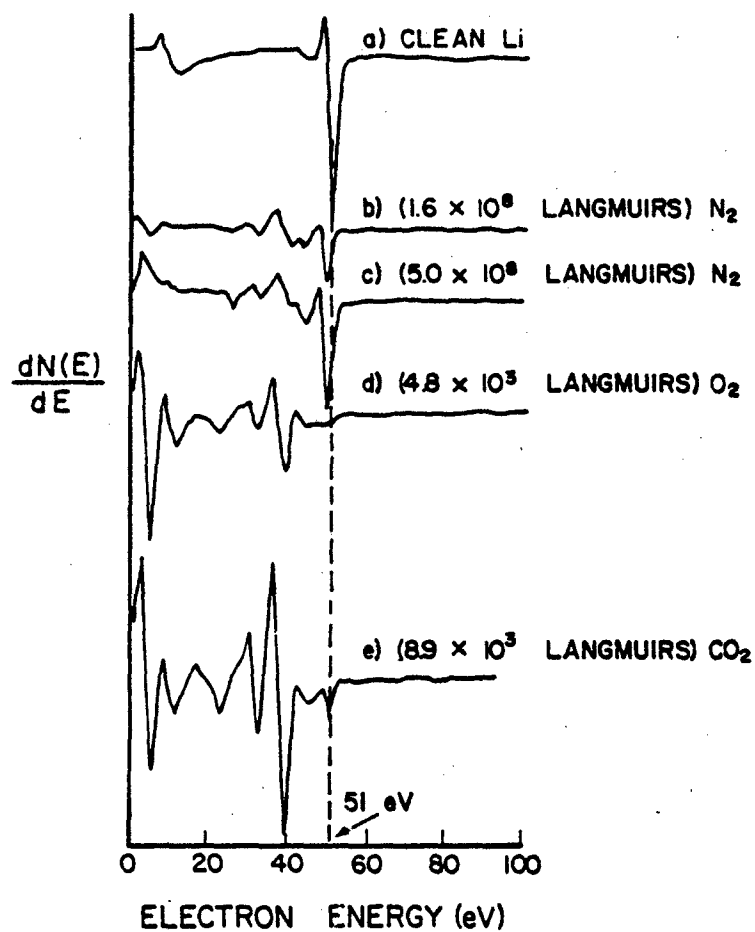


Figure 10. High Resolution Auger Spectra of Lithium.  
 a) clean surface; b) exposed to  $1.6 \times 10^8$  Langmuirs of nitrogen; c) exposed to  $5.0 \times 10^8$  Langmuirs of nitrogen; d) exposed to  $4.8 \times 10^3$  Langmuirs of oxygen; e) exposed to  $8.9 \times 10^3$  Langmuirs of carbon dioxide.

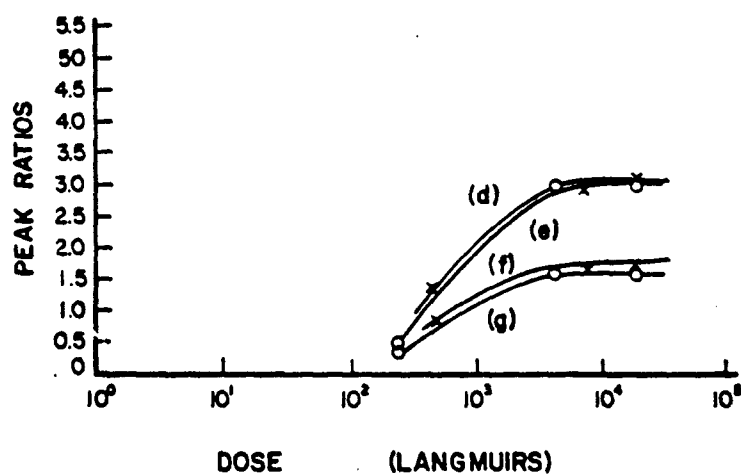
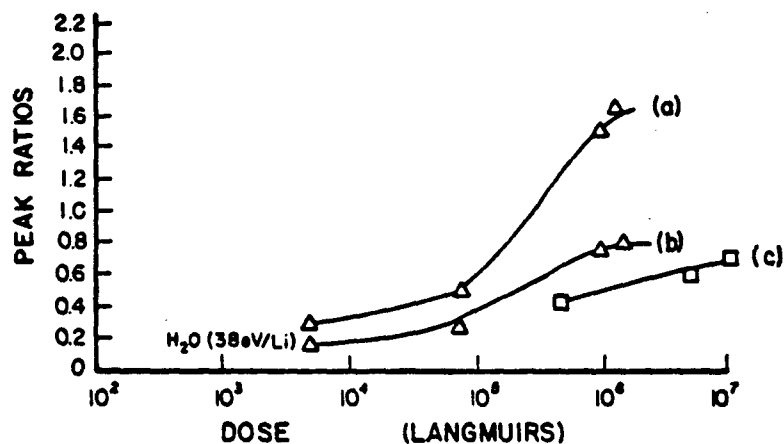


Figure 11. Relative Response Ratios of  $\text{H}_2\text{O}$ ,  $\text{N}_2$ ,  $\text{CO}_2$ , and  $\text{O}_2$  versus Dose. a) O (509 eV)/Li(51 eV) Auger peak ratios for  $\text{H}_2\text{O}$  exposures; b) Li (38 eV)/Li(51 eV) Auger peak ratios for  $\text{H}_2\text{O}$  exposures; c) N (380 eV)/Li(51 eV) Auger peak ratios for  $\text{N}_2$  exposures; d) O (509 eV)/Li(51 eV) Auger peak ratios for  $\text{CO}_2$  exposures; e) O (509 eV)/Li(51 eV) Auger peak ratios for  $\text{O}_2$  exposures; f) Li(38 eV)/Li(51 eV) Auger peak ratios for  $\text{CO}_2$  exposures; g) Li(38 eV)/Li(51 eV) Auger peak ratios for  $\text{O}_2$  exposures.

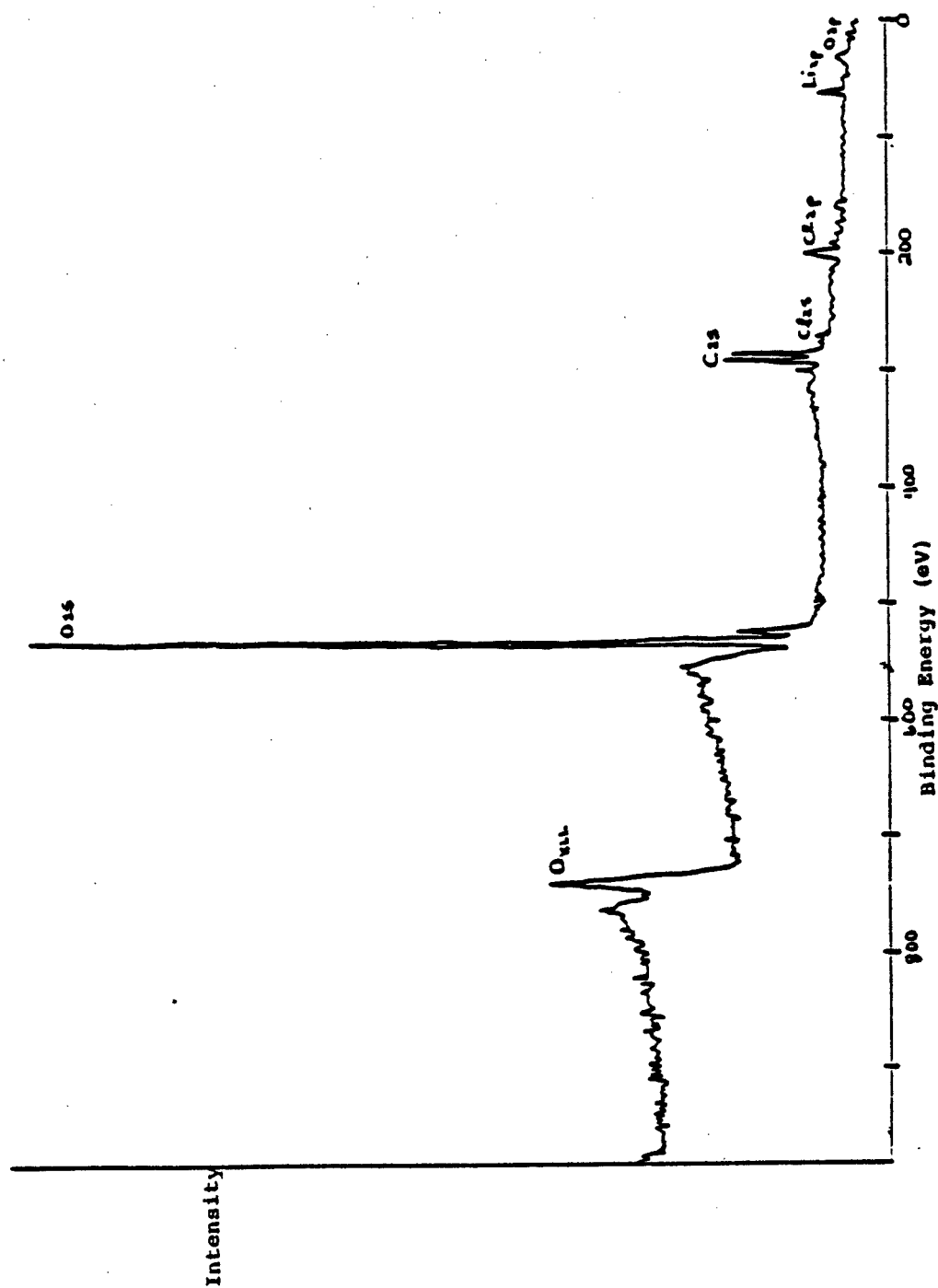


Figure 12. Typical Overall XPS Scan of Foote Mineral Lithium Freshly Cut in Inert Atmosphere.

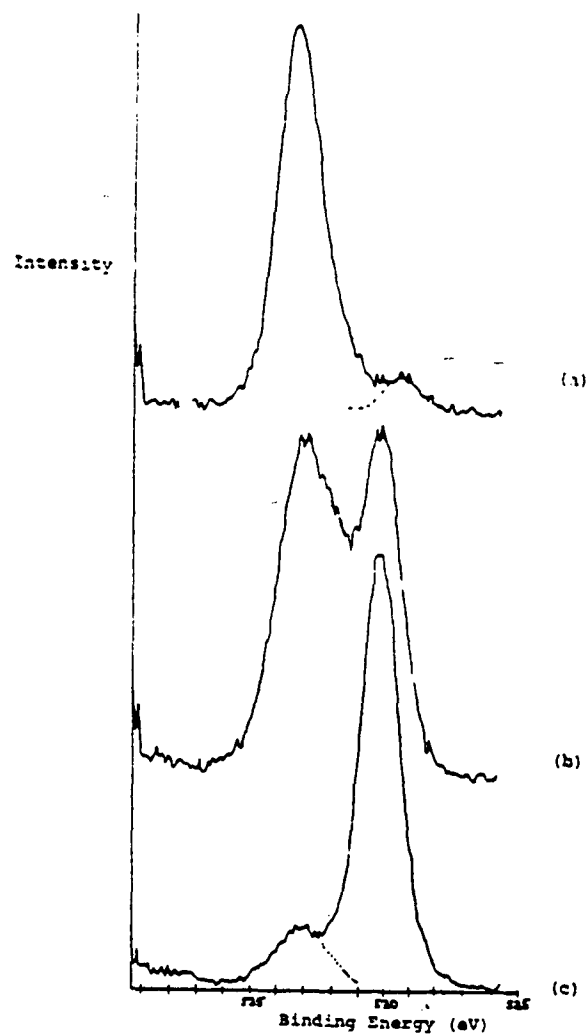


Figure 13. High Resolution O 1s XPS Spectra of: a) Lithium hydroxide; b) approximately equal amount of Lithium hydroxide and Lithium oxide, and c) Lithium oxide.

study done on water chemisorption on magnesium metal (28), and demonstrate the ability to observe the relative concentration differences of lithium oxide and lithium hydroxide on the surface of freshly cut lithium. A high resolution XPS spectrum of the oxygen O 1s peak for lithium exposed to thionyl chloride vapor gave a single oxide peak centered at 530.5 eV.

Lithium metal develops black nodules approximately 3 mm in diameter when exposed to dry nitrogen gas for a period of 12 hours. The AES trace obtained (Figure 14) shows a significant enrichment of nitrogen had taken place and that the black spotted area is a lithium nitride or oxynitride (28) type material. This conclusion is drawn because shortly (~6 minutes) after commencing to profile the "black spot" the relative intensities of the oxygen and nitrogen peaks become constant and of significant value. The circular symmetry and hemispherical shape of the spots from the surface inward indicate the presence of an active surface nucleation site. The nature of this site has not been established.

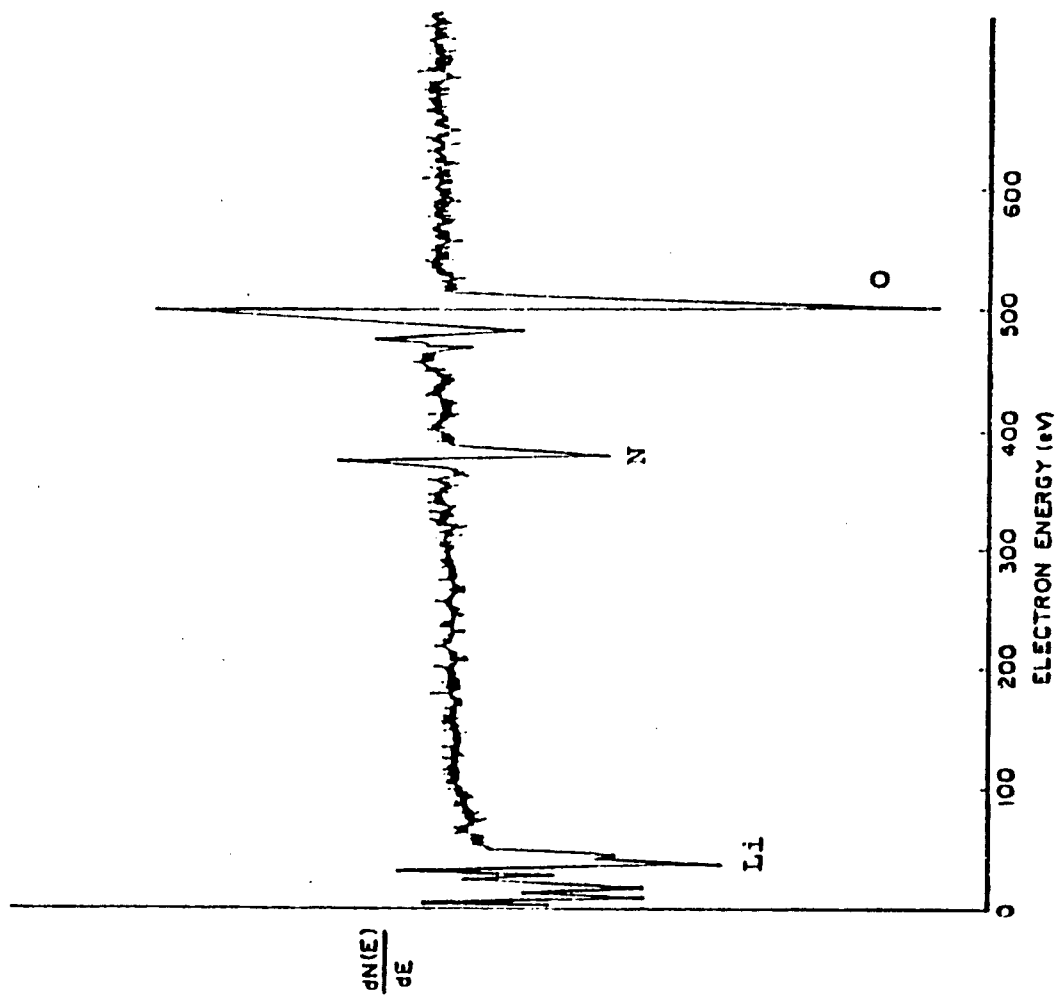


Figure 14. Auger Spectrum of Black Spot on a Lithium Surface  
After an Overnight Exposure to Nitrogen.

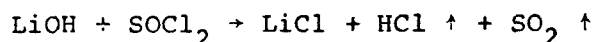


## SECTION 5

### NON-FARADAIC REACTIVITY OF LITHIUM

The reactivity of lithium metal to thionyl chloride was determined in a series of experiments in which the length of exposure and temperature were varied. The length of exposure varied from 90 minutes to 20 days while the effect of temperature upon the film properties was studied over the range of 2°C to 70°C. We anticipated that we would correlate the ion sputter time required to profile through the resulting film with the length of exposure and the temperature during exposure. Unfortunately, none but the thinnest films could be profiled in reasonable periods of time. The AES spectra of "as received" GTE lithium anode surface treated for 11 hours at room temperature with  $\text{SOCl}_2$  liquid (Figure 15a) and  $\text{SOCl}_2$  vapor (Figure 15b) is typical of these spectra. The major reaction product is lithium chloride; however, trace quantities of carbon, oxygen, and sulfur are also present in both. These surfaces are nearly identical and, on the basis of their profile times (400 seconds each), both contain films of equal thickness.

For lithium exposed to liquid thionyl chloride at room temperature the effect of an increase in exposure time is to cause a reduction in the sulfur (150 eV) and oxygen (503 eV) peak intensities (29). It is tempting to conclude that with time of exposure to  $\text{SOCl}_2$  the surface is cleansed of contaminant elements such as sulfur, carbon, and oxygen leaving lithium chloride as the major surface compound. If lithium hydroxide did form in an initial surface reaction between lithium and water in  $\text{SOCl}_2$ , it could subsequently react with  $\text{SOCl}_2$  to produce a passivating lithium chloride layer via the reaction



It is interesting to note that the high resolution XPS spectra of the O 1s peak for lithium discharged in a battery configuration contains but a single oxygen (oxide) peak centered at 533 eV. The

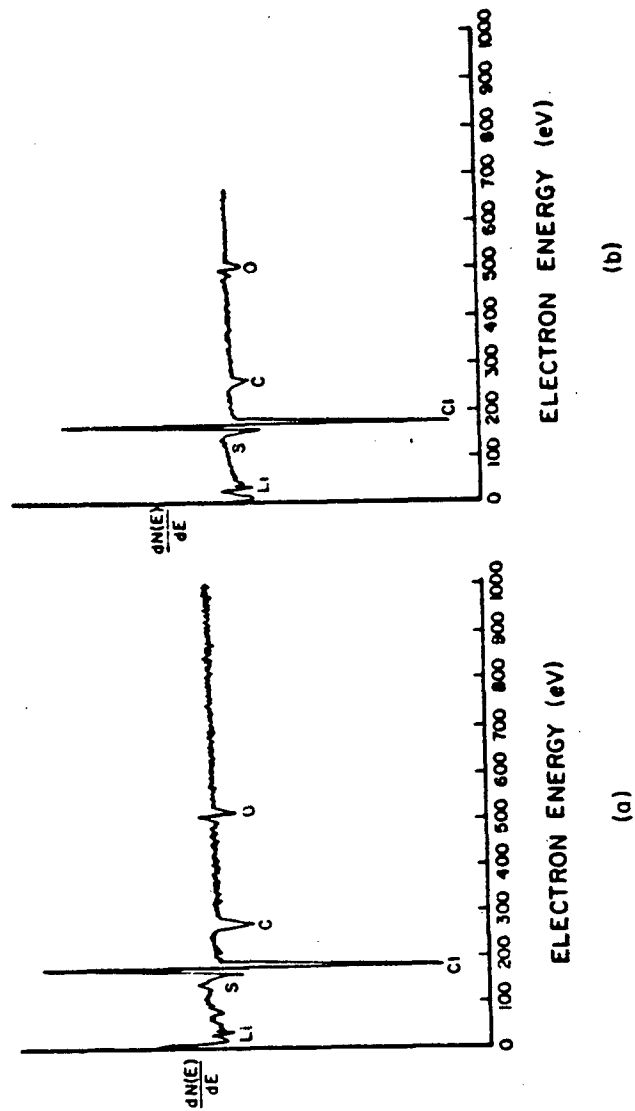


Figure 15. Overall AES Spectra of a Typical GTE Lithium Anode Surface "as received" which was Exposed to: a)  $\text{SOCl}_2$  liquid, 11 days, and b)  $\text{SOCl}_2$  vapor, 11 days.

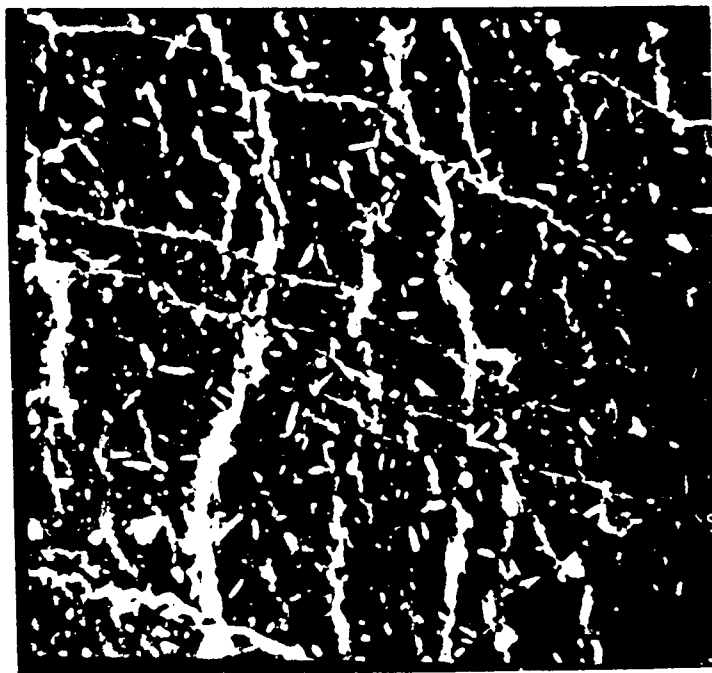
apparent reduction in the sulfur and oxygen peaks with increase in exposure time might be explained by growth of the lithium chloride crystals on the lithium surface. The thickness of the passive lithium chloride film on lithium was found to increase from increased length of exposure, or temperature or both.

SEM photomicrographs for lithium stored in thionyl chloride show little evidence for formation of aggregate lithium chloride crystals upon the surface. Some crystallizing is observed at elevated temperatures after a period of several days. Figure 16 is particularly interesting because in this case the lithium chloride crystals are not cubic as expected but rather prismatic. The SEM/EDAX trace (Figure 16d) supports both the XPS and AES results in that it also finds a minor quantity of sulfur present.

The surfaces of these samples were studied using the SEM where photomicrographs and EDAX traces were obtained. The lithium metal surface has been scraped prior to commencing the aging study and scraping is responsible for gross surface irregularities seen on the lithium surface. Aged samples were first removed and washed with pure thionyl chloride. The samples were then dried by pumping on them for a two-hour period to remove the majority of the physically adsorbed thionyl chloride. Samples were transferred to the SEM under an argon atmosphere. SEM photomicrographs at 100x, 300x, 1000x and an EDAX trace were obtained for each sample. The EDAX traces are similar for each sample within the series and indicate a major chloride peak ( $K_{\alpha}$  2.62,  $K_{\beta}$  2.81 keV) and minor concentrations of aluminum ( $K_{\alpha}$  1.49 keV) and sulfur ( $K_{\alpha}$  2.31 keV). Large concentrations of aluminum and sulfur are found in the unwashed samples. The EDAX results are consistent with AES and XPS results for these samples.

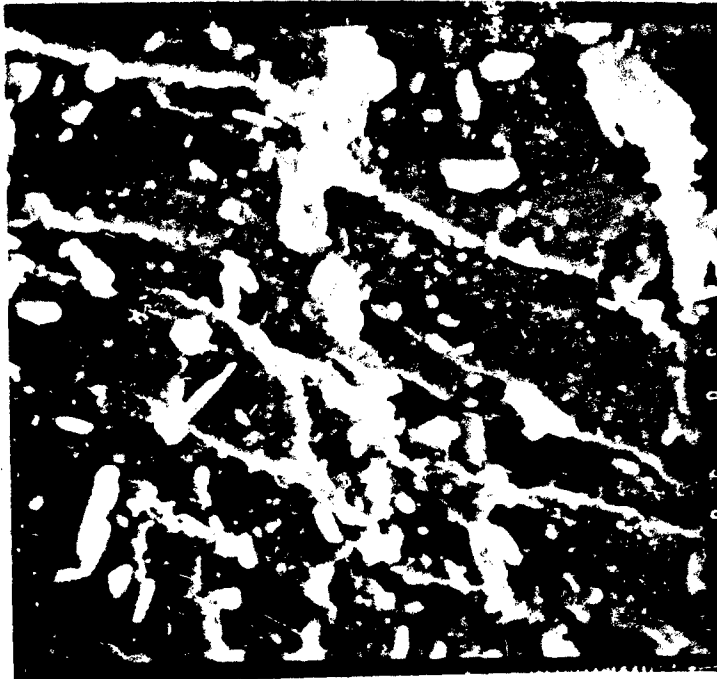


(a) 100X

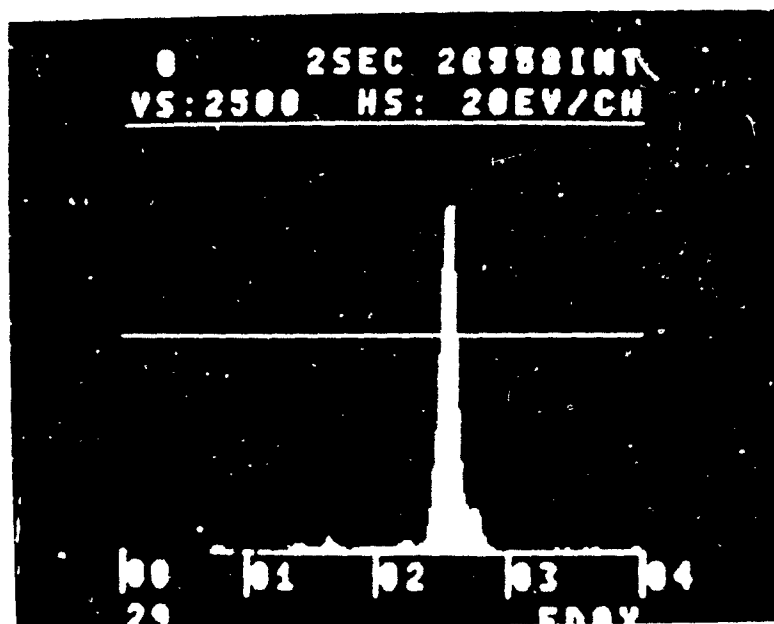


(b) 300X

Figure 16. SEM Photomicrographs for Lithium Aged in Thionyl Chloride, 55°C, Four Days.



(c) 1000X



(d) EDAX Trace

Figure 16. Concluded.

## SECTION 6

### THE NON-FARADAIC REACTIVITY OF LITHIUM WITH ELECTROLYTE

During the course of these studies the only electrolyte used was 1.8 M  $\text{LiAlCl}_4$  in thionyl chloride. This was supplied in sealed glass bottles by GTE-Sylvania. The most significant difference in the reactivity of lithium in thionyl chloride and electrolyte is the rate at which the passive lithium chloride film forms (Figure 17). Here, the ion sputter time required to reach a 10 percent chlorine signal versus exposure temperature is presented for a four day exposure of lithium in thionyl chloride and in electrolyte at different temperatures. The enhanced rate of film formation in electrolyte suggests the tetrachloroaluminate ion may be actively involved in a chloride exchange reaction.

In contrast to lithium anodes aged in thionyl chloride, the lithium anodes stored in electrolyte showed essentially complete coverage of the surface by crystalline material at temperatures above 20°C: Figure 18 (25°C), Figure 19 (55°C) and Figure 20 (70°C). The EDAX traces show trace quantities of sulfur are also present on the surface. The existence of macroscopic cracking of these films stored in electrolyte is noteworthy because the presence of such a film defect could minimize the "voltage delay" for an anode system.

The photomicrographs show clearly that crystal growth is enhanced along ridges or grain boundaries which represent high energy positions upon the surface (Figure 21). The surface morphology cannot be elucidated from these results because the particles seen here are crystal clusters (Figure 22) rather than a single crystal of lithium chloride. These aggregate clusters are seen to grow in "street lamp"-like fashion along high energy regions of the lithium surfaces. In the unwashed sample some "mudcracking" is found and the region is found to contain substantially larger quantities of aluminum (Figure 23).

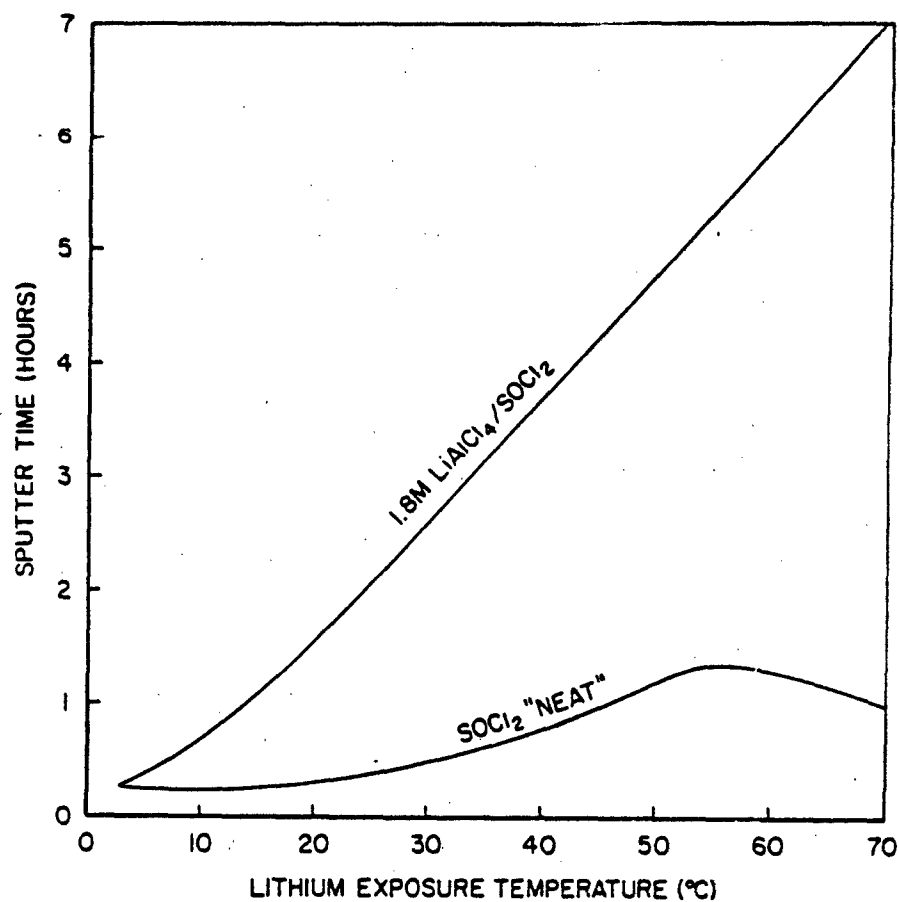


Figure 17. Sputtering Time Required to Read 10 Percent Signal versus Lithium Exposure Temperature for a Four-Day Exposure to "neat" Thionyl Chloride and 1.8 M Lithium Tetrachloroaluminate in Thionyl Chloride.



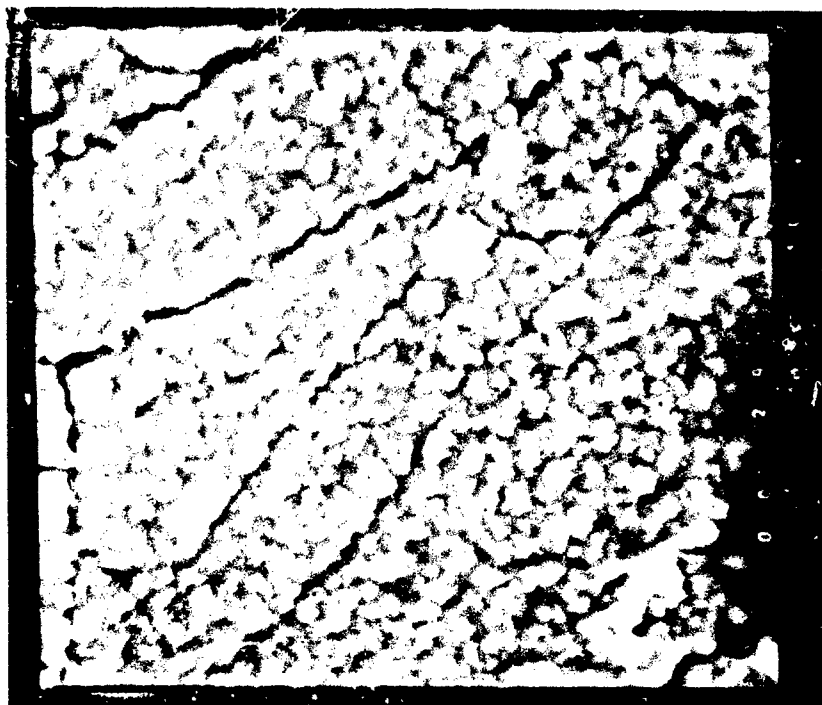
(a) 100X



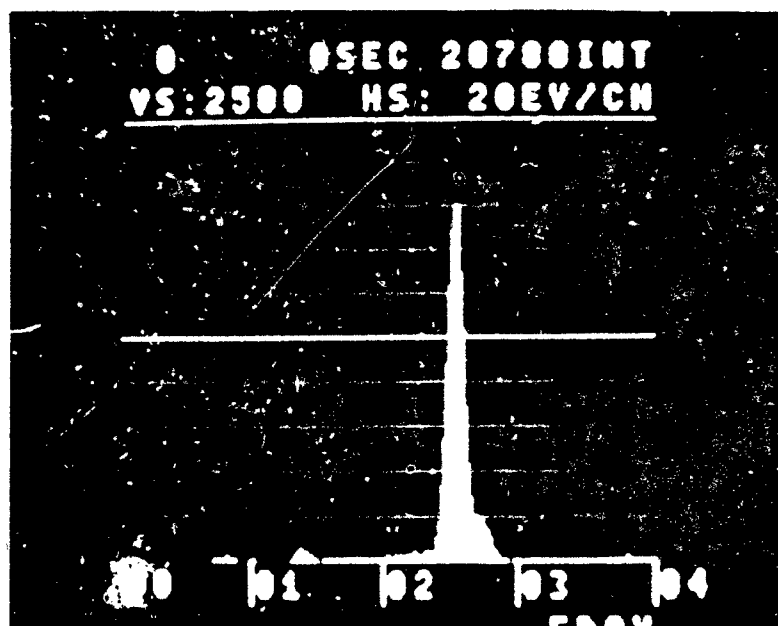
(b) 300X

Figure 18. SEM Photomicrographs for Lithium Aged in Electrolyte, 25°C, Four Days.





(c) 1000X

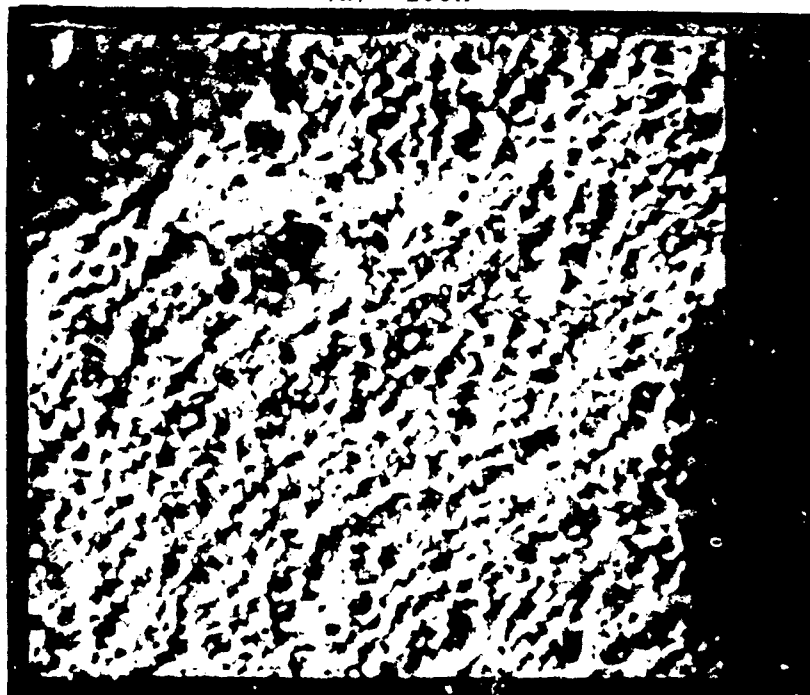


(d) EDAX Trace

Figure 18. Concluded.

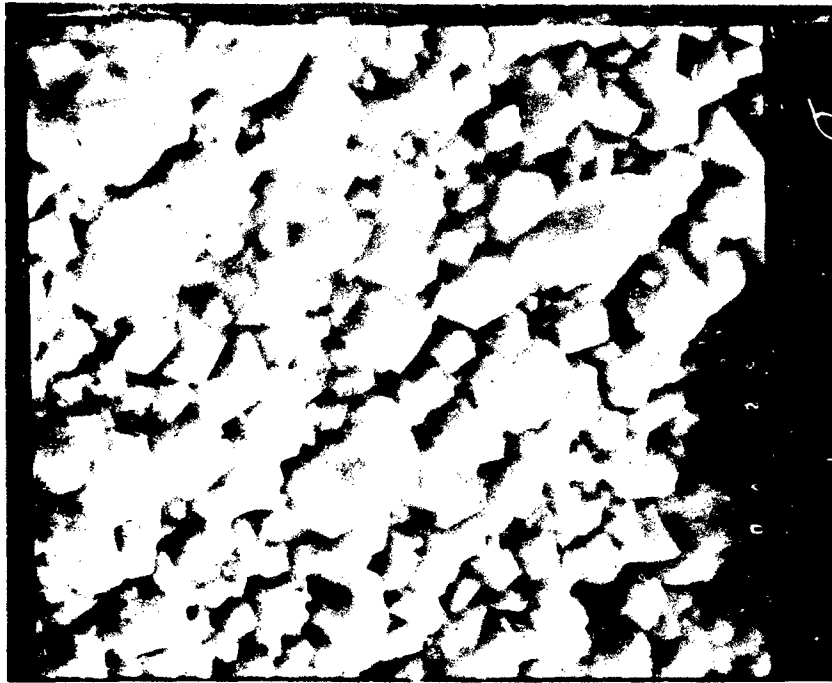


(a) 100X



(b) 300X

Figure 19. SEM Photomicrographs for Lithium Aged in Electrolyte, 55°C, Four Days.

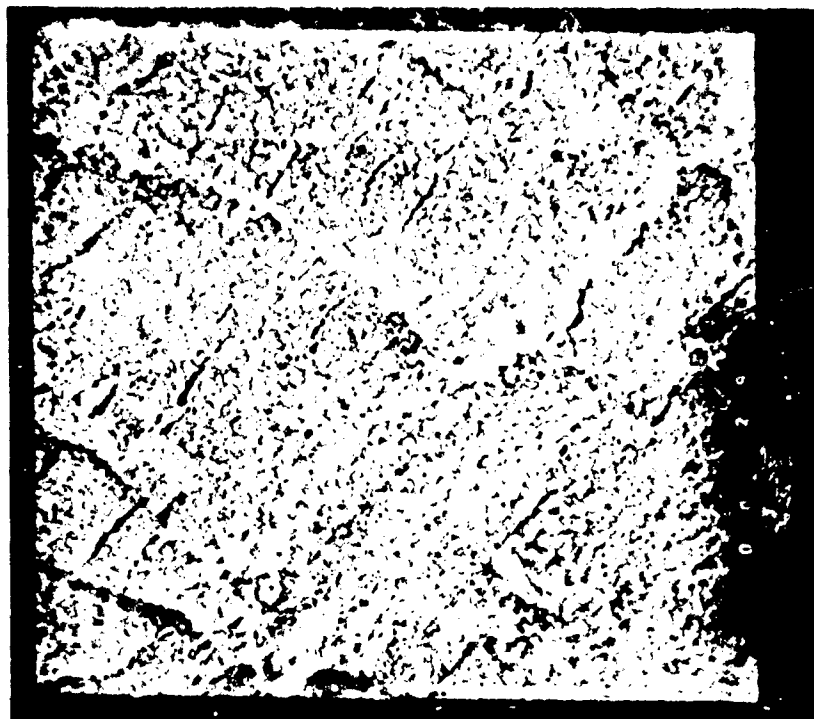


(a) 1000X

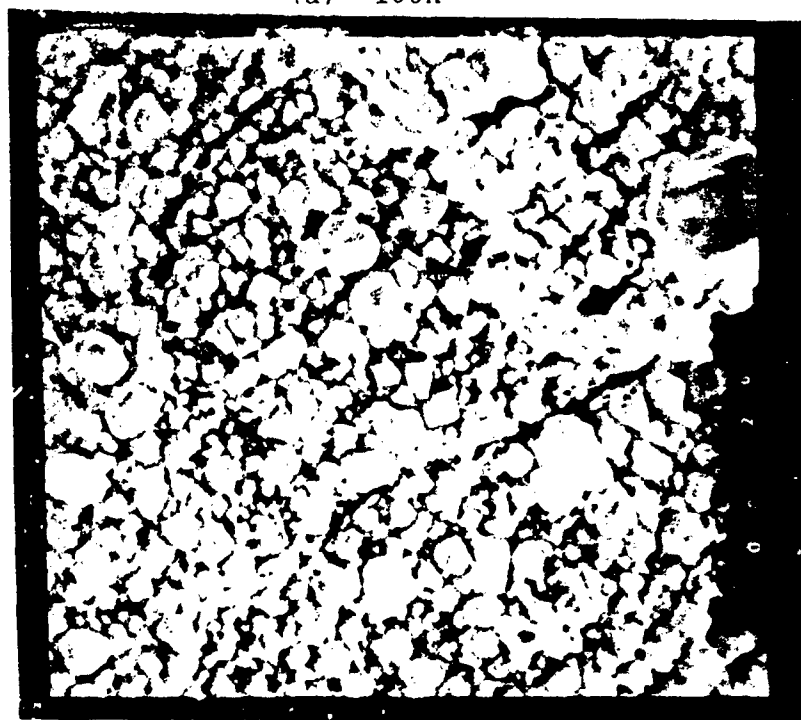


(d) EDAX Trace

Figure 19. Concluded.

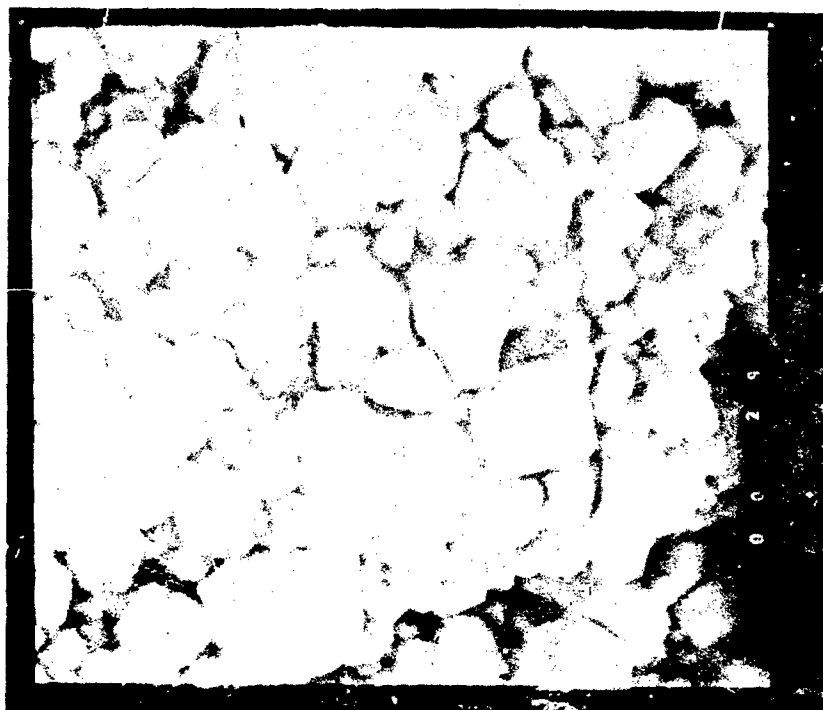


(a) 100X

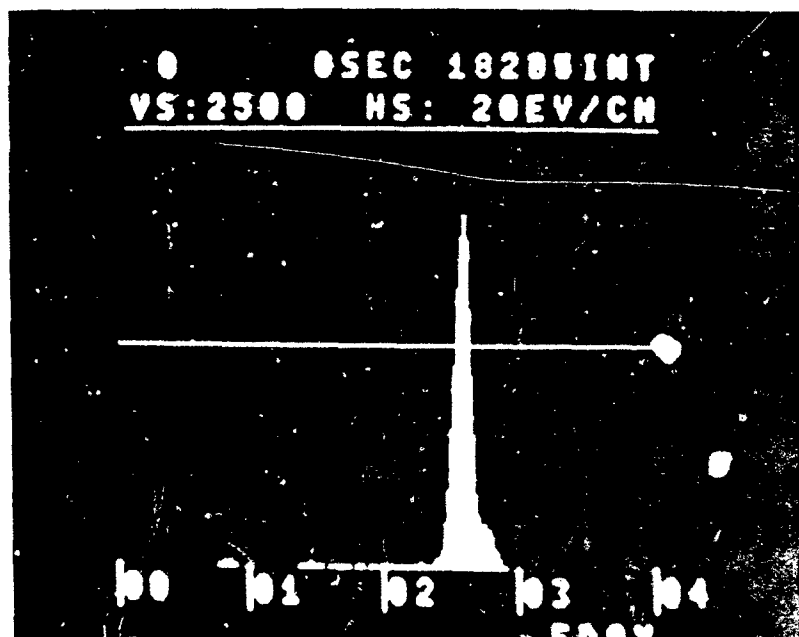


(b) 300X

Figure 20. SEM Photomicrographs for Lithium Aged in Electrolyte, 70°C, Four Days.

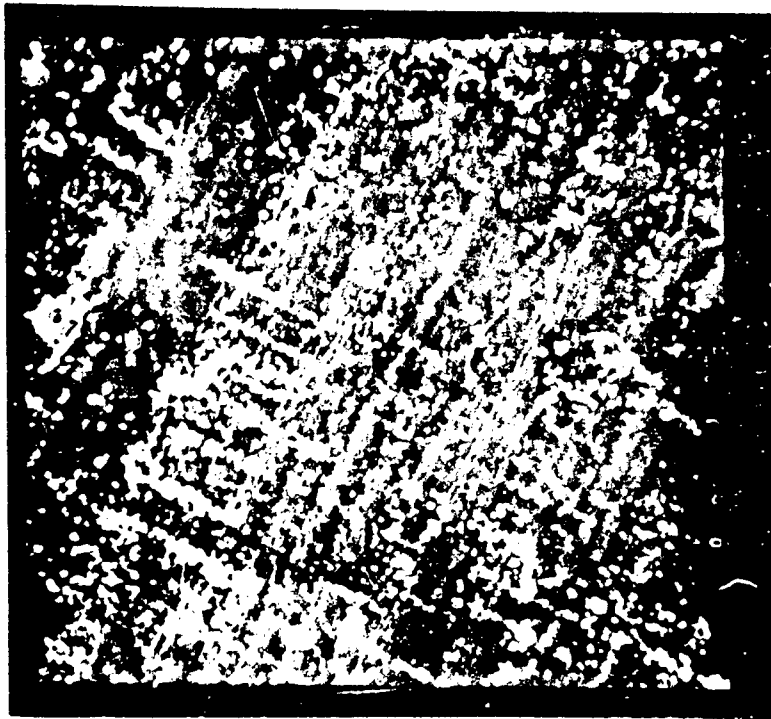


(c) 1000X

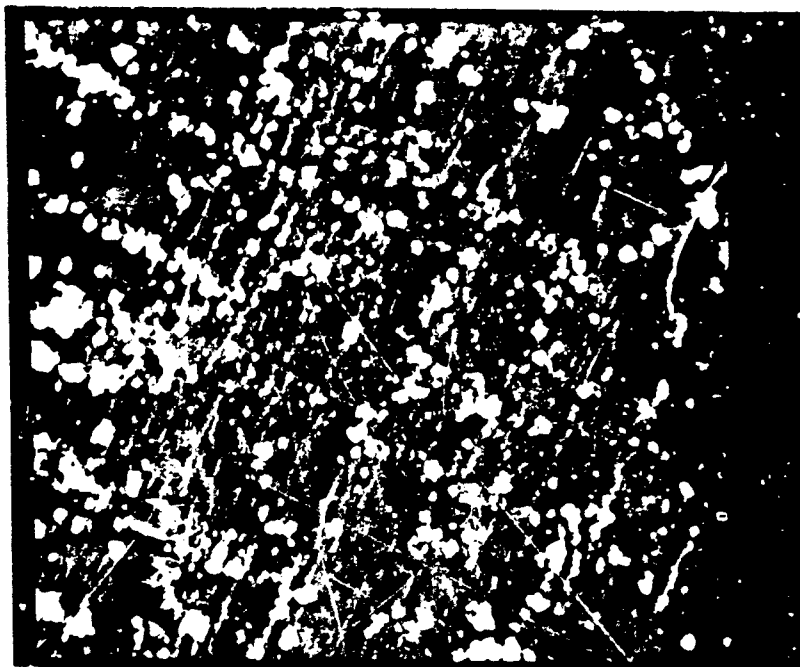


(d) EDAX Trace

Figure 20. Concluded.



(a) 100X



(b) 300X

Figure 21. SEM Photomicrographs for Lithium Samples Soaked in Electrolyte for 90 Minutes and Receiving Two Thionyl Chloride Washings.

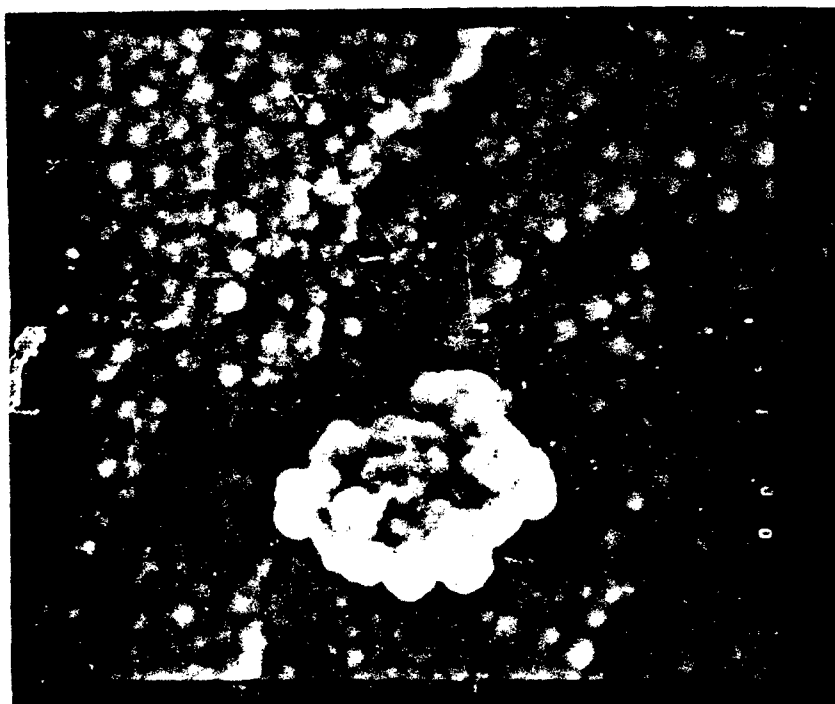
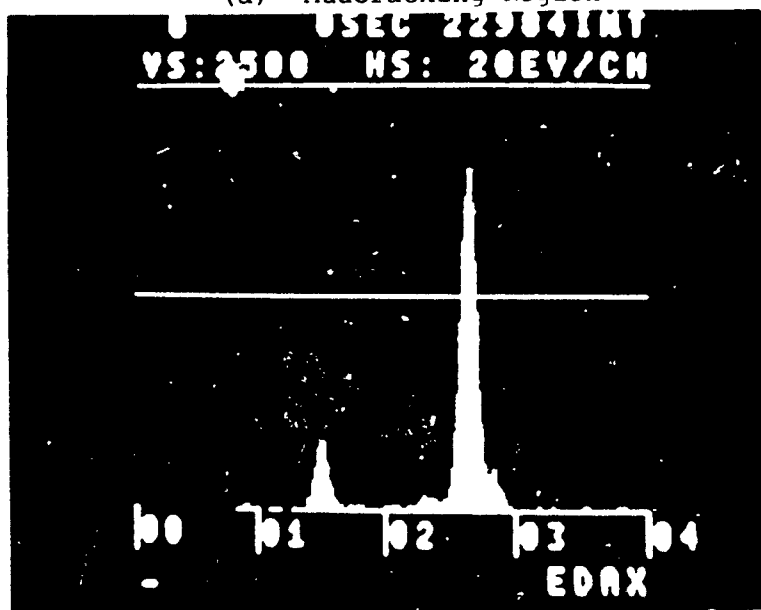


Figure 22. SEM (3000X) Photomicrographs of Aggregate Crystal Formed During a 90 Minute Electrolyte Soak.



(a) Mudcracking Region



(b) EDAX Trace

Figure 23. SEM (1000X) Photomicrograph and EDAX Trace of "mudcracked" Region for a Lithium Sample Soaked in Electrolyte 90 Minutes and Receiving No Thionyl Chloride Wash.



The presence or absence of aluminum is readily detected in these samples using AES. Figures 24 and 25 show clearly the effective removal of aluminum as a result of a single thionyl chloride wash upon a lithium anode stored in electrolyte for a short time.

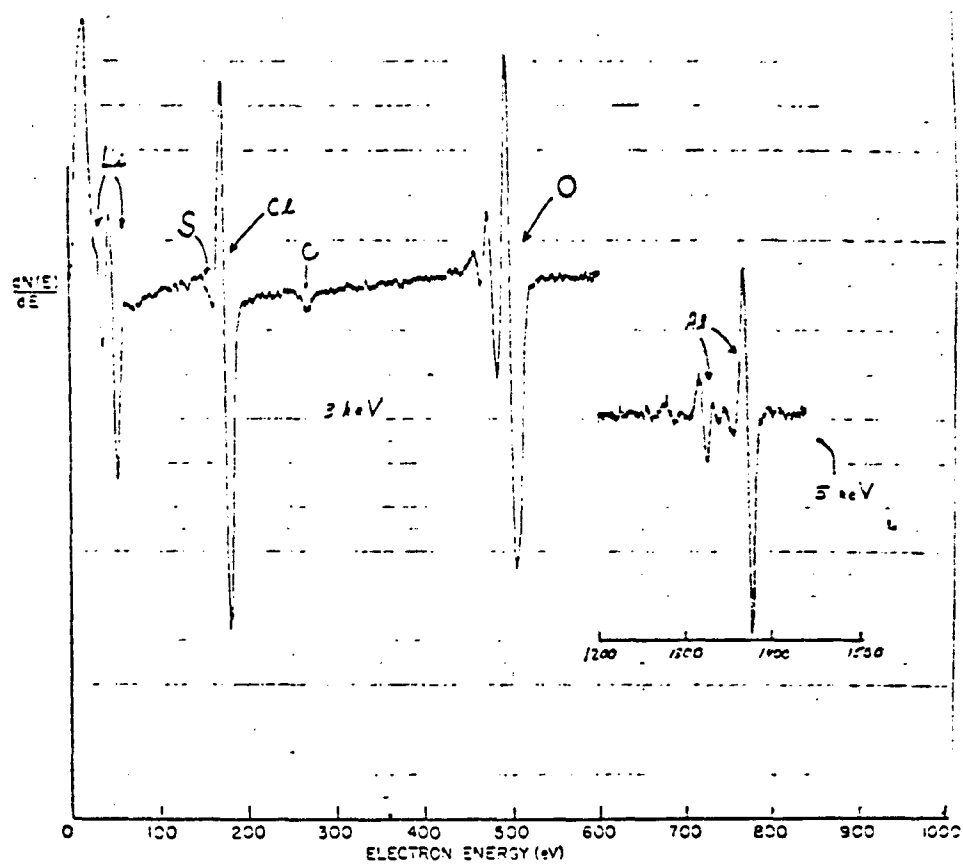


Figure 24. AES Spectrum of Lithium Exposed for 90 Minutes to  $\text{LiAlCl}_4/\text{SOCl}_2$ , No Wash.

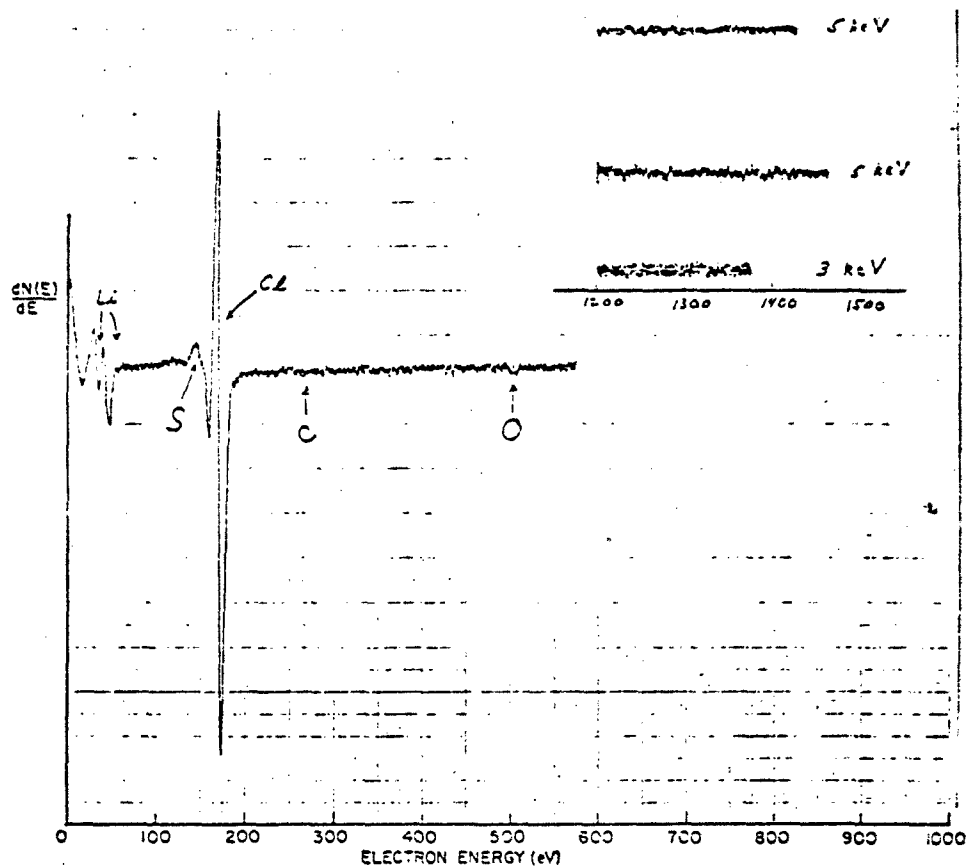
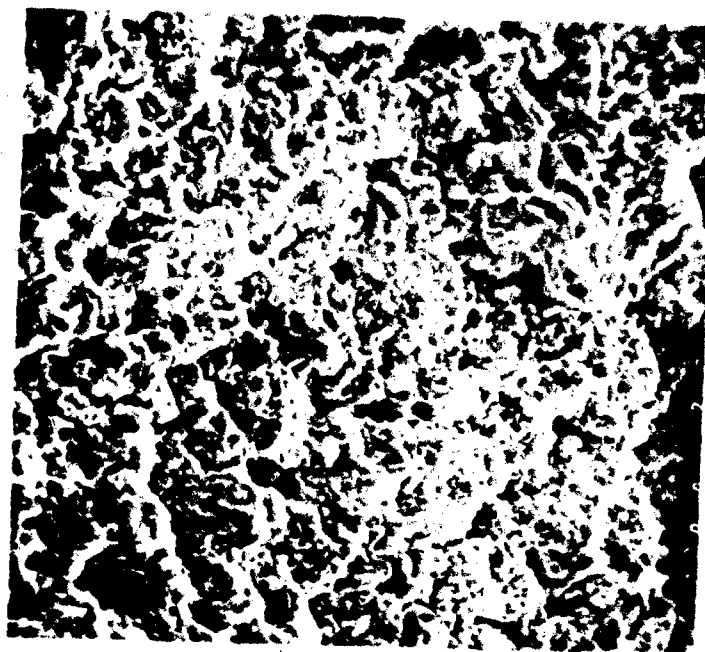


Figure 25. AES Spectrum of Lithium Exposed for 90 Minutes to  $\text{LiAlCl}_4/\text{SOCl}_2$ , One Wash.

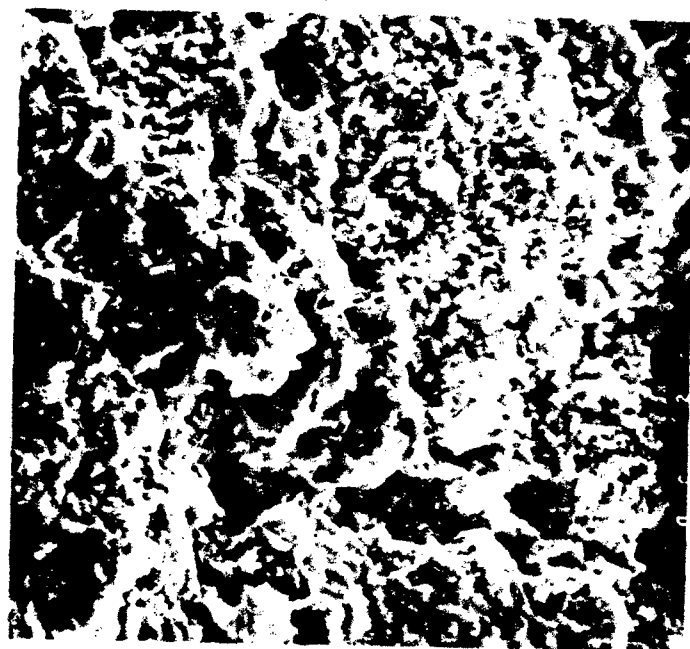
## SECTION 7

### THE FARADAIC REACTIVITY OF LITHIUM IN ELECTROLYTE

The passage of an anodic current across the lithium metal electrolyte interface produces a surface which appears "sponge-like", porous, and tortuous. Figures 26 and 27 represent SEM photomicrographs and EDAX traces for lithium discharged 10 percent of capacity at one milliamp per  $\text{cm}^2$  and at room temperature, unwashed and one wash respectively. There is no apparent difference in surface morphology and the EDAX traces indicate a quantity of aluminum and sulfur is present (2-5 percent), even after a wash with thionyl chloride. The aluminum and sulfur are occluded during discharge and can be seen throughout the AES profile. The AES spectra of anodes receiving only a slight discharge (0.5 percent of capacity) at one milliamp per  $\text{cm}^2$ , using a separator material which could easily be removed are shown in Figures 28, 29, 30, 31, and 32. The anodes received from zero to four washings with "neat" thionyl chloride, respectively. Inspection of the AES traces for slight or moderate (30,31) discharge depths reveals no significant differences. A significant difference exists between lithium metal which has been discharged and lithium metal which has received only an electrolyte soak (Figure 25). The difference is that in discharged samples, aluminum and oxygen peaks are detected even after four washings with "neat" thionyl chloride. Figure 33 shows the oxygen (503 eV) and aluminum (1378 eV) AES peak intensities for samples receiving a number of washings with thionyl chloride. After washing with thionyl chloride, the samples were evacuated to  $10^{-3}$  Torr for two hours to remove surface thionyl chloride. Considering the residual peak intensities for oxygen and aluminum in the AES spectrum after four washings and the ionization cross section for oxygen and aluminum for the Auger process, one can compute the approximate atomic ratio of oxygen to aluminum within the film to be unity.

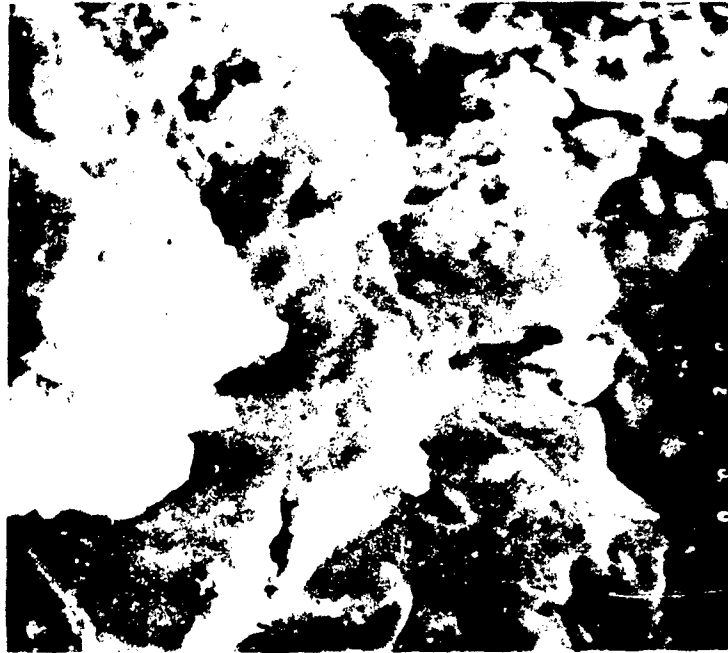


(a) 100X

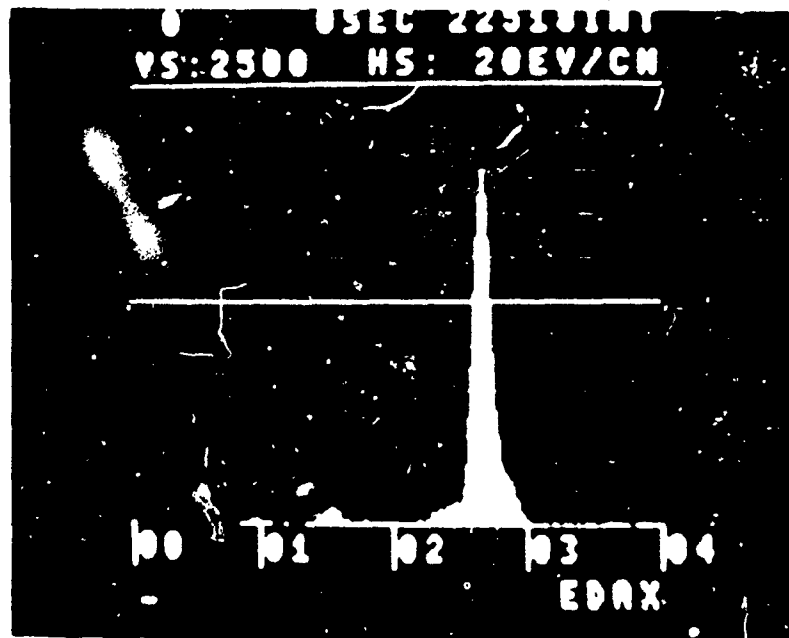


(b) 300X

Figure 26. SEM Photomicrographs for Lithium Discharged Ten Percent at One  $\text{mA}/\text{cm}^2$ , Room Temperature, Unwashed.

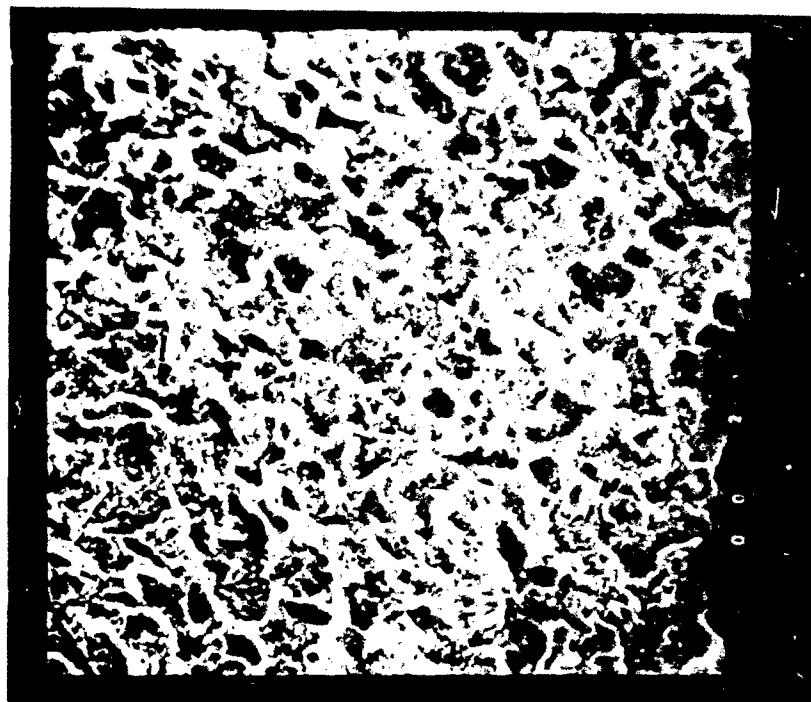


(c) 1000X

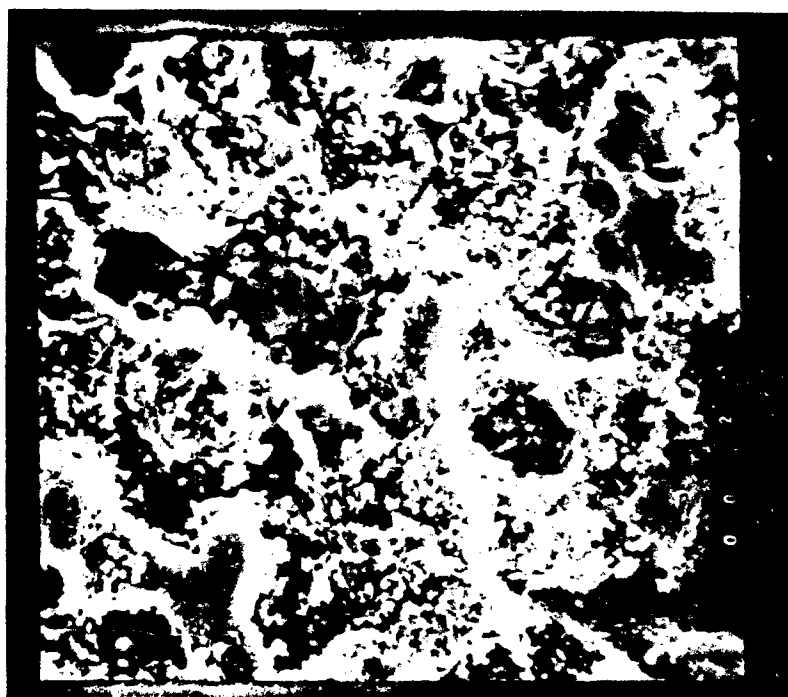


(d) EDAX Trace

Figure 26. Concluded.

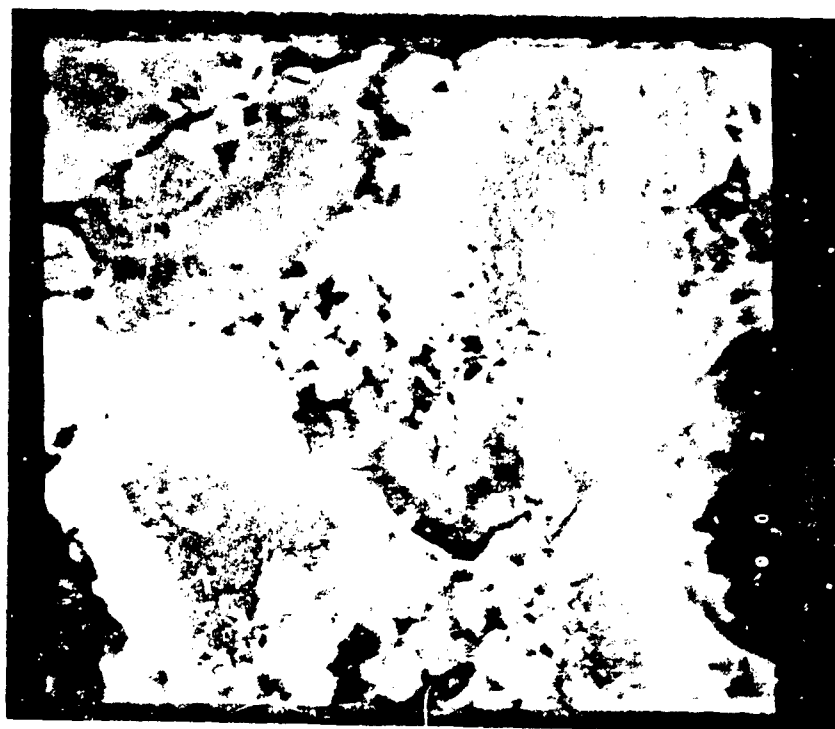


(a) 100X

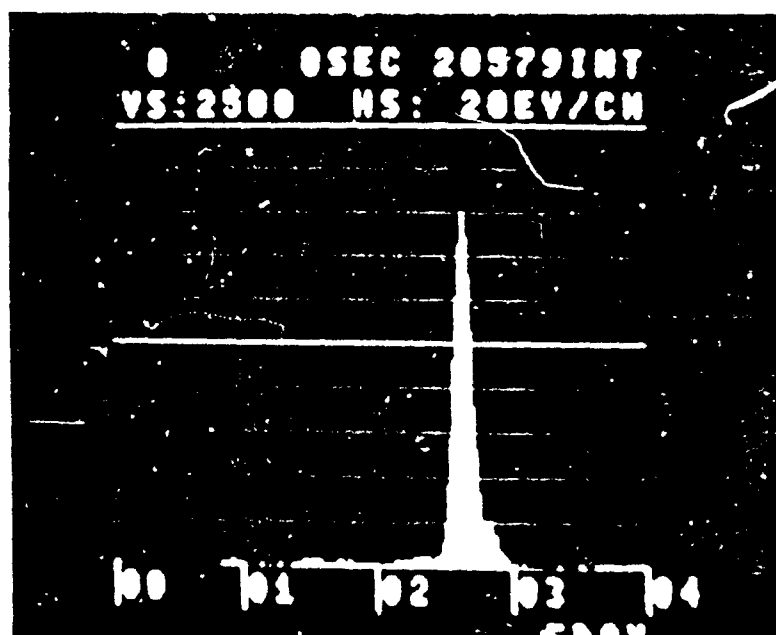


(b) 300X

Figure 27. SEM Photomicrographs for Lithium Discharged Ten Percent at One  $\text{mA}/\text{cm}^2$ , Room Temperature, One Washing.



(c) 1000X



(d) EDAX Trace

Figure 27. Concluded.



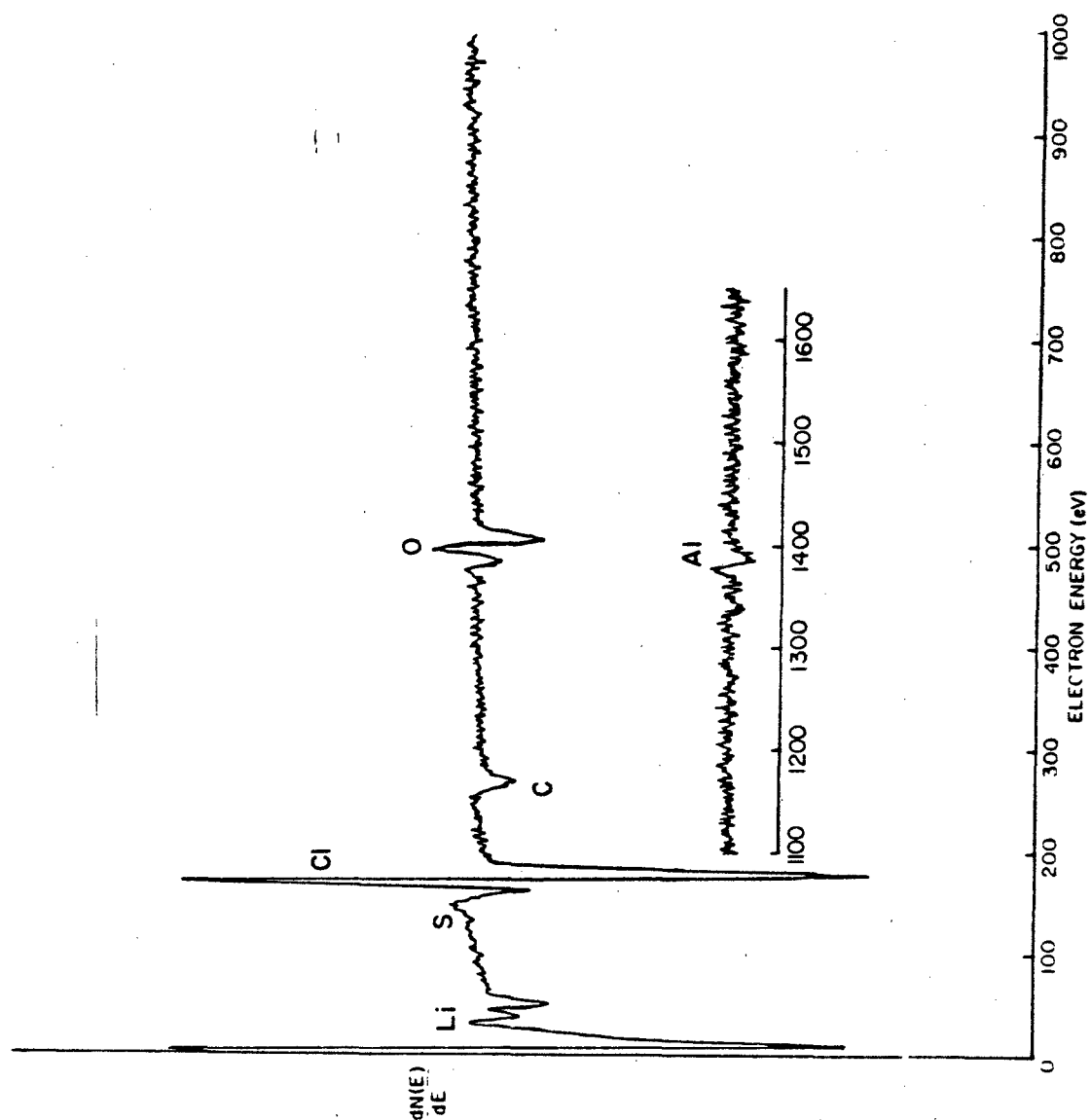


Figure 28. AES Spectrum of Lithium Discharged One-Half Percent in Electrolyte at One  $\text{mA}/\text{cm}^2$ , Room Temperature, No Thionyl Chloride Wash.

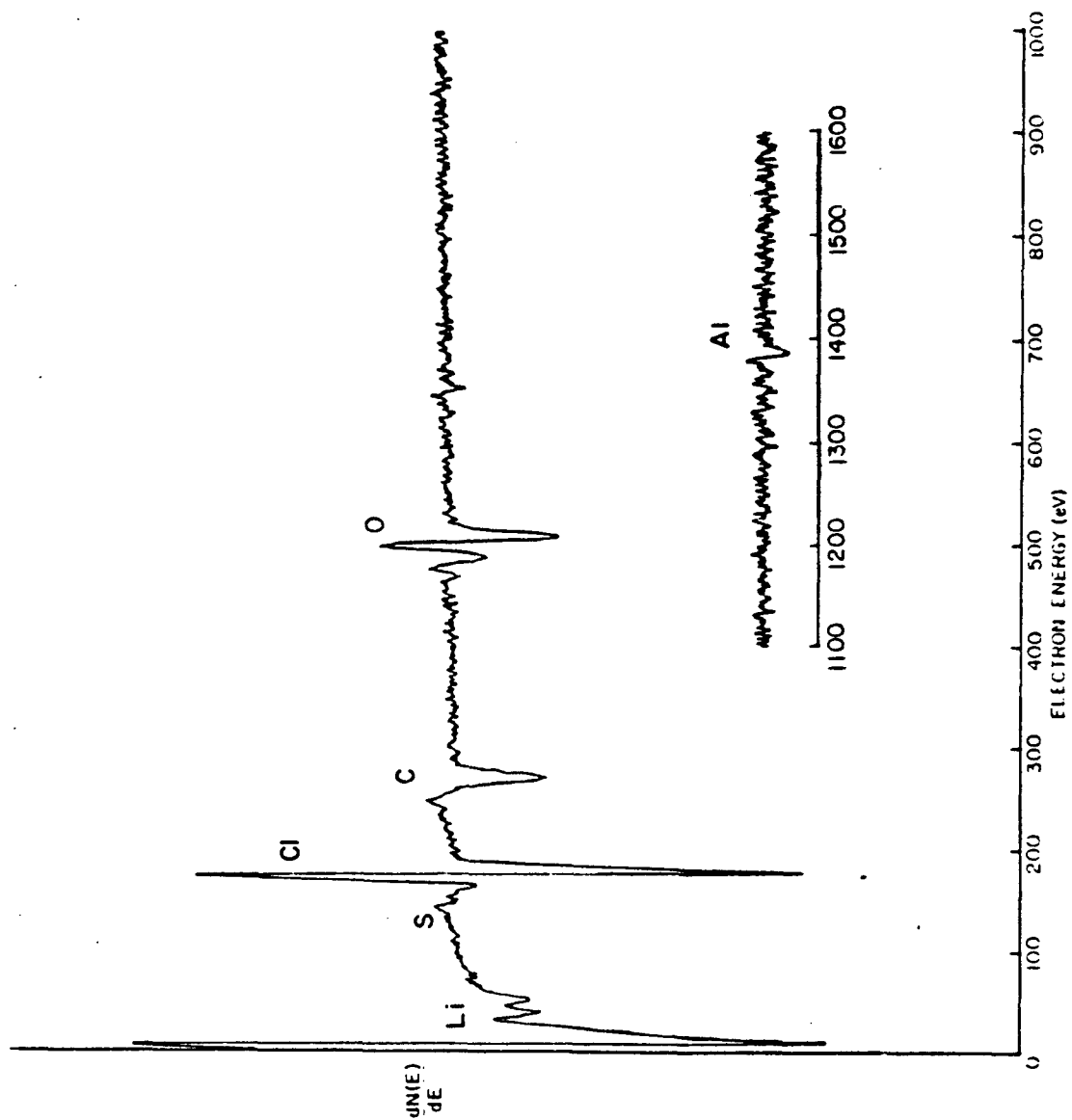


Figure 29. AES Spectrum of Lithium Discharged One-Half Percent in Electrolyte at One  $\text{mA}/\text{cm}^2$ , Room Temperature, One Thionyl Chloride Washing.

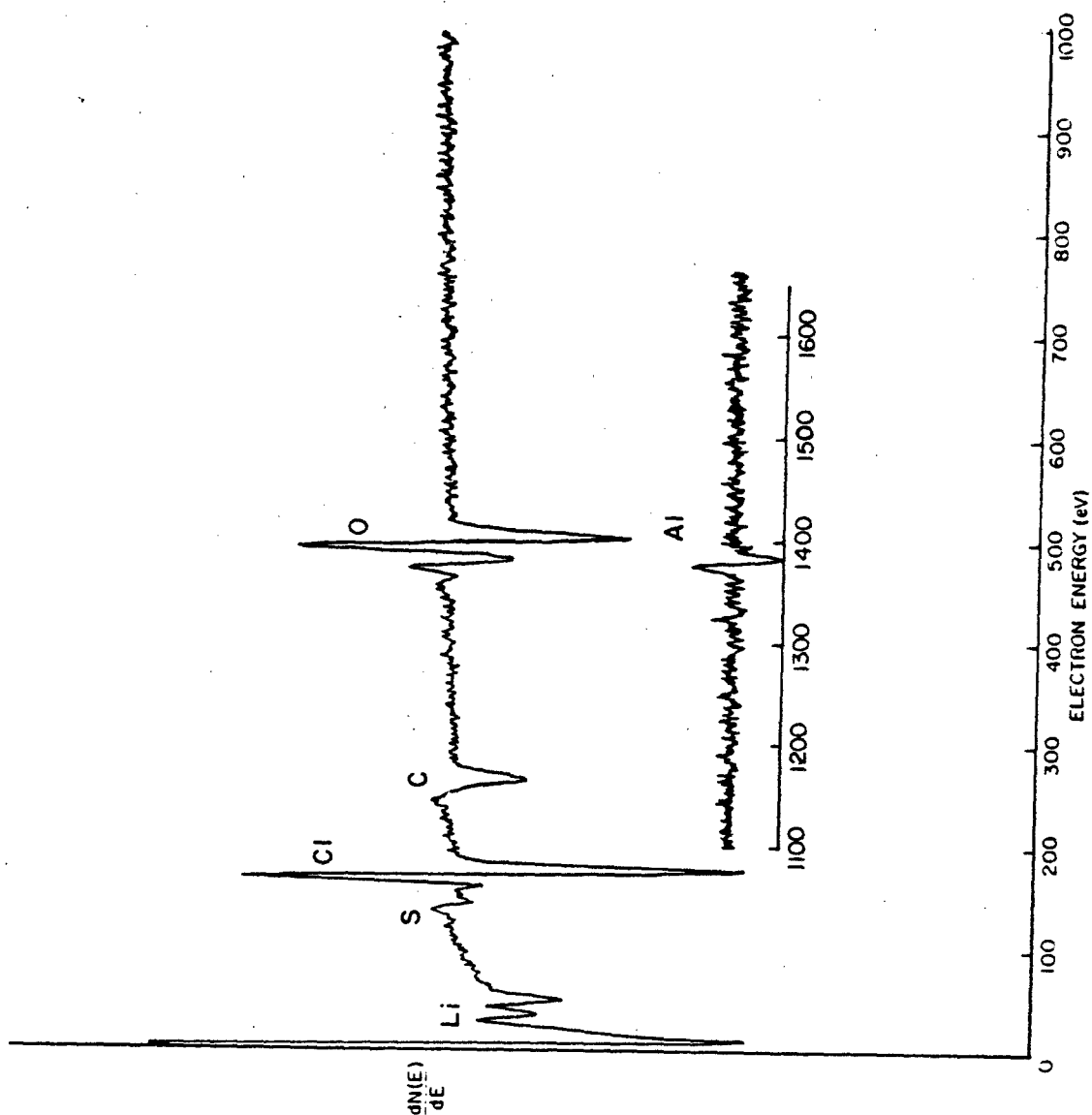


Figure 30. AES Spectrum of Lithium Discharged One-Half Percent in Electrolyte at One  $\text{mA}/\text{cm}^2$ , Room Temperature, Two Thionyl Chloride Washings.

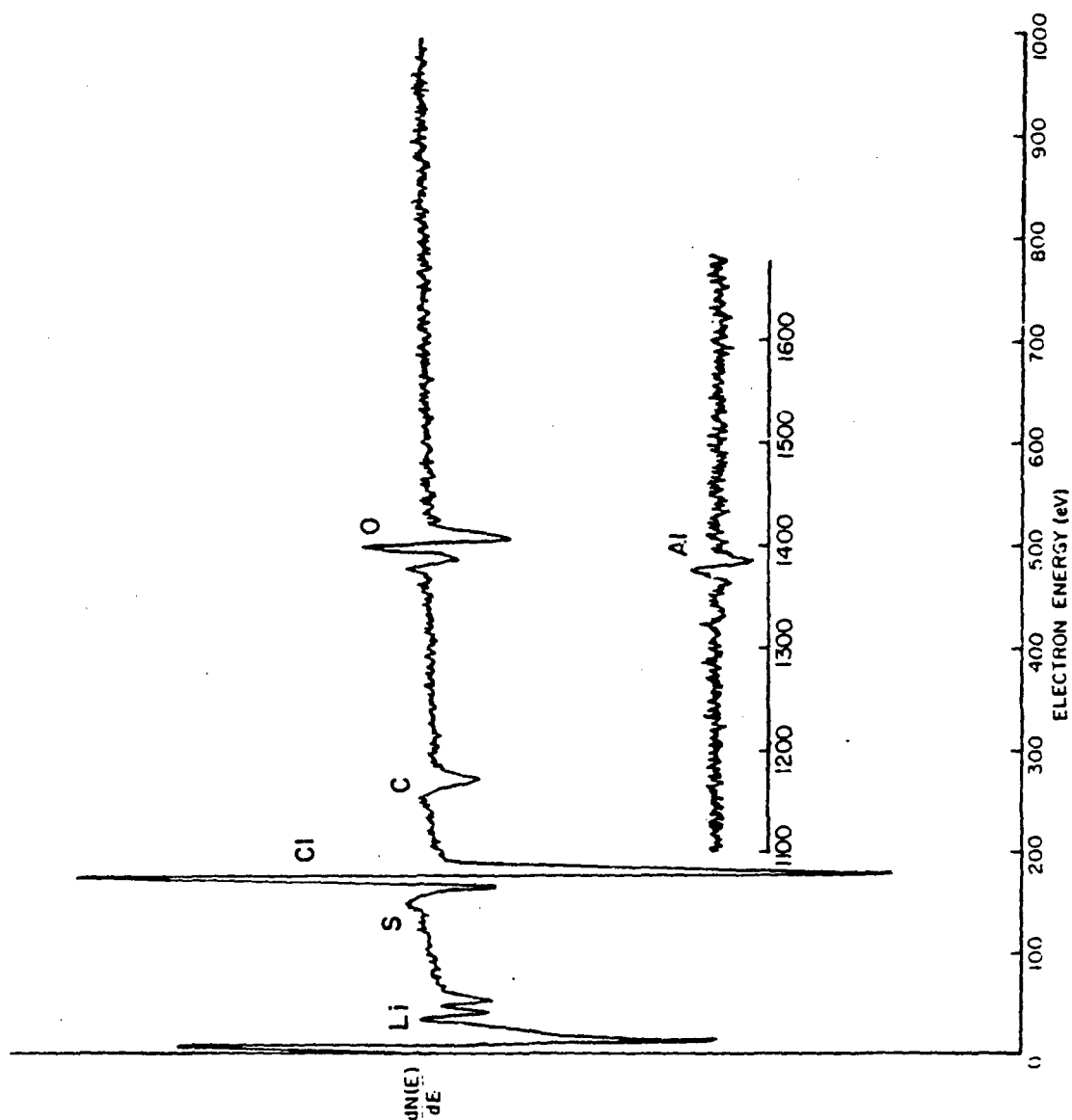


Figure 31. AES Spectrum of Lithium Discharged One-Half Percent in Electrolyte at One  $\text{mA}/\text{cm}^2$ , Room Temperature, Three Thionyl Chloride Washings.

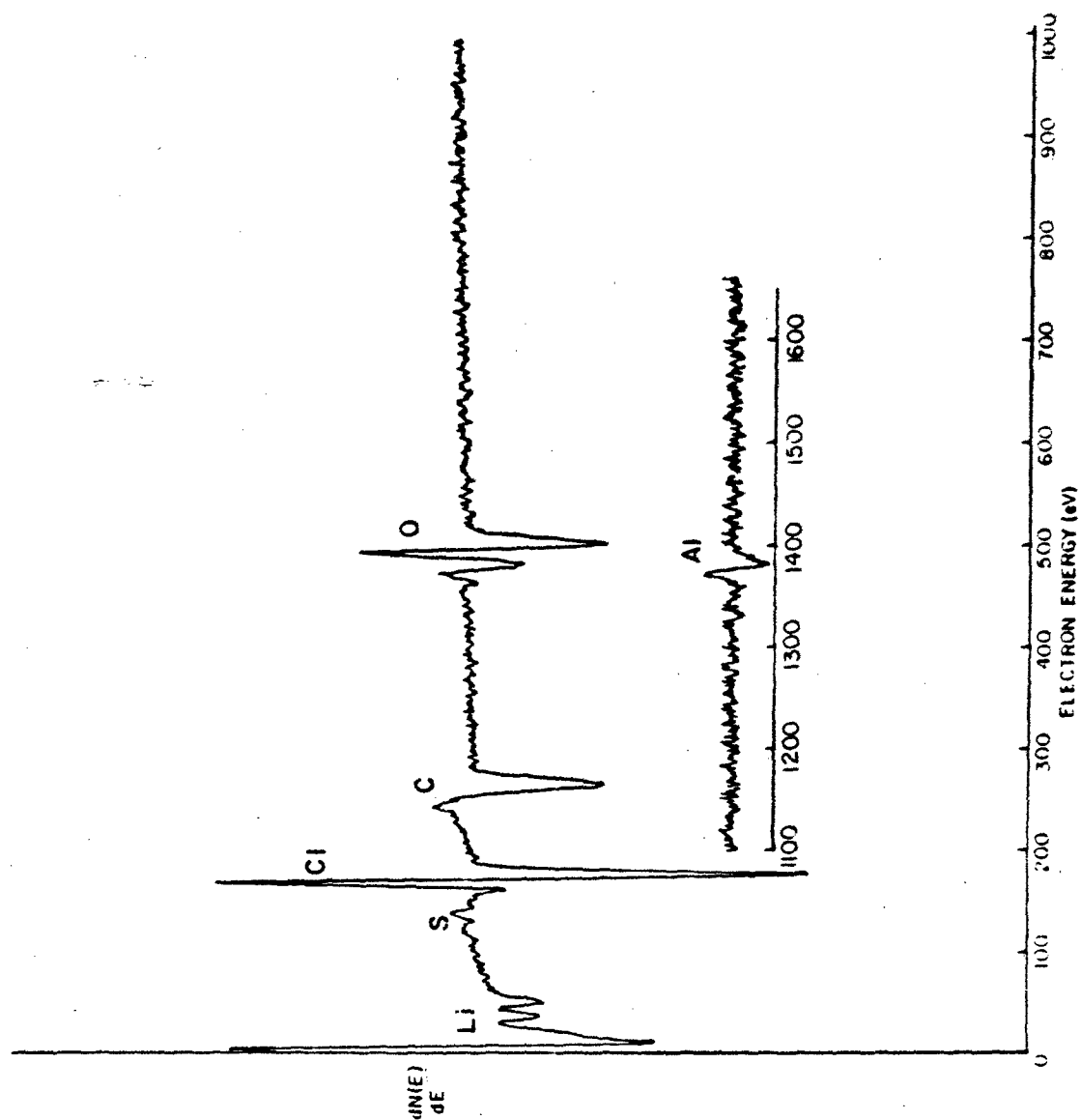


Figure 32. AES Spectrum of Lithium Discharged One-Half Percent in Electrolyte at One  $\text{mA}/\text{cm}^2$ , Room Temperature, Four Thionyl Chloride Washings.

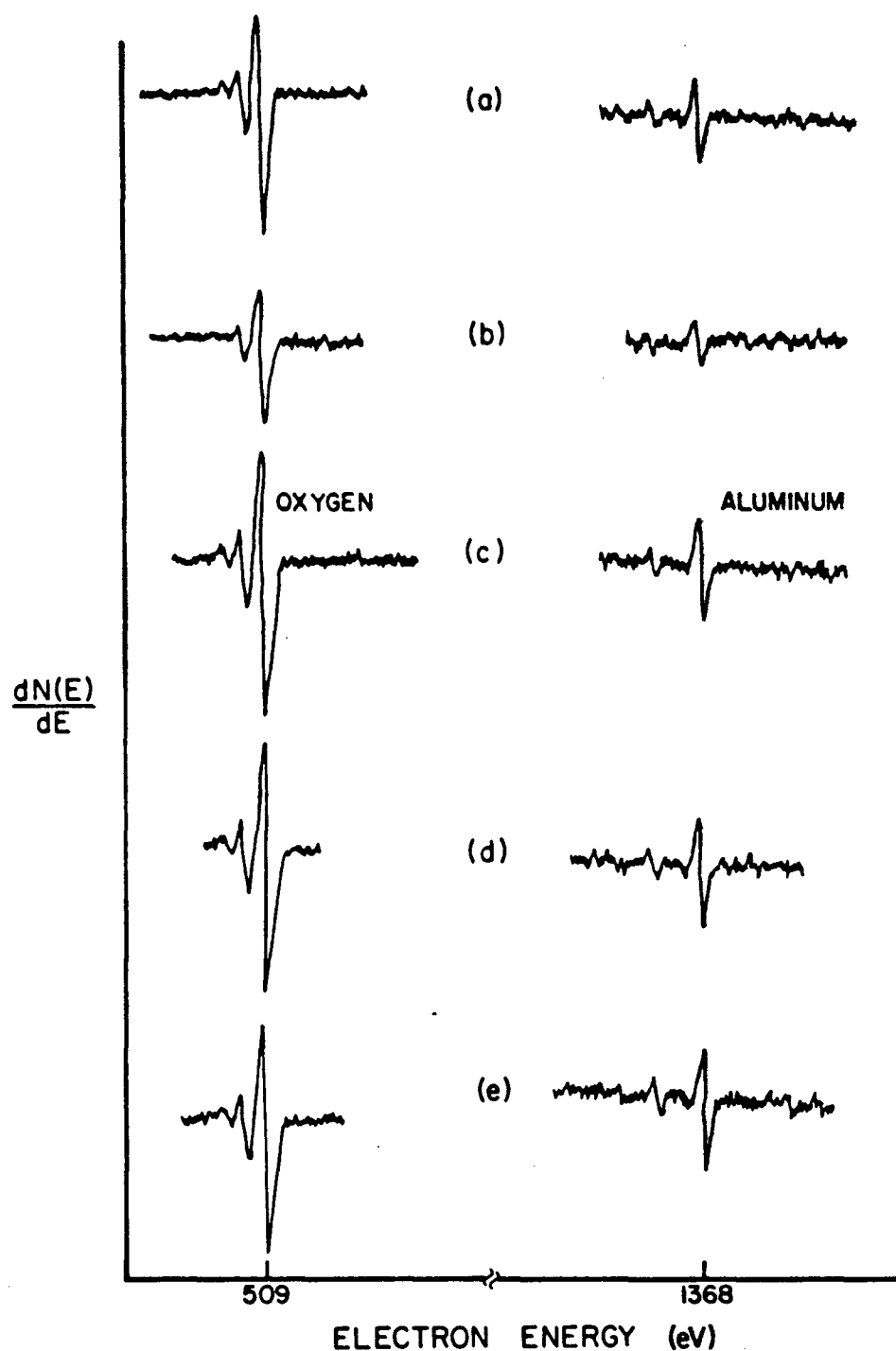
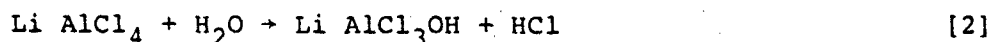


Figure 33. AES Oxygen and Aluminum Peak from a Lithium Anode Discharged Ten Percent at One  $\text{mA}/\text{cm}^2$ , and Room Temperature Receiving Thionyl Chloride Washings. a) no wash; b) one wash; c) two washings; d) three washings; e) four washings.

This ratio is interesting in view of data previously reported (30) which shows clearly that under identical storage conditions, a thicker lithium chloride film is formed when electrolyte salt,  $\text{LiAlCl}_4$ , is present. Assuming the chloride from the  $\text{AlCl}_4^-$  anion is responsible, it is necessary for that negative charge to be replaced by another, perhaps oxygen, if the aluminum is to remain in its +3 oxidation state. The observation may be somewhat fortuitous, given that the relative intensity of the oxygen to aluminum peak has not reached a constant value after four washings. The observation is consistent, however, with previously obtained data for lithium exposure to battery electrolyte (Figure 17). SEM data showed the surface of discharged lithium to be cavernous and tortuous. The electrolyte salt in discharged samples may well be chemically altered and occluded within the film as  $\text{AlOCl}_2^-$ .

In fabricated battery systems, water is introduced to some extent from the carbon. It is hypothesized (32) that water reacts in two ways with the electrolyte system, namely



Reaction 1 is thought to be predominant and evidence for the formed salt in Reaction 2 comes from the infrared (IR) hydroxyl band at  $3600 \text{ cm}^{-1}$ . Additional data in support of these reactions is that discharged batteries develop hydrogen gas pressure more rapidly than undischarged cells, leading to speculation that in discharged cells  $\text{H}_2(\text{g})$  comes from a salt of the form  $\text{LiAlCl}_3\text{OH}$ . In fact,  $\text{HCl}$  dissolved in  $\text{SOCl}_2$  does not react readily with lithium metal to liberate hydrogen gas (32).

With only trace quantities of sulfur occluded in the passive lithium chloride film, 12 hour periods were required to gather the high resolution XPS data. Figure 34 shows a high resolution XPS sulfur 2p trace (Figure 34-C). The trace shows clearly that three and perhaps four distinct sulfur species are present within the film

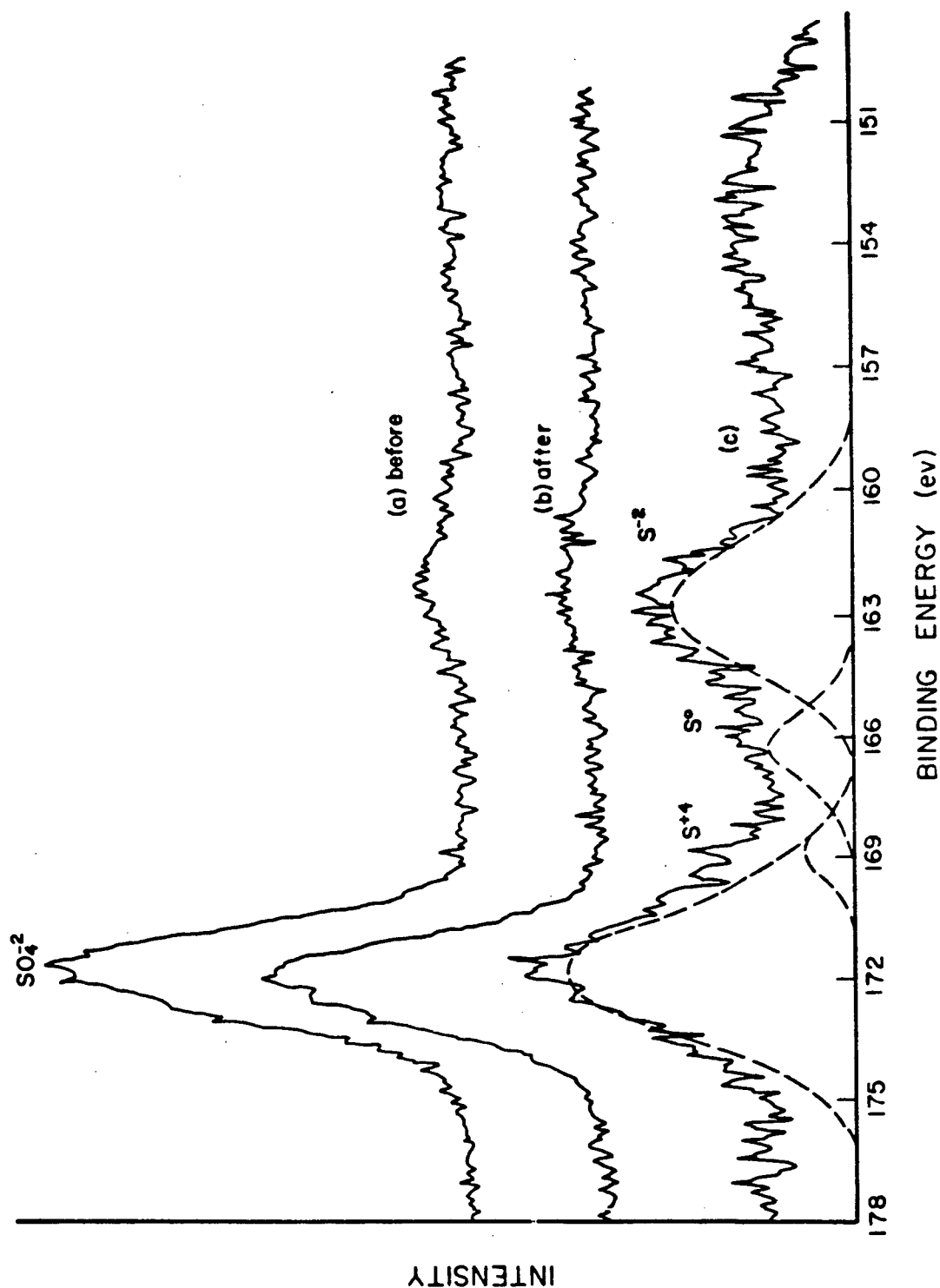


Figure 34. High Resolution XPS of Sulfur 2p in a)  $\text{Na}_2\text{SO}_4$  initial scan; b)  $\text{Na}_2\text{SO}_4$  after 11 hour beam exposure; and c) ten percent discharged lithium at one  $\text{mA}/\text{cm}^2$ , 50,000 counts, 11-hour beam exposure.



material. We identify these (Figure 34c) sulfur materials as  $\text{SO}_4^{-2}$  (50%),  $\text{S}^{+4}$  (5%) as  $\text{SO}_3^{-2}$  or residual  $\text{SOCl}_2$ ,  $\text{S}^0$  (15%) and  $\text{S}^{-2}$  (30%) sulfide. While a portion of the  $\text{S}^-$  peak can be attributed to  $\text{SO}_4^{=}$   $\text{K}_{\alpha 3,4}$ , its intensity allows the conclusion to be made that significant amounts of sulfide are formed during discharge of lithium anodes in battery cells at one milliampere per  $\text{cm}^2$ .

The combined chemical shift of 9 eV from sulfate ( $\text{SO}_4^{-2}$ ) sulfur to sulfide ( $\text{S}^{-2}$ ) sulfur enables separation of the sulfur oxidation states. It was thought that the x-ray beam might cause some sample damage. We, therefore repeated the experimental conditions using a sample of sodium sulfate which received little (Figure 34a) and equal (Figure 34b) beam radiation as our discharged sample. No significant beam damage to the sodium sulfate sample was observed after the 11-hour exposure.

In a recent study, Schliakjer et al (3) investigated the discharge reaction mechanism of lithium in thionyl chloride and concluded that significant quantities of elemental sulfur and  $\text{Li}_2\text{SO}_3$  may be formed. The experimental data published here and elsewhere (17,33,34) indicate considerable confusion exists regarding the reaction products and reaction intermediates which are formed during discharge of lithium in thionyl chloride and modified thionyl chloride systems (35,36). This is not surprising if one considers that the actual reaction products formed during the battery discharge may be kinetically, rather than thermodynamically, controlled. It should be pointed out that we do not infer that the surface analytical results represent the reaction products formed during the macroscopic reaction at the lithium electrode. However, knowledge of the presence of these reaction products is important because of the effect each might have upon the electrode kinetics.

## SECTION 8

### XPS OF THE LITHIUM SURFACE

Significant overall differences were observed in the XPS spectra on lithium samples which received different surface pretreatments. Figure 35a illustrates the XPS spectrum of lithium in the "as-received" condition. The surface of the metal is contaminated primarily by oxygen and carbon. Trace quantities of chlorine, sulfur and silicon are noted. The chlorine and sulfur are due to contamination from the dry box. Sputtering this surface with an inert argon ion beam easily removes all contaminants except for the oxygen (Figure 35b). This is not expected because of the affinity of lithium for oxygen. In fact, any fresh lithium metal produced through inert ion beam sputtering would rapidly react with residual oxygen in the vacuum chamber even at  $10^{-9}$  Torr pressure.

Figures 35c and 35d show the effect of exposing "as received" Foote lithium to  $\text{SOCl}_2$  vapor and liquid, respectively. The significant differences between these two exposures are the absence of sulfur and the increased chloride in the liquid exposure.

Figure 36a shows the result of exposing the Foote "as received" lithium metal surface to 1.8 M  $\text{LiAlCl}_4$  in thionyl chloride. In this case sulfur and aluminum are both detectable. Rinsing the surface with successive quantities of "neat" thionyl chloride and evacuating to remove the excess results in the following: (1) increased chloride signal, (2) sulfur and aluminum are removed below detectability and (3) the carbon and oxygen levels are reduced. The final surface contains lithium, oxygen and chlorine as seen by XPS.

High resolution scans of the chlorine 2p and oxygen 1s peaks following different surface treatments are shown in Figures 37 and 38 respectively. It is interesting to note the broadness in the

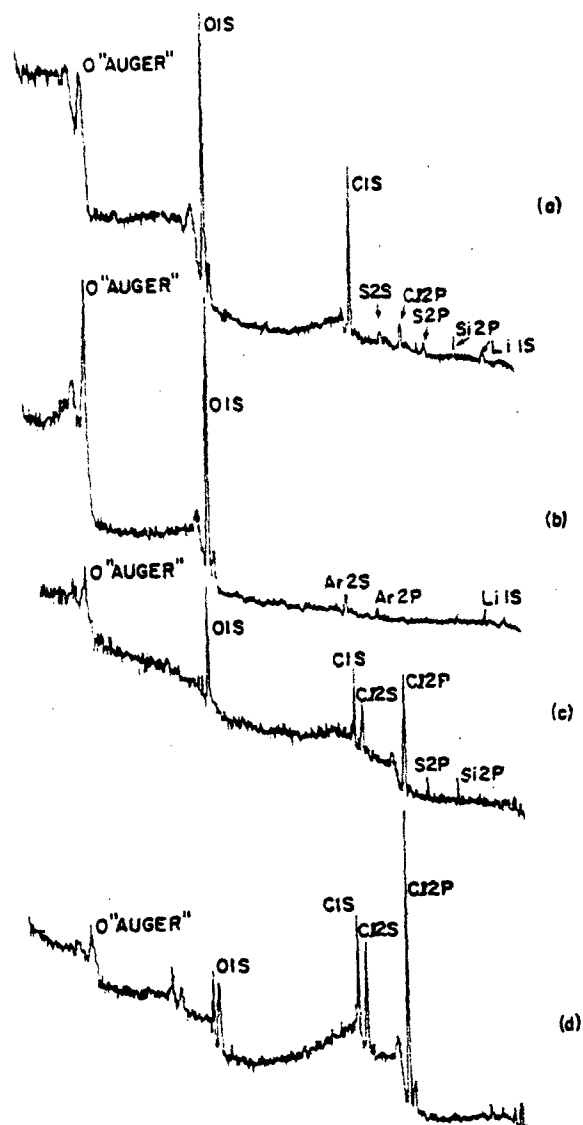


Figure 35. XPS Spectra of Lithium Surface a) "as received" and transferred from the dry box, b) after argon ion sputtering, c) after short exposure to  $\text{SOCl}_2$  vapor, and d) after short exposure to  $\text{SOCl}_2$  liquid.



Figure 36. XPS Spectra of a) after 90 minutes exposure of "as received" lithium to 1.8 M  $\text{LiAlCl}_4/\text{SOCl}_2$ . no wash; b) after one  $\text{SOCl}_2$  wash; c) after three  $\text{SOCl}_2$  washes, d) after four  $\text{SOCl}_2$  washes.

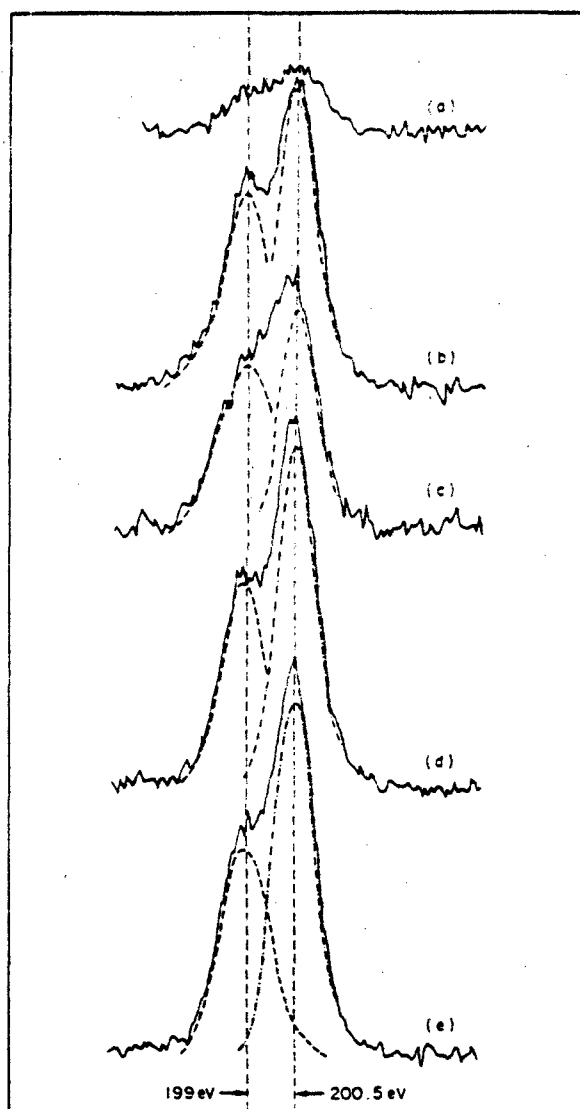


Figure 37. High Resolution XPS Spectra of Chlorine 2p on Lithium Metal Surfaces a) "as received" and transferred from the dry box, b) after 90 minutes exposure to  $\text{SOCl}_2$  liquid, c) after 90 minutes exposure to electrolyte, no wash, d) after 90 minutes exposure to electrolyte, one  $\text{SOCl}_2$  wash, and e) after 90 minutes exposure to electrolyte, four washings.

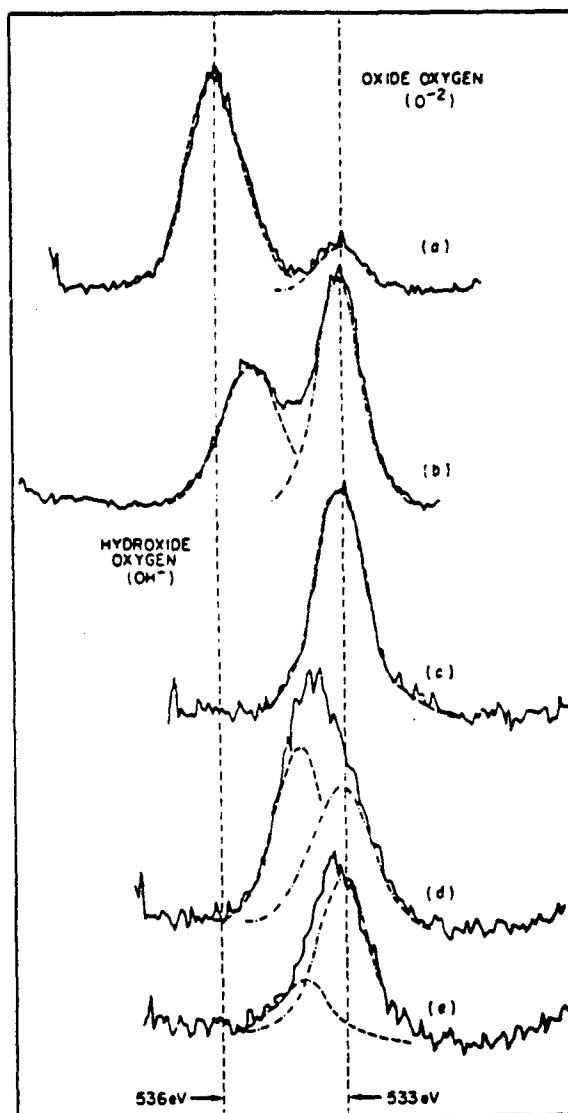


Figure 38. High Resolution XPS Spectra of Oxygen 1s on Lithium Metal Surfaces a) "as received" and transferred from the dry box, b) after receiving 90 minutes argon ion sputter, c) after exposure to  $\text{SOCl}_2$  vapor, d) after 90 minutes exposure to electrolyte, no  $\text{SOCl}_2$  wash, and e) after 90 minute exposure to electrolyte, four  $\text{SOCl}_2$  washings.

chlorine spectra of the lithium surface "as-received" (Figure 37a), exposed to  $\text{SOCl}_2$  liquid (Figure 37b) and exposed to electrolyte solution (Figure 37c). This peak broadness is characteristic of chlorine in more than one chemical environment. The chlorine 2p spectrum is normally a doublet,  $2p_{3/2}$  and  $2p_{1/2}$ , separated by 1.7 eV and found in a 2/1 ratio. This Cl 2p data suggests the presence of chlorine containing compounds, one a chloride and the other covalently bound chlorine. The latter is removed through  $\text{SOCl}_2$  washing (Figure 37d, e).

The oxygen 1s data shown in Figure 38 is also very interesting. The oxygen present at 533 eV binding energy is characteristic of lattice oxide,  $\text{O}^{2-}$ , while the oxygen appearing at a binding energy of 536 to 537 eV is most likely hydroxyl,  $\text{OH}^-$ . In Figure 38, evidence of the hydroxyl oxygen is seen in the "as received" lithium (Figure 38a). The hydroxyl intensity is severely reduced through sputtering (Figure 38b) and is absent from lithium surfaces exposed to  $\text{SOCl}_2$  vapor (Figure 38c). Exposure of lithium to battery electrolyte gives evidence of more than one type of oxygen (Figure 38d), an effect which can be removed through washing with  $\text{SOCl}_2$  (Figure 38c).

SECTION 9  
ELECTROCHEMICAL STUDIES:  
A MODEL FOR THE LITHIUM/ELECTROLYTE INTERFACE

From the available data (12,14,31) one can conclude that the "voltage delay" phenomenon is caused by the passivating film of lithium chloride at the lithium/electrolyte interface. It has recently been reported (21) that the interfacial capacities for the lithium electrode in thionyl chloride/LiAlCl<sub>4</sub> varies from 0.45 to 0.06  $\mu\text{Fcm}^{-2}$  compared to above 15  $\mu\text{Fcm}^{-2}$  for Au, Ni, W, and Pt electrode in SOCl<sub>2</sub> solutions (37).

Considering this data, it follows that a series capacitance model (38) is applicable to this electrode system because the passive film substantially reduces the effective capacitance (39) of the metal solution interface. Under conditions where cracks were produced over a substantial area of the lithium film, an increased lithium-solution capacitance would be expected.

The lithium chloride film can be considered to be the dielectric medium of a capacitor whose plates are composed of the substrate metal and the solution into which it is immersed. If lithium is polarized anodically under galvanostatic conditions, the film will transport charge (ion or electron) in some manner. The external current,  $i_e$ , in the circuit must equal the sum of this ion current plus current due to capacitance charging at the interfaces. To maintain a given current density across the lithium film, the lithium metal assumes some value of overpotential,  $n$ . The overpotential is the numerical difference between the potential of the lithium minus its reversible potential in the medium of interest. The differential equation which relates the current density through the film,  $i$ , the overpotential,  $n$ , and the external circuit current,  $i_e$ , is given by

$$i + C \frac{dn}{dt} = i_e \quad [3]$$



Should  $i_e$  become numerically equal to zero, an open circuit results and a voltage transient (decay) occurs.

If one can measure the change in the potential with time, the current through the film may be determined as a function of overvoltage, assuming a value for  $C$  is available. Conversely, at time  $t = 0$ , the instant the external current is interrupted,  $i_e$  equals  $i$  since  $dn/dt$  is at its steady state value, zero.

The capacitance of the film can then be determined from the relationship

$$C = -i / (dn/dt)_{t \rightarrow 0} \quad [4]$$

Here " $i$ " is assumed to be numerically equal to  $i_e$  at the instant the current is interrupted and  $(dn/dt)$  is the initial rate of overvoltage decay. The effective resistance of the film can be calculated, assuming ohmic behavior, by dividing the overvoltage by the formation current density.

For the current due to ion transport through a passive film to be activation-energy-controlled a substantial energy barrier must be surmounted during the transport process. The theoretical relation for such a process in the high-field case, is given in its simplest form by

$$i = 2anv \exp(-U/RT) \exp(qaE/RT) \quad [5]$$

where " $a$ " is the half jump distance of the activation barrier, " $n$ " the density of charge carriers, " $v$ " the frequency of oscillating ions, " $U$ " the activation energy for the process, " $q$ " the effective charge on the mobile ions and " $E$ " the electric field at the activation barrier. The other symbols have their usual meanings.

Ion transport in anodic films (40) is believed to be activation-energy controlled and a similar mechanism is postulated to be applicable to lithium chloride films. For anodic oxides, the relationship between overpotential and time upon commencement of the open-circuit follows an equation of the form

$$n = k - V_o \ln (t + \theta) \quad [6]$$

The quantity  $k$ ,  $V_o$  and  $\theta$  are parameters which are determined by the particular transient. Differentiating Equation 6 with respect to time yields

$$\frac{dn}{dt} = \frac{-V_o}{t+\theta} \quad [7]$$

Solving Equation 6 for the quantity  $(t+\theta)$  and substituting into Equation 7 yields

$$\frac{dn}{dt} = -V_o \exp(-k/V_o) \exp(V/V_o) \quad [8]$$

Substituting Equation 8 into Equation 3 and noting that  $i_e = 0$  (at the commencement of the open circuit transient) yields for the final result an equation of the form

$$i = i_o \exp n/V_o \quad [9]$$

where  $i_o = C V_o \exp(-k/V_o)$ . The point is that an equation of this form is the mathematical consequence of the differential equation describing the system and the experimental voltage-time profile for systems where ion transport is activation-energy-controlled. Here  $i_o$  and  $V_o$  are experimentally determined parameters whose dimensions are the same as  $i$  and  $V$ , respectively. Assuming the electrostatic field at the activation barrier is equal to the average electric field, a comparison of Equations 5 and 9 may be made which yields the relationship

$$V_o = \frac{kT}{qa} D \quad [10]$$

Thus,  $V_o$  is proportional to the thickness of the passive layer,  $D$ , and it provides an indirect measurement of the relative thickness of the passive films. An equation of this form would be expected for the lithium anode if a passive film is on its surface.

Consider now what the relationship would be between overpotential,  $n$ , and time if ion transport occurred via a mechanism in which the activation energy is a small fraction of that just considered. One would expect that the duration of the transient would be shortened markedly. Such a situation might result if ion transport can occur along large grain boundaries or under conditions where a substantial fraction of the metal surface is devoid of passive film. If the transient lifetime would be short compared to the previous example, the open-circuit voltage time profile might now be of the form

$$n = k - V_o t \quad [11]$$

Using similar arguments as before, the ion current at the interface would be given by

$$i = -C \left( \frac{dn}{dt} \right) = C V_o \quad [12]$$

Recognizing that at  $t = 0$ ,  $i_e = i_{e \max}$  and  $k = V_{\text{formation}}$  yields the film resistance,  $R$ , in ohms  $\text{cm}^{-2}$

$$R = \lim_{t \rightarrow 0} \left( \frac{n}{i_e} \right) \quad [13]$$

Similarly, the capacitance of the interface is calculated from the rate at which voltage decay occurs and the initial current at the commencement of the decay process using the relationship

$$C = i_e / V_o \quad [14]$$

Upon completion of the computer interface system, the anodic oxidation of tantalum, a well characterized system, was studied. An aqueous boric acid - sodium tetraborate medium was used for a growth medium. Platinum foil was used as the counter electrode. The overvoltage of the tantalum anode was monitored through a

high input impedance operational amplifier (Philbrick SP-102) versus an S.C.E. connected through a Luggin capillary. For each transient up to 256 data points were taken at intervals which were controlled through an external clock. The maximum acquisition rate was 6,500 points per second. This allowed transients with lifetimes as short as one millisecond to be monitored adequately.

Table II indicates the formation voltage, growth current density, data acquisition frequency and the table number which control an existing software. The data was stored on disc and subsequently analyzed using a number of curve fitting programs. A best-fit was obtained for the voltage transient data through a logarithmic relationship i.e.,

$$n = k - V_0 \ln(t + \theta) \quad [15]$$

In Equation 15,  $\theta$  is an adjustable quantity necessary to minimize the standard deviation and achieve a "best-fit". Numerical values for  $V_0$  and  $k$  were subsequently calculated. A summary of these calculated quantities which result in a minimal value of the standard deviation are listed in Table XV. The anodic tantalum oxide films were grown at room temperature on an electrode whose apparent surface area equaled  $0.23 \text{ cm}^2$ . Two-hundred-fifty-six voltage measurements were recorded for each transient. In the analysis,  $V_0$  is seen as a measure of the relative thickness of the passive layer. It is therefore expected to increase linearly with the film formation voltage. Figure 39 shows that  $V_0$  does increase approximately linearly with the film formation potential at a specific growth current density. In addition,  $V_0$  is seen to decrease with increasing current density at a given formation potential. This effect is attributed to the increase in the ion jump distance "a" at a larger formation current density.

TABLE II. EXPERIMENTAL CONDITIONS AND TABLE SOURCE FOR  
VOLTAGE DATA OBSERVED WITH TANTALUM METAL IN  
AQUEOUS BORIC ACID - SODIUM TETRABORATE  
SOLUTIONS AT ROOM TEMPERATURE AFTER CURRENT  
INTERRUPT

Formation Voltage (Volts)	Formation Current Density $\mu\text{A}/\text{cm}^2$	Table No.
3.7	2,174	III
5.3	2,174	IV
7.0	2,174	V
9.0	2,174	VI
3.0	1,087	VII
5.0	1,087	VIII
7.0	1,087	IX
9.0	1,087	X
3.1	217	XI
7.0	217	XII
9.0	217	XIII
5.0	217	XIV

TABLE III. OVERVOLTAGE TRANSIENT DATA FOR A 3.7 VOLT TANTALUM FILM ANODIZED IN AN AQUEOUS BORIC ACID SODIUM TETRA-BORATE SOLUTION AT  $2,174 \mu\text{a}/\text{cm}^2$  AND AT ROOM TEMPERATURE: TIME RESOLUTION  $158.5 \mu \text{ SEC}$ , VOLTAGE RESOLUTION 2.4414 MILLIVOLTS, DATA PRESENTED IN MILLIVOLTS

t=0	3269	1333	1210	1118	1025	957
	1660	1325	1208	1113	1030	952
	1638	1320	1206	1110	1027	952
	1574	1308	1201	1110	1020	949
	1501	1300	1198	1101	1015	947
	1520	1298	1196	1096	1015	939
	1499	1293	1191	1093	1005	937
	1484	1289	1186	1091	1005	
	1477	1284	1184	1083	1003	
	1462	1281	1179	1081	998	
	1450	1274	1176	1079	993	
	1440	1271	1169	1076	988	
	1430	1265	1162	1069	991	
	1420	1259	1157	1069	986	
	1411	1254	1154	1064	979	
	1393	1249	1152	1062	981	
	1391	1245	1152	1052	971	
	1381	1240	1145	1059	979	
	1374	1240	1145	1049	971	
	1367	1232	1140	1049	971	
	1354	1228	1135	1042	964	
	1350	1225	1127	1040	964	
	1345	1220	1125	1035	961	Final Voltage
	1335	1215	1123	1032	957	699

TABLE IV. OVERVOLTAGE TRANSIENT DATA FOR A 5.3 VOLT TANTALUM FILM ANODIZED IN AN AQUEOUS BORIC ACID SODIUM TETRABORATE SOLUTION AT  $2,174 \mu\text{a}/\text{cm}^2$  AND AT ROOM TEMPERATURE: TIME RESOLUTION  $158.5 \mu \text{ SEC}$ , VOLTAGE RESOLUTION 2.4414 MILLIVOLTS, DATA PRESENTED IN MILLIVOLTS

5310	2368	2036	1862	1740
3259	2351	2026	1855	1735
3205	2333	2019	1853	1730
3093	2319	2009	1848	1730
3039	2299	1999	1843	1726
2985	2287	1994	1835	1723
2941	2270	1984	1831	1718
2897	2258	1979	1823	1716
2861	2243	1970	1821	1711
2822	2231	1965	1816	1711
2788	2216	1955	1813	1708
2753	2207	1950	1806	1706
2722	2189	1943	1804	1701
2690	2180	1938	1799	1699
2663	2165	1933	1794	1696
2634	2153	1923	1791	1691
2609	2143	1921	1787	1689
2583	2128	1911	1782	1687
2558	2121	1909	1779	1684
2534	2109	1901	1772	1679
2512	2099	1898	1772	1677
2490	2087	1896	1765	
2463	2077	1887	1762	
2446	2067	1882	1755	
2426	2060	1877	1750	
2404	2053	1874	1748	Final Voltage
2390	2041	1865	1743	1484

TABLE V. OVERVOLTAGE TRANSIENT DATA FOR A 7.0 VOLT TANTALUM FILM ANODIZED IN AN AQUEOUS BORIC ACID SODIUM TETRA-BORATE SOLUTION AT 2,174  $\mu\text{a}/\text{cm}^2$  AND AT ROOM TEMPERATURE: TIME RESOLUTION 158.5  $\mu$  SEC, VOLTAGE RESOLUTION 2.4414 MILLIVOLTS, DATA PRESENTED IN MILLIVOLTS

7004	3281	2790	2470	2231	2155
4372	3254	2775	2458	2226	2148
4306	3229	2756	2448	2216	2141
4157	3203	2746	2438	2211	2131
4091	3181	2727	2429	2202	2128
4028	3156	2714	2419	2199	2121
3972	3134	2700	2407	2189	2116
3913	3112	2692	2399	2185	2109
3864	3090	2673	2387	2175	2102
3815	3081	2661	2380	2170	2099
3767	3049	2648	2368	2163	2089
3718	3029	2634	2360	2155	2087
3679	3010	2626	2351	2148	2080
3635	2990	2612	2341	2143	2072
3601	2973	2597	2331	2131	2067
3562	2956	2587	2321	2126	2060
3522	2941	2575	2314	2116	2058
3491	2919	2563	2292	2111	2050
3457	2907	2551	2294	2102	
3427	2888	2536	2285	2199	
3395	2871	2524	2277	2189	
3361	2853	2514	2265	2185	
3337	2841	2499	2260	2175	
3308	2822	2492	2248	2170	Final Voltage
	2810	2980	2243	2163	1652



TABLE VI. OVERVOLTAGE TRANSIENT DATA FOR A 9.0 VOLT TANTALUM FILM ANODIZED IN AN AQUEOUS BORIC ACID SODIUM TETRABORATE SOLUTION AT  $2,174 \mu\text{a}/\text{cm}^2$  AND AT ROOM TEMPERATURE: TIME RESOLUTION 158.5  $\mu$  SEC, VOLTAGE RESOLUTION 2.4414 MILLIVOLTS, DATA PRESENTED IN MILLIVOLTS

9047	4890	4077	3544	3181	2888
6535	4884	4052	3527	3166	28880
6345	4807	4023	3513	3156	2868
6249	4768	4003	3491	3142	
6152	4731	3972	3481	3129	
6061	4692	3952	3459	3120	
5966	4663	3925	3447	2105	
5893	4621	3903	3432	3093	
5810	4587	3881	3417	3085	
5744	4548	3859	3403	3068	
5671	4519	3835	3386	3056	
5600	4479	3813	3378	3046	
5534	4450	3796	3359	3032	
5476	4414	3771	3347	3024	
5417	4387	3752	3334	3010	
5361	4350	3730	3317	2998	
5307	4326	3708	3303	2985	
5253	4291	3691	3291	2976	
5205	4267	3669	3276	2963	
5153	4235	3652	3264	2954	
5107	4211	3630	3249	2944	
5061	4182	3618	3234	2929	
5014	4157	3596	3220	2919	
4975	4128	3581	3205	2907	Final Voltage
4931	4106	3562	3193	2900	2062

TABLE VII. OVERVOLTAGE TRANSIENT DATA FOR A 3.0 VOLT TANTALUM FILM ANODIZED IN AN AQUEOUS BORIC ACID SODIUM TETRA-BORATE SOLUTION AT 1,087  $\mu\text{a}/\text{cm}^2$  AND AT ROOM TEMPERATURE: TIME RESOLUTION 158.8  $\mu$  SEC, VOLTAGE RESOLUTION 2.4414 MILLIVOLTS, DATA PRESENTED IN MILLIVOLTS

3068	1499	1423	1479	1386
1745	1484	1437	1484	1394
1748	1489	1420	1484	1394
1643	1477	1423	1484	1389
1625	1486	1416	1484	
1601	1474	1418	1479	
1591	1481	1418	1464	
1603	1462	1411	1474	
1579	1462	1384	1472	
1562	1464	1401	1481	
1579	1474	1398	1459	
1552	1474	1374	1491	
1550	1462	1394	1486	
1555	1464	1389	1476	
1547	1462	1374	1484	
1535	1459	1381	1484	
1540	1452	1394	1484	
1535	1459	1379	1474	
1525	1462	1406	1486	
1525	1447	1389	1481	
1542	1452	1396	1486	
1520	1459	1386	1489	
1533	1437	1386	1481	
1520	1435	1396	1484	
1511	1430	1379	1484	
1530	1423	1386	1484	
1503	1455	1381	1474	
1516	1428	1389	1474	
1501	1433	1372	1484	
1501	1442	1364	1403	Final Voltage
1484	1418	1381		1325

TABLE VIII. OVERVOLTAGE TRANSIENT DATA FOR A 5.0 VOLT TANTALUM FILM ANODIZED IN AN AQUEOUS BORIC ACID SODIUM TETRABORATE SOLUTION AT  $1,087 \mu\text{a}/\text{cm}^2$  AND AT ROOM TEMPERATURE: TIME RESOLUTION  $158.8 \mu\text{ SEC}$ , VOLTAGE RESOLUTION 2.4414 MILLIVOLTS, DATA PRESENTED IN MILLIVOLTS

5024	2861	2565	2294	2116
3591	2849	2543	2312	2092
3581	2841	2548	2299	2084
3439	2822	2480	2280	2099
3405	2829	2517	2260	2094
3369	2814	2512	2263	2092
3359	2795	2487	2255	2087
3286	2770	2482	2258	2067
3281	2753	2468	2250	2070
3254	2739	2478	2233	2075
3227	2734	2460	2236	2058
3205	2714	2448	2241	2036
3193	2707	2438	2214	2043
3161	2700	2434	2214	2038
3132	2686	2414	2202	2036
3122	2675	2412	2182	2023
3095	2670	2404	2187	
3063	2661	2402	2165	
3039	2644	2387	2165	
3027	2639	2373	2170	
3007	2622	2375	2153	
2978	2622	2365	2141	
2971	2604	2358	2116	
2951	2602	2351	2126	
2939	2583	2343	2119	
2919	2602	2329	2128	
2900	2583	2316	2116	Final Voltage
2905	2573	2316	2128	1669

TABLE IX. OVERVOLTAGE TRANSIENT DATA FOR A 7.0 VOLT TANTALUM FILM ANODIZED IN AN AQUEOUS BORIC ACID SODIUM TETRA-BORATE SOLUTION AT  $1,087 \mu\text{a}/\text{cm}^2$  AND AT ROOM TEMPERATURE: TIME RESOLUTION  $158.8 \mu \text{ SEC}$ , VOLTAGE RESOLUTION 2.4414 MILLIVOLTS, DATA PRESENTED IN MILLIVOLTS

7026	4479	3791	3327	2927
5788	4448	3786	3303	2915
5729	4428	3859	3295	2902
5556	4389	3725	3271	2893
5490	4357	3730	3261	2878
5427	4326	3725	3225	2875
5361	4299	3681	3222	2858
5258	4267	3659	3207	2849
5251	4238	3642	3193	2841
5190	4218	3618	3186	2822
5131	4184	3601	3178	2819
5092	4160	3601	3156	2814
5053	4128	3581	3146	2788
4997	4128	3564	3129	2778
4963	4091	3544	3112	2780
4899	4072	3520	3098	2744
4890	4023	3503	3085	2770
4809	3996	3593	3059	2756
4809	3977	3586	3078	2736
4780	3952	3549	3032	2719
4736	3930	3537	3029	2727
4716	3901	3508	3012	2709
4663	3884	3403	3007	2712
4626	3862	3383	2988	
4584	3845	3361	2956	
4545	3830	3366	2966	Final Voltage
4533	3791	3334	2927	1979

TABLE X. OVERVOLTAGE TRANSIENT DATA FOR A 9.0 VOLT TANTALUM FILM ANODIZED IN AN AQUEOUS BORIC ACID SODIUM TETRA-BORATE SOLUTION AT  $1,087 \mu\text{a}/\text{cm}^2$  AND AT ROOM TEMPERATURE: TIME RESOLUTION  $158.8 \mu \text{ SEC}$ , VOLTAGE RESOLUTION 2.4414 MILLIVOLTS, DATA PRESENTED IN MILLIVOLTS

9025	6054	5166	4494	4025
7595	6018	5126	4475	4006
7429	5957	5090	4472	4001
7365	5927	5075	4436	3991
7285	5886	5029	4421	3967
7209	5847	5007	4401	3950
7136	5815	4990	4377	3040
7067	5771	4960	4348	3020
7004	5737	4902	4340	3008
6921	5700	4899	4323	3879
6874	5644	4873	4301	3884
6811	5615	4843	4284	3854
6745	5612	4821	4262	3852
6680	5544	4804	4265	3828
6630	5534	4782	4221	3823
6594	5495	4755	4216	2818
6530	5480	4728	4191	3786
6477	5415	4702	4191	3771
6420	5417	4704	4160	3779
6381	5363	4655	4138	3740
6330	5336	4633	4145	3720
6279	5302	4631	4103	3723
6240	5273	4592	4089	3701
6186	5246	4562	4082	3691
6142	5209	4536	4055	Final Voltage
6098	5168	4531	4042	

TABLE XI. OVERVOLTAGE TRANSIENT DATA FOR A 3.1 VOLT TANTALUM FILM ANODIZED IN AN AQUEOUS BORIC ACID SODIUM TETRA-BORATE SOLUTION AT  $217 \mu\text{a}/\text{cm}^2$  AND AT ROOM TEMPERATURE: TIME RESOLUTION  $158.8 \mu \text{ SEC}$ , VOLTAGE RESOLUTION 2.4414 MILLIVOLTS, DATA PRESENTED IN MILLIVOLTS

3154	2727	2565	2460	2355
3027	2722	2561	2458	2351
3020	2714	2556	2453	2351
3005	2714	2563	2451	2348
2941	2702	2546	2446	2343
2924	2690	2563	2443	2338
2912	2683	2548	2463	2333
2902	2678	2546	2436	2329
2895	2668	2539	2431	2329
2885	2663	2536	2424	2324
2875	2653	2529	2421	
2863	2651	2526	2416	
2856	2644	2521	2414	
2844	2639	2517	2409	
2836	2648	2512	2404	
2829	2626	2509	2414	
2832	2614	2507	2399	
2810	2617	2502	2397	
2807	2614	2497	2390	
2795	2614	2495	2390	
2790	2609	2492	2382	
2780	2604	2487	2387	
2775	2597	2485	2377	
2768	2590	2480	2390	
2763	2585	2478	2375	
2757	2583	2473	2370	
2749	2578	2470	2363	
2741	2575	2465	2358	Final Voltage
2734	2570	2465	2353	2028

TABLE XII. OVERVOLTAGE TRANSIENT DATA FOR A 7.0 VOLT TANTALUM FILM ANODIZED IN AN AQUEOUS BORIC ACID SODIUM TETRA-BORATE SOLUTION AT  $217 \mu\text{a}/\text{cm}^2$  AND AT ROOM TEMPERATURE: TIME RESOLUTION  $158.8 \mu\text{ SEC}$ , VOLTAGE RESOLUTION 2.4414 MILLIVOLTS, DATA PRESENTED IN MILLIVOLTS

7023	6318	5908	5595	5336
6874	6308	5898	5585	5327
6862	6293	5886	5578	5324
6835	6276	5876	5573	5327
6760	6264	5913	5563	
6735	6247	5852	5554	
6716	6230	5837	5544	
6696	6218	5827	5534	
6679	6206	5820	5524	
6655	6193	3749	5517	
6643	6179	6081	5510	
6625	6166	5788	5500	
6608	6154	5776	5490	
6591	6140	5766	5483	
6564	6127	5754	5476	
6557	6115	5744	5468	
6542	6103	5732	5458	
6520	6091	5717	5451	
6508	6079	5715	5446	
6489	6064	5703	5439	
6475	6052	5693	5436	
6459	6037	5683	5424	
6447	6025	5673	5417	
6433	6013	5664	5410	
6420	6000	5659	5400	
6406	5988	5649	5454	
6391	5961	5646	5383	
6374	5959	5634	5380	
6359	5947	5622	5366	
6347	5932	5615	5358	Final Voltage
6332	5917	5603	5346	4457

TABLE XIII. OVERVOLTAGE TRANSIENT DATA FOR A 9.0 VOLT TANTALUM FILM ANODIZED IN AN AQUEOUS BORIC ACID SODIUM TETRABORATE SOLUTION AT  $217 \mu\text{a}/\text{cm}^2$  AND AT ROOM TEMPERATURE: TIME RESOLUTION  $158.8 \mu\text{SEC}$ , VOLTAGE RESOLUTION 2.4414 MILLIVOLTS, DATA PRESENTED IN MILLIVOLTS

9091	8249	7785	7409	7070
8935	8232	7770	7399	7058
8913	8215	7756	7390	7045
8806	8198	7741	7377	7033
8786	8178	7724	7365	7033
8759	8161	7712	7355	7014
8732	8137	7702	7346	7001
8708	8117	7692	7331	6987
8684	8100	9678	7324	6977
8662	8083	7661	3702	6965
8640	8063	7648	7299	6955
8608	8046	7634	7285	6943
8586	8029	7622	7268	6433
8580	8012	7604	7258	
8542	8015	7595	7246	
8522	7980	7578	7233	
8500	7963	7568	7221	
8481	7949	7556	7209	
8459	7936	7541	7199	
8439	7922	7526	7187	
8420	7907	7514	7177	
8398	7888	7502	7165	
8381	7875	7490	7150	
8361	7858	7480	7138	
8344	7841	7468	7131	
8325	7829	7456	7119	
8308	7810	7443	7109	
8286	7802	7431	7099	Final Voltage
8269		7419	7084	5786



TABLE XIV. OVERVOLTAGE TRANSIENT DATA FOR A 5.0 VOLT TANTALUM FILM ANODIZED IN AN AQUEOUS BORIC ACID SODIUM TETRA-BORATE SOLUTION AT  $217 \mu\text{a}/\text{cm}^2$  AND AT ROOM TEMPERATURE: TIME RESOLUTION  $158.8 \mu \text{ SEC}$ , VOLTAGE RESOLUTION 2.4414 MILLIVOLTS, DATA PRESENTED IN MILLIVOLTS

5301	4509	4248	4001	3845
4897	4497	4243	4006	3840
4882	4487	4233	3999	3832
4863	4440	4223	3999	3828
4775	4467	4213	3989	3823
4760	4453	4204	3981	3818
4746	4440	4199	3972	2815
4731	4433	4189	3964	2811
4719	4421	4187	3957	2806
4704	4411	4179	3962	3798
4694	4401	4169	3962	3796
4677	4394	4162	3955	3791
4665	4384	4152	3942	3789
4653	4377	4143	3935	3789
4641	4365	4135	3928	
4631	4355	4125	3923	
4621	4350	4118	3913	
4609	4340	4108	2911	
4599	4331	4099	2906	
4587	4321	4086	3901	
4577	4328	4079	3896	
4567	4311	4069	3886	
4567	4299	4060	3881	
4567	4289	4052	3876	
4553	4279	4045	3867	
4543	4267	4035	3864	
4536	4262	4030	3859	
4526	4252	4020	3854	Final Voltage
4516	4248	4013	3850	3251

TABLE XV. ELECTROCHEMICAL RESULTS; CALCULATED VALUES OF "k", " $V_0$ ", AND "s" FOR FILM GROWN AT SPECIFIED CURRENT DENSITY AND VOLTAGE. THE VALUE OF  $\theta$  WHICH YIELDS THE MINIMAL VALUE IS "s" IS PRESENTED

Formation Overvoltage (Volts)	Formation Current Density $\mu\text{a/cm}^2$	k (Volts)	$-V_0$ (Volt/Sec)	Minimum Standard Deviation "s"	$\theta$ (Sec)
3.1	217	1.21	0.281	0.054	$5.0 \times 10^{-4}$
5.3	217	0.57	0.883	0.026	$7.2 \times 10^{-3}$
7.0	217	-0.491	1.70	0.021	$1.3 \times 10^{-2}$
9.0	217	-1.55	2.59	0.027	$1.8 \times 10^{-2}$
3.0	1,087	0.93	0.115	0.088	$9.5 \times 10^{-4}$
5.0	1,087	-0.198	0.582	0.079	$8.0 \times 10^{-4}$
7.0	1,087	-1.70	1.15	0.085	$8.0 \times 10^{-4}$
9.0	1,087	-3.80	1.95	0.078	$2.3 \times 10^{-3}$
3.7	2,174	0.042	0.226	0.056	0.000
5.3	2,174	+0.191	0.389	0.042	0.000
7.0	2,174	-0.436	0.646	0.082	$1.0 \times 10^{-5}$
9.0	2,174	-2.31	1.350	0.13	$1.0 \times 10^{-3}$

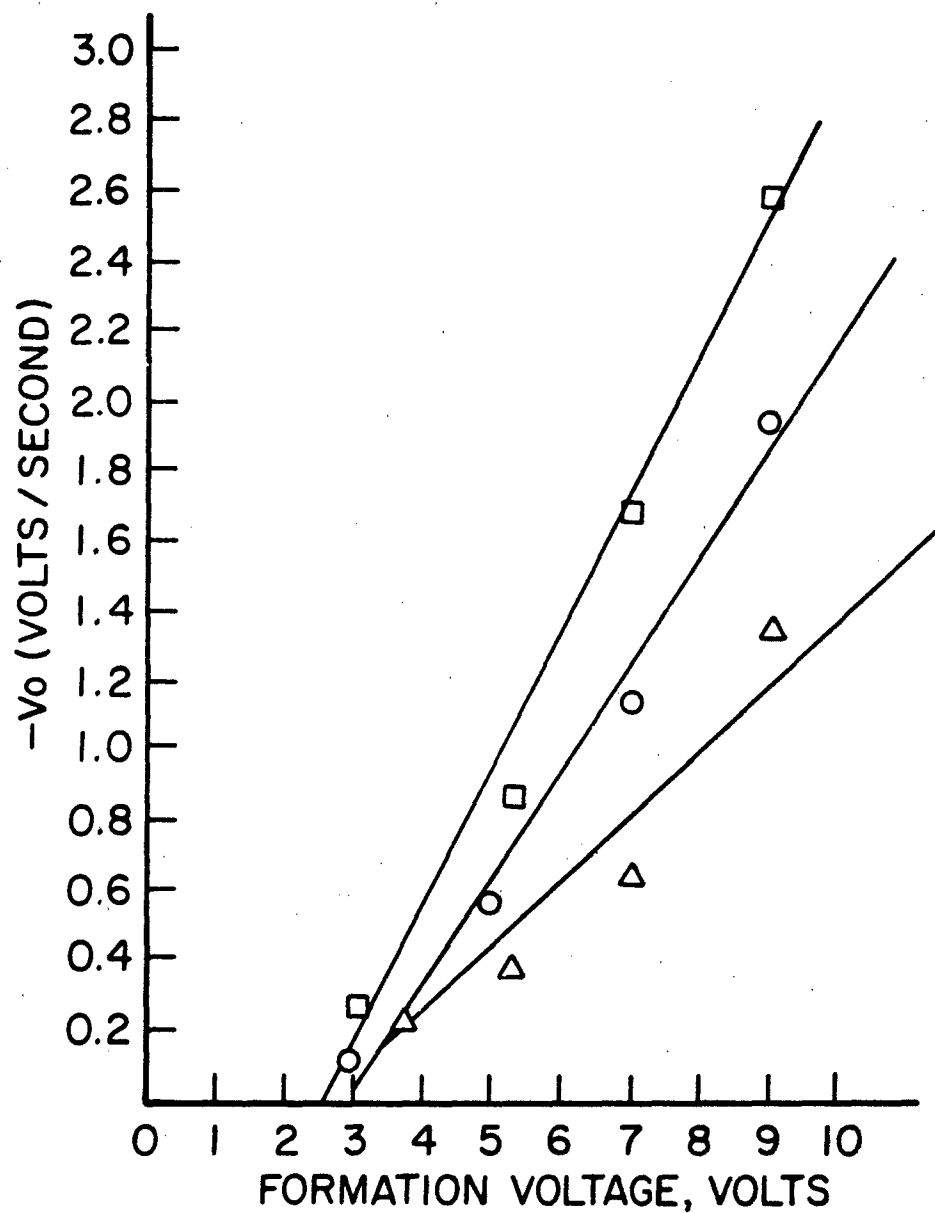


Figure 39. Plot of Minus  $V_o$  versus Formation Potential (Volts) for Tantalum Anodized in An Aqueous Boric Acid-Sodium Tetraborate Solution at Room Temperature.

The data acquisition system and associated software are functional. The data acquired for the tantalum system is in concert with that reported (41) by other researchers. The tantalum anode does contain a passive anodic film. The lithium anode system in thionyl chloride electrolyte would be expected to exhibit similar transient characteristics if its surface contains a passive non-porous lithium chloride layer. Some preliminary data has been gathered for the lithium system but none of sufficient quality to justify its inclusion within this final report. We do however have every reason to believe that the current-interrupt method coupled with surface analytical determinations can yield valuable information concerning the lithium anode in the thionyl chloride electrolyte-system and other non-aqueous electrolyte systems.

## SECTION 10

### SUMMARY AND CONCLUSIONS

The results obtained during this research program are substantial and broad in scope. They are as follows. A technique to prepare atomically clean lithium surfaces was developed. This technique allowed a thorough study of the reaction of high purity gases with the lithium metal surface to be made. The order of reactivity of lithium with the four gases studied is  $N_2 \ll CO < O_2 < CO_2$ . Fundamental information concerning the chemical state of lithium, oxygen, chlorine, sulfur and aluminum on the surface of lithium was obtained using high resolution XPS. The "black spots" formed from prolonged exposure to nitrogen were identified as a lithium oxynitride.

The reactivity of lithium with thionyl chloride is slow compared to the reaction with the electrolyte. The primary reaction product is crystalline lithium chloride. Passive film growth is enhanced by increased temperature and length of exposure. Substantial mechanical film failure was observed and may provide a mechanism to minimize the voltage delay problem in the future. Under certain conditions small prismatic crystals as opposed to cubic crystals were formed suggesting crystal growth studies might prove useful. The passive films contain several percent of occluded impurities. The tetrachloroaluminate ion is thought to provide a chloride ion which increases the rate of passivation and in so doing forms  $AlOCl_2^-$ .

The passage of an anodic current produces a "spongelike", porous and tortuous film. Sulfur occluded in this film is present in four distinct chemical states identified as (a)  $SO_4^{-2}$  (50%), (b)  $S^{+4}$  (5%),  $S^0$  (15%), and  $S^{-2}$  (30%). Electrochemical techniques were developed to study the ion transport across the passive layer. A model for the system was developed and its implication discussed. A computer interface system to study passive films using the current interrupt method was developed along with the necessary software.

## REFERENCES

1. Lattimer, W. M., "The Oxidation States of the Elements and Their Potentials on Aqueous Solutions," 2nd Ed., Prentice Hall, Inc., Englewood Cliffs, N.J. (1952).
2. Jasinski, R., "High Energy Batteries," Chap. 4, Plenum Press, New York (1967).
3. Klaus, H. M., Braeuer, M., and Harvey, J. A., "Status Report on Organic Electrolyte High Energy Density Batteries," ECOM, May 1967.
4. Gabano, J. P., Gerbier, G., and Laurent, J. F., "High Energy Cells with a Lithium Electrode," Proc. 23rd Annual Power Sources Conference, pp. 80-83, May 1969.
5. Jasinski, R. Gaines, L., Hansen, G., and Carroll, S., "Lithium Nickel Sulfide Batteries," Proc. 24th Power Sources Symposium, pp. 93-100, May 1970.
6. Dey, A. N., "Lithium Metal Oxide Organic Electrolyte Primary Batteries," Abstract #54, Meeting of Electrochemical Society, October 1973, Boston, Mass.
7. Auburn, J. J., Frerich, K. W., Lieberman, S. I., Shah, V. K., and Heller, A., J. Electrochem. Soc., 120, 1613 (1973).
8. Behl, W., Choistopulos, J., Ramirez, M., and Gilman, S., J. Electrochem. Soc., 120, 1619 (1973).
9. Gilman, S., "An Overview of the Primary Lithium Battery Program," Proceedings 26th Power Sources Symposium.
10. Dey, A. N., "Sealed Primary Lithium-Inorganic Electrolyte Cell," Third Quarterly Report, ECOM-74-0109-3, March 1975.
11. Driscoll, J. R., Holleck, G. L., Taland, D. E., and Brummer, S. B., "Lithium-Inorganic Electrolyte Batteries," Eighth Quarterly Report, ECOM-74-0030-8, January 1976.
12. Dey, A. N., and Schlaikjer, C. R., "The Voltage Delay Problem with the Thionyl Chloride System and Some SEM Studies of Lithium Film Growth," 26th Power Sources Symposium, 26, 47 (1975).
13. Dey, A. N., Electrochimica Acta, 21, 855 (1976).

14. Chua, D. L., Merz, W. C., and Bishop, W. S., "Lithium Passivation in the Thionyl Chloride System," Proceedings 26th Power Sources Symposium.
15. Dey, A. N. , "Primary Li/SOCl<sub>2</sub> Cells II. Thermal Runaways and Their Prevention in Hermetic D. Cells," Proceedings 26th Power Sources Symposium.
16. Brooks, E. S., "Evaluation of Designs for Safe Operation of Lithium Batteries," Proceedings 26th Power Sources Symposium.
17. Schlaikjer, C., Goebel, F., and Marincic, N., Journal of the Electrochemical Society, 126, #4, 513 (1979).
18. McDonald, R., Private Communication, November 1978.
19. Driscoll, J. R., Holleck, G. L., Toland, D. E., "Reactions in Lithium Thionyl Chloride Cells," Proceedings 26th Power Sources Symposium.
20. Holleck, G. L., Turchan, M. J., and Cogley, D. R., 4th Quarterly Report, Contract DAAB07-74-0030 (ECOM), EIC, Inc., January 1975.
21. Peled E. and H. Yamin, Israel Journal of Chemistry, 18, 131 (1979).
22. Ebner, W., "Kinetics of the Solid Lithium Electrode in Various Nonaqueous Electrolyte Systems", Preprint, 29th Power Sources Conference, Atlantic City, 1980.
23. Keil, R. G., J. R. Hoenigman, W. E. Moddeman, T. N. Wittberg and J. A. Peters, Technical Report AFWAL-TR-80-2018, March 1980.
24. Physical Electronics Industries, Handbook of Auger Spectroscopy.
25. Froning, M. H., Moddeman, W. E., Wittberg, T. N., and David, D. J., "Non-Aqueous Electrode Research", Interim Technical Report, AFAPL-TR-79-2003, February 1979.
26. Clausing, R. E., D. S. Easton and G. L. Powell, Surface Science, 36, 377 (1973).
27. Johansson, L. I., S. B. M. Hagstrom, and S. E. Karlsson, in the Program and Extended Abstracts of the International Conference of the Physics of X-ray Spectra, 122 (1976).
28. Fuggle, J. C., L. M. Watson, and D. J. Fabian, Surface Sci., 49, 61 (1975).

29. Keil, R., et al., Technical Report UDR-NM-QPR-79-33, November 1979.
30. Keil, R., et al., Technical Report UDR-NM-QPP-80-04, February 1980.
31. Keil, R., et al., Technical Report UDR-NM-QPR-80-15, March 1980.
32. McDonald, R. C., Private Communication, March 1980.
33. Dey, A. and R. W. Holmes, Journal of the Electrochemical Society, 127, #4, 755 (1980).
34. Dey, A., Journal of the Electrochemical Society, 126, #10, 1637 (1979).
35. Klinedinst K. and M. Domeniconi, Journal of the Electrochemical Society, 127, #3, 539 (1980)
36. Dey, A. and J. Miller, Journal of the Electrochemical Society, 126, #9, 1445 (1979).
37. Meitov, A. and E. Peled, submitted for 30th ISE Meeting, Trondheim, Norway.
38. Peled, E., Journal of the Electrochemical Society, 126, #12, 2047 (1980).
39. Yun, K., S. Wilhelm, S. Kapusta and N. Hackerman, Journal of the Electrochemical Society, 127, #1, 85 (1980).
40. Young, L. and D. J. Smith, Journal of the Electrochemical Society, 126, #5, 765 (1980).
41. Ord, J. and E. Lushiku, Journal of the Electrochemical Society, 126, #8, 1374 (1979).